ADDIS ABABA UNIVERSITY

COLLEGE OF NATURAL AND COMPUTATIONAL SCIENCE

SCHOOL OF EARTH SCIENCE

APPLICATION OF INTEGRATED GEOPHYSICAL METHODS TO MAP GEOLOGICAL STRUCTURE AND CHARACTERIZE GROUNDWATER AQUIFERS IN MEKI AREA, EAST SHEWA ZONE

A Thesis Submitted to The School of Earth Science of Addis Ababa University in Partial Fulfillment of The Requirements for The Degree of Masters of Science in Geophysics (Applied Geophysics)

By

EPHREM ALEMU MEHAMMED

Advisors:

Mebatseyon Shawel (PhD)

Tilahun Azagegn (PhD)

Addis Ababa, Ethiopia

May, 2023

ADDIS ABABA UNIVERSITY

COLLEGE OF NATURAL AND COMPUTATIONAL SCIENCE

SCHOOL OF EARTH SCIENCE

APPLICATION OF INTEGRATED GEOPHYSICAL METHODS TO MAP GEOLOGICAL STRUCTURE AND CHARACTERIZE GROUNDWATER AQUIFERS IN MEKI AREA, EAST SHEWA ZONE

A Thesis Submitted to The School of Earth Science of Addis Ababa University in Partial Fulfillment of The Requirements for The Degree of Masters of Science in Geophysics (Applied Geophysics)

By

EPHREM ALEMU MEHAMMED

Addis Ababa University

May, 2023

ADDIS ABABA UNIVERSITY

COLLEGE OF NATURAL AND COMPUTATIONAL SCIENCE

SCHOOL OF EARTH SCIENCE

APPLICATION OF INTEGRATED GEOPHYSICAL METHODS TO MAP GEOLOGICAL STRUCTURE AND CHARACTERIZE GROUNDWATER AQUIFERS IN MEKI AREA, EAST SHEWA ZONE

By

EPHREM ALEMU MEHAMMED

A Thesis Submitted to The School of Earth Science of Addis Ababa University in Partial Fulfillment of The Requirements for The Degree of Masters of Science in Geophysics (Applied Geophysics)

Approved by Board of Examiners: -

Prof. Worash Getaneh	________________	________________
Chairman	Signature	Date
Dr. Mebatseyon Shawel	________________	________________
Advisor	Signature	Date
Dr. Tilahun Azagegn	________________	________________
Co Advisor	Signature	Date
Dr. Abera Alemu	________________	________________
Examiner	Signature	Date
Dr. Dessie Nedaw	________________	________________
Examiner	Signature	Date

Declaration

The work titled "Application of Integrated Geophysical Methods to Map the Geological Structure and characterize Aquifers in the Meki Area, east Shewa zone " undersigned below is my own work being performed under the guidance of Dr. Mebatseyon Shawel and has not been presented to any institutions for the degrees or diploma awards, and all the sources utilized for research paper are properly acknowledged.

Name: Ephrem Alemu

Signature: _____________

Date: ________________

I hereby confirm that the above declaration by the applicant is correct to the best of my knowledge and has been submitted for examination with my consent as a university advisor.

1. Dr. Mebatseyon Shawel

Signature _____________

Date: ________________

2. Dr. Tilahun Azagegn

Signature _____________

Date: ________________

1. Abstract

Groundwater is the water found beneath the Earth's surface at depths where the soil, sediments, or rock are totally filled with water. This study focuses on mapping geologic structure and characterization of the groundwater aquifers of Meki to Alemtena area. The magnetic and electrical resistivity methods of prospecting give an effective presentation of the subsurface structures and delineation of groundwater aquifers. Aquifer characterization is essential for managing water resources. The interpretation of VES gives five to seven layers across all the three profiles with the average aquifer thickness of approximately 30 to 70 m. Fractured ignimbrite, sand, and alluvial deposit make up the lithologic unit of the aquifer layer, which is severely weathered and fractured. Protective capacity of aquifers with in the area is in the range of moderate to good. In terms of aquifers water potential, the areas of high longitudinal conductance, high transmissivity, low transverse resistance, low longitudinal resistivity shows the areas of high groundwater aquifers. Based on these, the study area has the highest groundwater potential in the northwestern part. Similarly, magnetic result shows that the lithological trend running from NE – SW along the research area's sides to the north and south as well as deep structures that follow the E-W trend. The groundwater flow direction to the south and north of the survey region may be determined by this structure. Most anomaly sources in the research region related to deep structures, as determined by 3D Euler deconvolution and a 2D magnetic model. The results are combined to produce a comprehensive representation of the subsurface groundwater, structures and hydrogeology. Integration of method's offers more detailed information on the aquifer characteristics, groundwater potential and identification of various lithologic structures in the area.

Keyword: Aquifer, Dar Zarrouk parameter, Euler deconvolution, flow path, Groundwater, Trend, VES

2. Acknowledgement

First and foremost, I want to express my gratitude to the Almighty God for giving me strength in my life. Next, I want to thank Dr. Mebatseyon Shawel for the constructive ideas and suggestions he gave me to successfully complete this thesis. Thank you for everything you have done for me and I appreciate Dr. Tilahun Azagegn for his technical support and tolerance during the challenging times I encountered while performing this research. I always remember and appreciate your valuable contributions. Their experience enabled the successful completion of this thesis.

My deepest appreciation goes to Prof. Tigistu Haile who gave me the important instrument and sound suggestion during the field investigation, Mr. Seyum who provided me a magnetic instrument in incredible condition and Murtessa Tegenu who helped me during the data collection in the field. You are the wonderful person I meet in my life. Next, I like to appreciate all the instructor who taught me different courses because they passed on their knowledge to me.

At last, but not the least, God Bless you all of my friends for your technical support during the writing stage of my thesis. I didn’t realize that I have such kind of friend. The school of Earth Sciences is highly acknowledged for the providing the field instrument.

3. Contents

1. Abstract v

2. Acknowledgement vi

4. List of Figures ix

5. List of Tables xi

6. Acronyms xii

CHAPTER ONE 1

1. Introduction 1

1.1. Background 1

1.2. Description of the research area 2

1.2.1. Location 2

1.2.2. Climate 3

1.3. Statement of Problem 6

1.4. The objective of the study 6

1.4.1. General Objective 6

1.4.2. Specific Objectives 7

1.5. Methods 7

1.6. Literature Review 9

1.7. Significance of the study 10

1.8. Research Question 10

1.9. Hypothesis 11

1.10. Organization of the thesis 11

Chapter Two 12

2. Geologic setting 12

2.1. Tectonic setting 12
2.2. Regional Geology 13
2.2.1. The Miocene–Pliocene formation 14
2.2.2. Quaternary Sediments 14
2.2.3. Volcanoes and Volcanic complexes 15
2.2.4. Nazreth pyroclastic 15
2.3. Local Geology 16
2.3.1. Alluvial and Lacustrine Sediments 17
2.3.2. Chefe Donsa Pyroclastic deposit (CDp) 18
2.3.3. Zikwala trachyte 18
2.3.4. Wonji basalt 18
2.3.5. Bora Bericha Rhyolites 19
2.3.6. Dino Formations 19
2.4. Geologic structure 19
2.5. Hydrogeology 20
2.5.1. Groundwater potential 20
2.5.2. Ground water flow direction 21
2.5.3. Groundwater Recharge 21
Chapter Three 22
3. Theoretical Background Geophysical methods 22
3.1. Electrical Resistivity methods 22
3.1.1. Vertical Electrical soundings (VES). 23
3.1.2. Principles of VES Survey 24
3.1.3. Basic principles of the DC resistivity method 25
3.1.4. Electrode configuration 30

3.1.5. The resistivity of earth material ... 31
3.2. Dar Zarrouk Parameter ... 32
3.2.1. Longitudinal conductance (C) ... 33
3.2.2. Traverse Resistance (R) ... 33
3.2.3. Longitudinal Resistivity ($\boldsymbol{\rho l}$) ... 34
3.2.4. Hydraulic conductivity(K) ... 34
3.2.5. Transmissivity (T) ... 34
3.2.6. Coefficient of Anisotropy ($\boldsymbol{\lambda}$) ... 35
3.2.7. Aquifer protective capacity ... 35
3.3. Magnetic method of prospecting ... 35
3.3.1. Principles and elementary theory ... 37
3.3.2. Earth's magnetic field and susceptibility ... 37
3.3.3. Correction of Magnetic Data ... 39
3.3.4. Qualitative interpretations ... 40
Chapter Four ... 45
4. Data Acquisition and processing ... 45
4.1. VES Data acquisition and instrumentation ... 45
4.1.1. Data Acquisition ... 45
4.1.2. VES data Processing ... 45
4.1.3. VES data Presentation ... 46
4.2. Magnetic data acquisition ... 47
4.2.1. Data Reduction and processing ... 48
4.2.2. Magnetic Data Processing ... 49
4.2.3. Magnetic data presentation ... 49
Chapter Five ... 50

5. Result and Discussion 50
5.1. Introduction 50
5.2. Interpretation and Discussion of VES 50
5.2.1. 1D modeling of VES data 50
5.2.2. Sliced stacked section 52
5.2.3. Pseudo depth and Geo-electric section 53
5.3. Aquifer Characterization Using Dar Zarrouk Parameter 62
5.3.1. Longitudinal conductance (C) 63
5.3.2. Traverse Resistance (R) 64
5.3.3. Longitudinal Resistivity($\boldsymbol{\rho l}$) 65
5.3.4. Hydraulic conductivity (K) 66
5.3.5. Transmissivity (T) 66
5.3.6. Coefficient of Anisotropy ($\boldsymbol{\lambda}$) 67
5.3.7. Aquifer protective capacity 68
5.3. Interpretations and Discussions of Magnetic Data 69
5.3.1. Total magnetic field anomaly 69
5.3.2. Reduction to equator 71
5.3.3. Residual magnetic field anomaly 72
5.3.4. Upward continuation 73
5.3.5. First order Vertical derivative 75
5.3.6. Analytic signal (AS) 76
5.3.7. Horizontal gradient 77
5.3.8. Tilt derivative 78
5.3.9. Second order vertical derivative 80
5.3.10. 3D Euler deconvolution 81

5.3.11. Geological Interpretation of the Structure 83
5.3.12. Magnetic 2D modelling 84
5.4. Discussion on Integration of VES and Magnetic method 86
Chapter Six 90
6. Conclusion and Recommendations 90
6.1. Conclusion 90
6.2. Recommendations 91
6. References 93
Appendix 99
Resistivity curves 99
Borehole data 101

4. List of Figures

Figure 1. 1. Location map of Meki to Alemtena area. 3
Figure 1. 2. 3D map of the area identifying variation in the elevation of Meki area 5
Figure 1. 3. flow chart of the methods 8
Figure 2. 1. Geological map of the research area taken from (Abebe et al., 2005) 17
Figure 3. 1. Current and equipotential lines produced by a current source and sink 23
Figure 3. 2. Electrical resistivity equipment 24
Figure 3. 3. Current flow in continuous medium 25
Figure 3. 4. Schlumberger electrode arrangement 30
Figure 3. 5. Resistivity variation of Water and rock material 31
Figure 3. 6. 3D electro stratigraphic model with total longitudinal conductance (C) and transverse resistance (R) 33
Figure 3. 7. magnetic direction of the earth 38
Figure 4. 1. Location map of Electrical survey profiles, boreholes and magnetic data. 47
Figure 5. 1. Interpreted VES curves of the three sounding points. 51
Figure 5. 2. Sliced stacked apparent resistivity plot 53
Figure 5.3. Pseudo depth section of first transverse 54
Figure 5. 4. Geoelectric section of first transverse 55
Figure 5. 5. Pseudo depth section along profile two 57
Figure 5. 6. Geoelectric layer section along profile two 58
Figure 5. 7. Pseudo depth section of third Profile. 60
Figure 5. 8. Geoelectric cross section of Profile three. 61
Figure 5. 9. Longitudinal conductance contour map 63
Figure 5. 10. Traverse resistance contour map 64
Figure 5. 11. Longitudinal Resistivity contour map 65
Figure 5. 12. Distribution of aquifer hydraulic conductivity contour map 66
Figure 5. 16. Reduced to the equator anomaly map of Meki to Alemtena area 72
Figure 5. 18. upward continued map of the equator reduced anomaly map 74
Figure 5. 19. first order vertical derivative map of Meki-Alemtena area 75
Figure 5. 20. Analytic signal map of Meki-Alemtena area 76

Figure 5. 21. Total horizontal derivative map of Meki-Alemtena area 78
Figure 5. 22. Tilt derivative of Meki-Alemtena area 79
Figure 5. 23. THDR_TDR map of the Meki to Alemtena area 80
Figure 5. 24. Second order vertical derivative 81
Figure 5. 25. 3D Euler deconvolution map 82
Figure 5. 26. Lineament map of Meki - Alemtena area 83
Figure 5. 27. Power spectrum of anomaly map 85
Figure 5. 28. magnetic 2D modelling 86

5. List of Tables

Table 1. 1. present land use of the Dugda and Bora Woreda 6

Table 3. 1. Susceptibility range of different rock materials 38

Table 5. 1. the curve nature and type of all VES data 52

Table 5. 2. Summary statistics of the VES variables for the entire data set considered in the Dar Zarrouk parameter. 62

6. Acronyms

AS	Analytic signal
2D	Two-dimensional
3D	Three-dimensional
CMER	Central Main Ethiopian Rift
EARS	East African Rift System
EC	Electrical Conductivity
ER	Ethiopian Rift
ERT	Electrical resistivity tomography
FFT	Forward Fourier Transform
FVDR	First vertical derivative
GPS	Global positioning system
GSE	Geological survey of Ethiopia
IGRF	International Geomagnetic Reference Field
m asl	meter above sea level
MER	Main Ethiopian Rift
msl	Mean Sea level
nT.	Nano Tesla
NE	North East
NE –SW	North East – South West
N - S	North – South
NMER	Northern Main Ethiopian Rift
SI	Structural Index
SMER	Southern Main Ethiopian Rift
TDR	tilt derivative
VES	Vertical electrical sounding
VDR	Vertical derivative
WFB	Wonji Fault Bel

CHAPTER ONE

1. Introduction

1.1. Background

The water found beneath the Earth's surface at depths where the soil, sediments, or rock are totally filled with water is known as groundwater. The groundwater from a shallow or a deep well is refilled (recharged) by rainfall. Greatest portion of the recharge source of the groundwater is rainfall (Raghunath, 1982). Rainwater gets stored in aquifers after percolating through the soil and filling pores and openings in rocks and soils. It is a critical component of the freshwater resources. Prospective locations must be identified before drilling wells in order to maximize the use of the groundwater supply (Hagos & Andualem, 2021).

Since little or no treatment is required before use, groundwater resources are the most preferred ones. Quantitatively understanding the aquifer system and groundwater conditions is necessary for evaluating groundwater potential (Kawo & Karuppannan, 2018). The assessment of water resource needs more attention as a result of the rising demand for water for a number of purposes, including agricultural, domestic, industrial, etc. Since uneven distribution of rainfall produces an irregular distribution of surface water, groundwater evaluation is essentially important. In order to meet the community's daily water needs, notably for agricultural operations, industrial uses, and environmental concerns, new water resources are required.

The porosity, the amount of rainfall, the terrain, permeability and the type of overburden material have impact on the distribution of groundwater (Raji & Abdulkadir, 2020). The water demand research area is increasing from time to time due to expansion of agricultural and industrial activities in addition to domestic use.

According to a report on the Awash River basin, population projections show additional 11Mm^3 of water will be needed for the Mojo catchment (which includes the towns of Mojo, Bishoftu, and Dukem), and 6 Mm^3 of water will be needed for the Koka catchments (which includes the town of Koka) for domestic consumptions in 2030 (REACH, 2020). This suggests that the research area require water resource for both economic and domestic use. Additionally, groundwater investigation needs more attention because water use has been rising quickly in recent years as a result of increasing industrialization and urbanization.

In the research area, a surface water divide exists at the boundary of the Awash Valley and rift valley basin. This boundary trends east- west and controls flow direction of surface water. This research also helps to identify groundwater flow direction and compare interaction of surface and subsurface at the water divide. This research project combines the results of electrical drilling (VES) and magnetic surveys with borehole data, to evaluate and characterize the groundwater potential as well as to map the subsurface hydrogeologic units, structures, and fractures in the investigation region.

1.2. Description of the research area

1.2.1. Location

The survey region is situated on the Central MER's northern edge. It is located in Oromia Regional National State, on the edge of the Rift Valley and Awash River basin. It is located in East Shewa Administrative zone, the special zone between Alemtena and Meki town. It is located in the south-central part of Ethiopia. From the capital of Ethiopia, the research area well site is 140–160 km away. The research region is in the Meki area, between the latitudes of 8^0 06’ to 8^0 18’ N and the longitudes of 38^o 40’00’’ to 39^0 00’00’’ E, with an average elevation of between 1603 and 2250 m above sea level. The aerial coverage of research area is near to 84 Km^2 as seen in Fig 1.1

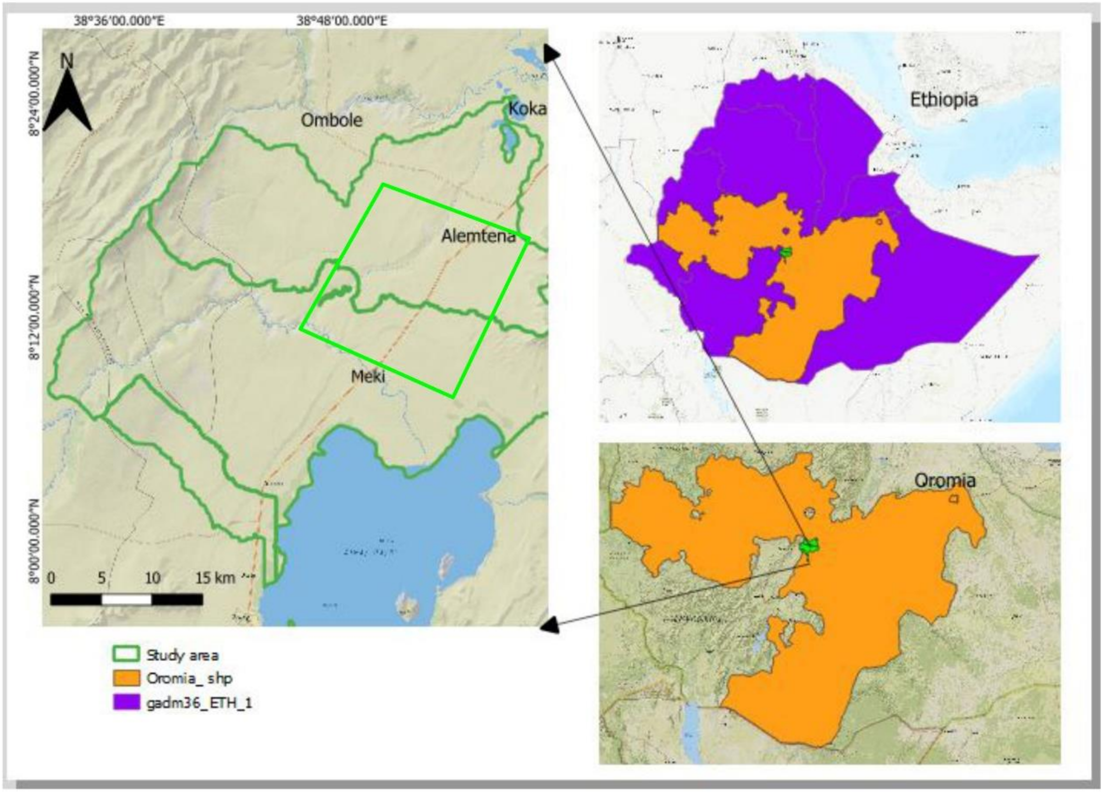

Figure 1. 1. Location map of Meki to Alemtena area.

1.2.2. Climate

1.2.2.1. Rainfall

According to data from the Ethiopian National Meteorological Agency for the years 1981–2005 the research area's precipitation data were gathered from a different nearby station. The Nazret hydrogeological map shows that the average annual precipitation distribution in the region surrounding Lake Ziway is not more than 650 mm (MoWIE, 2015) and in Koka is slightly more than 700–800 mm. The study area experiences rainy and dry seasons from June through September and from October to February, respectively, according to this paper. This region has bimodal rainfall, with a short rainy season from March to May and a long-wet season from June to September (KEBEDE, 2007). The annual amount of rainfall is sufficient for crop production even when it is low. But there is large spatial and temporal variability of rainfall.

1.2.2.2. Temperature

The main daily air temperature was 21.6 °C, while highest and lowest mean monthly temperatures may have been 27 °C and 18 °C, respectively (MoWIE, 2015). Koka and Wonji stations received reports of mean annual temperatures of 21.25^{0}C and 19.95^{0}C, respectively, and the annual daily temperature was 20.32^{0}C. Koka and Wonji stations as well as the entire rift valley, it is frequently claimed that the mean monthly evaporation rate is much higher than the mean monthly precipitation (KEBEDE, 2007). To generalize, temperature drops as altitude rises. The typical maximum temperature in the watershed is between 25°C and 29°C with maximum and minimum temperature is recorded in May and August respectively. While the mean low temperature ranges from 14.3 to 20.5 °C with maximum temperature was recorded in July and the lowest in December, (Melat, 2021).

1.2.2.3. Humidity

The amount of moisture in the air that is required to completely saturate at a given temperature is known as humidity. Around the research region, February and August has the year's lowest (51%) and maximum relative humidity (73%) values respectively. These maximum and minimum values also coincide with exceptionally wet and dry months, respectively. In general, the dry months have the lowest humidity levels while the wet months have the greatest levels (Tsegaye, 2008).

1.2.2.4. Physiography

According to (Woldegabriel, et al., 2000), the physical landscape in the research area today is the result of late Tertiary tectonic and volcanic activity as well as erosion processes that have occurred since transpired. The study's topographic elevation of the catchment extends from 1590 m asl in the lowland's flat portion to 2500 m asl at the peak of the mountain ridge (Tsegaye, 2008), and in its western and eastern regions, a little portion of the rift escarpment as well as some mountains may be seen. The catchment region shows a decline in height away from the water divide, towards Ziway and Koka Lake (KEBEDE, 2007). (Fig.1.2). With a few peaks and mountains, including Bericha and Bora, the survey area is primarily flat. With low-lying surfaces covering the low topographical basins and ridges in between, the topography is primarily flat and hilly. Flat topography is a common feature of the project region, which is primarily composed of various volcanic rock as noted by Tamiru and Antonio in (1995). The research region is somewhat elevated away from each of the two water bodies, Lake Ziway and Koka. Which is regarded as the boundary between groundwater and surface water by the previous researcher (KEBEDE, 2007).

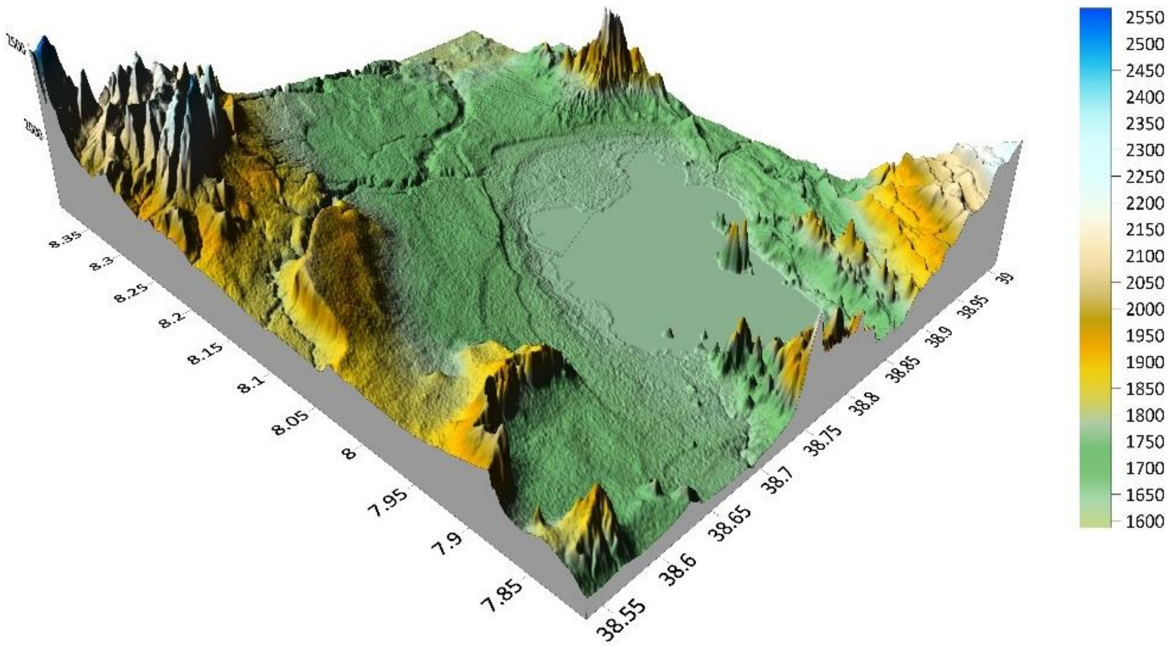

Figure 1. 2. 3D map of the area identifying variation in the elevation of Meki area

1.2.2.5. Land use land cover

According to the (Yifru et al., 2021) majority of the research area is made up of agricultural land, forest, grassland, shrubland, wetland, and bodies of water. The Dugda and Bora Woreda's current land use is also divided into four categories: farming, woodland, shrub and bush, grazing land, and others including roads. The extent of each land use category is summarized table 1 (JICA, 2002).

Table 1. 1. present land use of the Dugda and Bora Woreda

Land use category	Coverage (ha)	Percentage (100%)
Farmland	67,828	46
Forest, Bush, and Shrub	19,971	14
Grazing land	36,326	25
Others	9,758	7
Total	146,882	100

1.3. Statement of Problem

The primary issue of society has always been the availability of resources for freshwater (quality water). Due to the constantly rising demand of water in the Meki town and its surrounds, it is difficult to find an acceptable supply of quality water in the area. This problem requires a detailed study of the subsurface groundwater system. Poor quality groundwater production wells have previously been drilled in various locations throughout the region due to a lack of understanding of the groundwater system. In order to delineate the water resource, it is crucial to evaluate and characterize groundwater resources. This study is being done to characterize the aquifer in the study area and assess the potential for groundwater. Furthermore, interaction of surface and subsurface a water divides in the research area at the border of the Awash Valley and rift valley basin is also considered. This study maps the subsurface stratigraphic and structural setup and its role in controlling groundwater flow and also its relationship with the surface water divide.

1.4. The objective of the study

This geophysical study will have both general and specific objectives. Here VES, and magnetic surveys mainly focus on the characterization of the groundwater aquifers.

1.4.1. General Objective

Main objective of the research focuses on the delineation and characterization of the groundwater in Meki to Alemtena area.

1.4.2. Specific Objectives

The following particular goals are the focus of the research work, which is carried out to develop an understanding of the subsurface geology in the research area:

- ✓ To map the major geologic structures like faults, and fractures and weak zones that serve as storage areas or conduits for groundwater movement
- ✓ To recognize the key subsurface geological components in the area by combining magnetic and electrical resistivity and to map possible water-saturated horizons.
- ✓ To detect subsurface layers, their thicknesses, and resistivity.
- ✓ To determine depth of productive groundwater and to map ground water potential zones.

1.5. Methods

Several various initiatives have been undertaken in order to achieve the project's objective. These consist of a review of a large number of prior works, including material on the geology, hydrogeology, and geophysical applications (in groundwater exploration and the identification of geological formations). For this project two appropriate geophysical methods were (magnetic and Vertical electrical sounding Methods) were applied. According to (Degife, 2018) VES is used to verify groundwater potential, variations in subsurface resistivity, and the geoelectric characteristics of subsurface layers. The subsurface structure controlling groundwater flow is identified and mapped using the magnetic approach. The presence of rift faults, which play various roles in the flow and occurrence of groundwater, determines the distribution of the water within the rift. This is frequently seen in regions of geological structure where faults line up with the topographic slope, causing grabens and horsts to occur. Despite their great permeability, volcanic rocks typically do not create significant aquifers outside of the barrier faults (Fikre, 2006).

The integrated VES and magnetic methods are efficient techniques in groundwater evaluation; in facilitating better data analysis and their interpretations of groundwater potential. In this work, an attempt had been made to assess and classify possible groundwater potential zones in the Meki area using integrated VES and magnetic techniques.

To categorize the different types of rocks, the strategic positioning of the geological structures, and the likely aquifer system in the area, traverses were undertaken roughly in the NE-SW directions of the research area. In addition to that, the estimate of aquifer parameters was a key issue in defining the occurrence of the groundwater under the VES data collection. The detailed methodological process shown in the (fig. 1:3) is fully helpful to meet the objective of this thesis project.

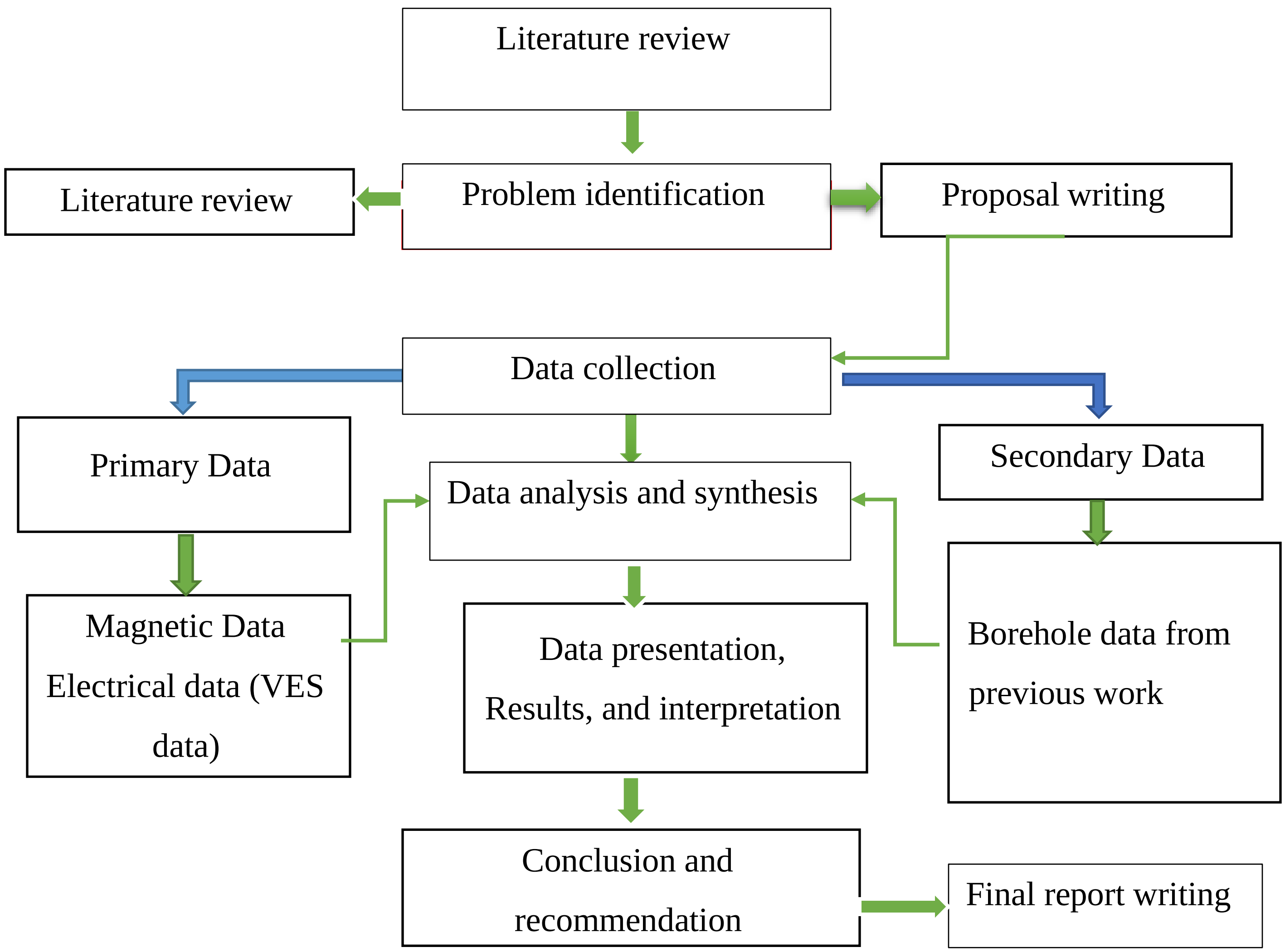

Figure 1. 3. flow chart of the methods

The Earth Resistivity meter was used to collect VES data in various predetermined directions. In VES measurement the increments of distance between main electrode increases the investigation depth.

The VES data were analyzed using proper software such as Win RESIST, and IPI2Win, and were presented by using plotting software like SURFER. In a similar manner, the magnetic data were analyzed with a combination of Microsoft Excel spread and the Oasis Montaj, SURFER16 software and presented as a map or profile on Oasis Montaj software.

1.6. Literature Review

Three-dimensional hydro-stratigraphic models supporting the assessment of fluoride enrichment in groundwater in the Lakes Basin (central Ethiopia) were studied (Ghiglieri et al., 2020; Mo WIE, 2015). According to (Kebede, 2002), groundwater is the most significant natural resource found underneath the surface of the earth. It is kept in the geological structures and is essential for domestic use, economic growth, and biological diversity. Construction of the landforms such high mountains, rift valleys, and flat places, as well as their function in surface runoff and infiltration of the Floor, affect the occurrence and flow system of groundwater.

The diverse and complicated hydrogeology in Ethiopia, which is influenced by various geological processes such as tectonic activity and climate change. The occurrence and groundwater flow are significantly influenced by the natural geological features, which also defines the aquifer's productivity (Fetter,2001). By utilizing faults and weak zones, the weathered and fractured ignimbrite and sand or alluvial layers contribute more to groundwater recharge and flow (Mequanent, 2015). Because of this, there are differences in groundwater distribution across the nation, and these differences are driven by a variety of geological and environmental factors (Alemayehu et al., 2006).

According to (Tamiru Alemayehu, 2006), the holes caused by lava flow, the vertical permeability provided by primary and secondary cracks, the horizontal permeability generated by horizons, and the gas expansion during solidification, and the occurrence of impermeable horizons and dikes are the main features that determine storage and flow of groundwater in volcanic rocks. Similar to this Zohdy, (1974) states; the electrical characteristics of the geologic formations and their fluid content have been correlated using the geoelectrical approach, which is commonly employed in groundwater investigation. The main variables affecting a formation's ER are its fluid salinity concentration, saturation, aquifer lithology, and porosity. This approach has been used to research groundwater and its condition successfully all over the world.

According to (Angasu, 2016) Over-pumping shallow groundwater for irrigation has a severe influence on the ecosystem as seen by the declining lake size and increased salinity of the water, both of which impair soil fertility and productivity. The shallow groundwater level data in the area demonstrates that as we move away from the lake, the groundwater table gets deeper and deeper. This causes the lake's size to change continuously as the shallow groundwater pumping rises day by day. The excessive extraction of groundwater caused by disparity between the amount of water demanded and supplied in the region. To address this issue groundwater exploration is conducted to analyze subterranean structure and gain insight into the hydrological process, evaluate the quality of groundwater, and recognize the characteristics, quantity, and classification of aquifers (Haile and Semir, 2016).

1.7. Significance of the study

The findings of this study can be used to identify groundwater characteristics and trace conductive geological features. They can also be used to identify subsurface layers, their thicknesses, and resistivity. It was also utilized to determine the possible region for groundwater aquifer regions by examining the hydrological conditions. Besides that, it provides scientific bases/ guidelines for future researchers and academic institutions especially geoscience disciplines, who are interested to work on related topics.

1.8. Research Question

- ✓ What is the general geologic setting of the Meki area looks like? Can we get the groundwater potential around the research area?
- ✓ What is the depth to the subsurface water table in the research area?
- ✓ What are the geophysical characteristics of soil covering the study areas?
- ✓ What are the lateral and vertical subsurface stratification of the subsurface layers and their thickness?
- ✓ What geologic structure of the area looks like?

1.9. Hypothesis

The variation in subsurface resistivity and magnetic susceptibility can be correlated with change in lithology and hydrogeological conditions, which can provide valuable information for groundwater potential investigation and geologic structures.

1.10. Organization of the thesis

There are six chapters in this thesis project. The general introduction, goals, methodology, literature review, and the description of the research area are all covered in chapter one. Chapter two describes the tectonic setting of the research area, including regional geology, local geology, site structure and hydrogeology. An overview of the geophysical techniques such as the VES, Dar Zarrouk parameter and magnetic data employed in the research is provided in third chapter. The Data acquisition is categorized under chapter four. The results and discussions of the data that have been analyzed and presented are found in chapter five. The study's conclusions and recommendations are covered in the final chapter.

Chapter Two

2. Geologic setting

2.1. Tectonic setting

The MER is a region that displays dynamic extensional tectonics (Agostini et al., 2011). It is a 700 km long, 80 km wide, NNE-SSW trending rift valley that is bordered to east and west by the Somali Plateau and the Ethiopian Plateau, respectively (Benvenuti, et al., 2002). A sequence of normal faults that typically trend parallel or sub-parallel to the NNE-SSW rift axis visibly separate the rift valley from the plateau (Ayenew, 2007). The Rift is characterized by powerful and recent faulting, making it a tectonically active region. These geological features indicate a high level of tectonic activity and volcanic processes in the region, contributing to its dynamic nature (Benvenuti, et al., 2002). There is NNE-SSW dense swarms along the SDZFZ on the west and the WFB consists an offset of 1500–2000 m between the rift and plateau (Woldegabriel et al., 1990; Ebinger et al., 1993).

The elevated eastern and western escarpment falling to east and west, are divided by the rift (Benvenuti, et al., 2002). The MER formation was from middle to late Miocene (Ebinger et al., 1993; Wolfenden et al., 2004; Woldegabriel et al., 1990). As noted by (Furi, et al., 2011) high volcanic-tectonic activity is occurred throughout the Oligo-Miocene period. The Middle Awash Basin exhibits diverse geology and intricate geologic features. These geological processes have produced two unique landscapes: the mid-sector NNE-SW trending rift floor and the mountain blocks that encloses the west and east graben. Southern, Central, and Northern MERs are the three main divisions of the MER, each of which represent a different stage in the development of a continental rift based on differences in fault timing, patterns, and lithospheric properties.

The SMER is one portion of the great EAR system located within the limit of 37^o-38.5^o east and 5.5^o-7^o north. According to (Benvenuti, et al., 2002) the Amaro Horst divides the southern section of the SMER extending from Hawassa to the Ethiopian-Kenya border to the two basins. The central MER is bounded on the north by the Yerer-Tullu-Wellel volcano tectonic line and on the south by the Goba-Bonga line. It is also bounded to the east and west by fault escarpments such as the Munesa and Guraghe rift ridges.

The NMER bounded between Afar Rift in the north and Koka Lake in the southern direction with border faults that trend at N50°E. which was formed during 10–11 Ma(Woldegabriel et al., 1990). Late Miocene and Pliocene-Pleistocene sediments are found along ancestral marginal grabens on both sides of the NMER, between the Kesem-Kebena and Middle Awash regions of the southern Afar Rift. The WFB, also known as border fault and the rift floor faults, are both well-developed fault systems that are visible in the NMER (Boccaletti et al,1998; Mohr & Wood, 1976).

The Quaternary volcanic rocks are composed of a range of volcanic elements including tuff, pumice, ignimbrite, pyroclastic flows, scoria, and basalt flows. According to (Angasu, 2016) the region's geological formation consists of tertiary-aged acidic and basic volcanic rocks as well as quaternary-aged acidic and basic volcanic rocks, lacustrine and alluvial deposits (Furi et al., 2011). A Bishoftu Scoria cones and basalt flows, is observed in the northern and southern regions and are possibly associated to the Bishoftu volcanic activity, are probably the result of volcanic activity.

According to (Woldegabriel et al., 1990) Ethiopia had extensive volcanic activity and a stretched tectonic activity during the Tertiary and Quaternary periods. Late Oligocene fissure eruptions of tholeiitic and transitional basaltic lavas, as well as a small number of ignimbrites forms the tertiary volcanic activity.

2.2. Regional Geology

The MER was formed by of extensional tectonics with trend in the NNE-SSW direction, which began to develop during in the Miocene period. According to Zennettin et al., (1980), volcanic rocks related to the rift were formed after fissural volcanism in the adjacent plateau had died out. It runs between Afar and Kenya rift and is roughly NE-oriented (Gibson, 1968); Wolfenden et al., 2004. The Ethiopian plateau is divided by MER. The Mozambique Belt, a huge movable belt of the Proterozoic that stretches from Ethiopia south to Kenya, Tanzania, and Mozambique, is where the MER originated.

South and north ends of the rift consists some irregular Precambrian rocks as well as volcano-tectonic, and sedimentation events during the Cenozoic era, are considered to be responsible for geology and geomorphology of the region (Benvenuti, et al., 2002). Extensive volcanism, which is characterized by the eruption of fissural basaltic lava flows and the deposition of volcanoclastic materials which is responsible for the rift's creation. (Ayenew, 2007). The Tertiary volcanic rocks dominate the geological sections along the rift borders. However, the crystalline basement is irregularly covered by Tertiary volcanic rocks and Mesozoic sedimentary rocks in a few particular places. This indicates a complex geological history in the region, with different rock formations being present and stacked in certain areas (Woldegabriel et al., 1990).

Examining regional structures reveals that rift and its escarpments are heavily faulted. The MER's faults are not randomly dispersed; rather, they frequently gather in groups. The WFB system of faults is the most prominent collection of faults in this area, and it is located near to the rift's eastern edge (Benvenuti, et al., 2002). Normal type of WFB faults is upthrown to both the north-west and south-east as noted by (EIGS, 1984). The Wonji Fault, the most active portion of the MER, exhibits larger grabens inside the rifts that are both oriented in NNE-SSW direction, much like the MER. The MER stretches from the region around Lake Abbe in Central Afar to the south of Lake Chamo in Southern Ethiopia (MoWIE, 2015). The Upper Awash River Basin dated from the Upper Miocene to the Holocene consists volcanic rocks (Plateau and Rift volcanic), lacustrine, and alluvial deposits.

2.2.1. The Miocene–Pliocene formation

This volcanic group consists of transitional, sub-alkaline basalts connected to rhyolite and trachyte. The majority of the principal unit of this formation is composed of rhyolite domes with subordinate basalt beneath the transitional and alkaline basalt (Abebe et al., 1998a). In a handful of the study area's north-west highland localities, there have been a few exposures. The unwelded tuffs, ash flow, rhyolite, and trachyte of this group are located in the west and south-east of the research region as a transitional zone between the highlands and the rift (Boccaletti et al.,1999).

2.2.2. Quaternary Sediments

These youngest strata in the research area are composed of formations from the late Pleistocene, Holocene, and upper Quaternary. These geological formations cover a majority of the rift. Rhyolite, tuff, pumice, scoria, and pyroclastic rocks, also referred to as the Dino formations, make up the rock's bottom unit (Abebe et al., 1998).

During the Pleistocene to Holocene period's, rift floor was covered with lacustrine sediments (lake deposits) which comprised of sands, clays, tuffs, pumice, and diatomite. These deposits are the remnant of a vast lake that used to fill the rift valley's floor before it eventually dried up, leaving behind these sedimentary materials (Mohr & Wood, 1976). Massive rocks including trachy basaltic lavas, rhyolitic ignimbrites, and basaltic lavas are found in the highlands. These rocks are connected by well-developed fracture networks, which makes them effective aquifers for the flow and storage of groundwater.

2.2.3. Volcanoes and Volcanic complexes

They are some of the pyroclastics that make up the flow of thick, viscous silicic lava. When magma that is rich in silica gas erupts, it can produce Ignimbrite and pumice. This same magma can later erupt as thick, viscous lava flows and domes after losing its gases due to explosive activity. These lava flows, composed of Rhyolites, trachytes, pumice, ash, and obsidian, often have craters or calderas ranging in size from 2 to 40 Km. These craters and calderas are often filled with small lakes. The sinking of the Gedemsa, shalla, and Corbetti caldera, located in three different regions, can be easily explained by the presence of large and wide spread ignimbritic formation and other silicic pyroclastics in the MER (Dipoala, 1972).

2.2.4. Nazreth pyroclastic

The Nazreth Units are exposed at their footwall and overlain by lake deposits in majority of the CMER (Agostini et al., 2011). North-west and eastern regions of research area is covered by this unit. According to Woldegabriel et al., (1990) this unit consists collection of lithological distributions such as a thick cluster of ignimbrites, unwelded tuffs, ash flows, welded rhyolitic ignimbrites and trachytic lava domes. The Nazareth unit (welded ignimbrites) shows poor permeability except the weathered and fractured areas (Gebere et al., 2021a). On the plateau margins, they are from 1 to 30 meters thick whereas, the group attains a maximum thickness of up to 250m in the Rift (Abebe et al., 2005). Presence of numerous widely dispersed rhyolitic domes suggests the evolution of Nazreth volcanoes.

According to (Kazmin, 1978), Nathret group can be classified into Upper and lower Nazreth pyroclastic deposits. The upper Nazreth group is made up of rhyolitic compacted tuff that ranges in color from white to blue grey, greyish green welded tuff with fiamme, and tuff breccia that contain white pumice, rhyolitic lava fragments, crushed and lightly worn obsidian fragments, and infrequent reddish-brown basaltic lava fragments. Similarly, the northeastern shore of Lake Koka also contains this type of geology (MoWIE, 2015). This unit unconformably overlies the lower part of Nazreth pyroclastic deposits. The thickness is more than 2m at Koka dam. Yellowish-white pumice fall deposits, tuff, crystal tuff, an alternation of fine volcanic sands, and pumiceous tuff make up the Lower Nazreth pyroclastic deposits (Abebe et al., 2005).

2.3. Local Geology

According to (EIGS, 1984) volcanic rocks and ash sediment, which comprise alluvial and lacustrine phases the predominant units. The different geological units covering the Meki area include; lacustrine deposit, and Zikwala trachyte, Magdela volcanic and Basaltic lava flows. Lacustrine deposits are geological units dominating about 75% of the plain, and other minor units make up the remaining 25% (Abebe et al., 2010; Kebede et al., 2021).

According to report by (MoWIE, 2015; Abeba, 2020; Kawo & Karuppannan, 2018; Mesele & Mechal, 2020) the significant aquifers in the Meki area to the north east region of the town consist of alluvial and lacustrine sediment, fractured ignimbrite & quaternary sediment, Basaltic aquifer. Alluvial, fractured ignimbrite, and lacustrine aquifers, which are known for having abundant groundwater resources, are found in the basin's flat parts.

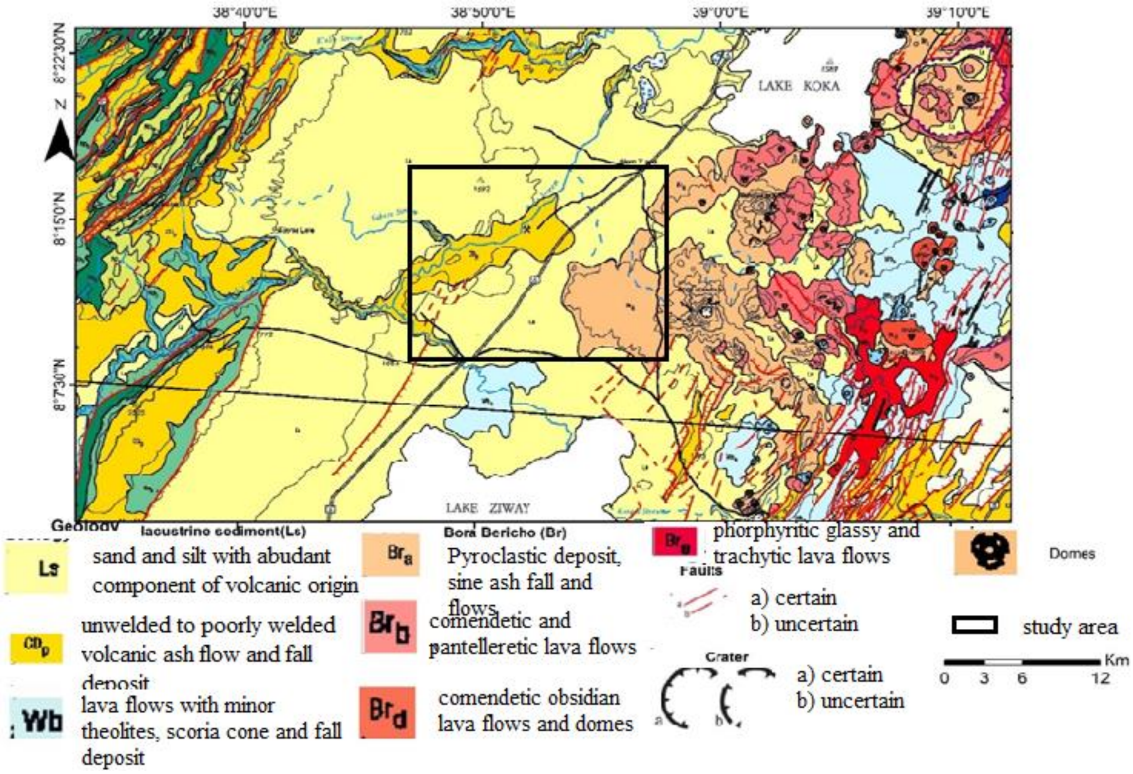

Figure 2. 1. Geological map of the research area taken from (Abebe et al., 2005)

2.3.1. Alluvial and Lacustrine Sediments

Local shallow aquifers are formed in the valley plains by lacustrine and fluvial deposits in alluvial sediments. Which covers most of the research area. The thickness of this rock is about 600m in the northern section of the researched area (Abebe, et al., 2005). The entire low-lying flat land on the western, southwestern, northern, and north-eastern side of Ziway Lake's is covered by lacustrine sediments, which are primarily made of silt and clay size material with a small amount of volcanoclastic sediment and tuff. These lacustrine deposits are supposed to be Pleistocene to Recent in age (Haile, 1998). In the Rift Valley, these deposits which are linked to volcaniclastic deposits can be found below the water beds of Lake Ziway and the Koka Dam (Bedane, 2008). The lithology of the sediments varies depending on their mode of origins (Ayenew, 1998).

The coarse sediments of alluvial and lacustrine deposits in the research regions make them highly permeable. In the north-eastern part of the survey area, it is up to 80 m thick (Kawo & Karuppannan, 2018). They interact with Quaternary volcanic products to create a particular kind of volcanic sedimentary rock. Lake deposits could be found lateral to the surface in the study region. These deposits seemed to be loosely cemented material with a range of granular textures from fine to coarse. The lacustrine sediments contain tuff, diatomaceous earth and ignimbrite that are partially embedded and occasionally form a thick layer (Furi, et al., 2011).

2.3.2. Chefe Donsa Pyroclastic deposit (CDp)

This group of rocks is made up of unwelded to insufficiently welded rock, volcanic ash flow, and fall deposits. Maximum exposed thicknesses range from a few to 40 m (Abebe et al., 2005). The Chefe Donsa unit, which is located in the easternmost part, is composed of pyroclastic fall that is approximately 12 m thick (Furi, et al., 2011; Bedane, 2008).

2.3.3. Zikwala trachyte

This group is located in the northeastern region of the Research area. Dark grey, aphyric, and phyric lava flows with interbedded pyroclastic make up its lithology. These unit consists dark gray, porphyritic trachyte with intercalation of pyroclastic material around Mt. Zikwala. It has thickness of more than 130m at Mt. Zikwala MoWIE, 2015).

2.3.4. Wonji basalt

Wonji basalt is primarily restricted to the WFB that runs parallel to the MER and is made from a variety of Quaternary lava, pyroclastic rocks, and volcaniclastic layers. (Woldegabriel et al., 1990). Alkaline to olivine basaltic lava flows with small tholeiites, Hawaiites, Benmoreites, rhyolitic, trachytic lava domes, and welded pyroclastic flows are found in the formation. It runs along the eastern shore of Ziway Lake. It is well-known for its basaltic lava flows, scoria cones, phreato-magmatic deposits, and Quaternary volcanics. Maximum exposed thickness of this rock is 10 m (Abebe, et al., 2005).

Basaltic Lava Flows is located in the east and north east lakes. Basalts can have a wide range of permeability from a hydrogeological standpoint. Dense, unfractured, and unjointed Basaltic rocks have relatively low permeability while heavily weathered and fractured basaltic rocks have high permeability (Haile, 1998). They are the product of explosive activity, and because of intense faulting in the area, basaltic hyaloclastites have a very high groundwater potential.

2.3.5. Bora Bericha Rhyolites

The Bora-Bericha group of volcanic rocks extends from southwestern corner of Koka Lake to the south Alemtena area. It comprises peralkaline trachytes and rhyolites from the central volcanoes with comenditic and pantelleritic affinity (Abebe, et al., 2005). According to (Agostini et al., 2011), the Bora-Bericha silicic rock characterizes later quaternary volcanic activity and builds huge core volcanoes with well-developed calderas. Ignimbrites, lava flows, domes, and phreatomagmatic deposits with compositions ranging from trachyte to peralkaline rhyolites are produced by these volcanoes.

2.3.6. Dino Formations

This kind of volcanic rock is made up of welded rhyolitic to andesitic tuff that ranges in color from greenish-yellow to light grey and has elongated obsidian lenses. It can be found up to Shala Lake, south-west of Ziway Lake, west of Meki town, and south-west of Koka Lake (Kebede et al., 2021). Along the Awash River, Dino ignimbrite is about 20 m thick. At the Awash River, the unit is divided into two flow units. The lowest unit is composed of rhyolite, green welded tuff, white pumice, and medium to coarse-grained tuff with a grayish-yellow tint. Rhyolite, white pumice, and unusual green welded tuff, which are all huge lithic clasts, are graded both normally and in reverse in the higher part. Rhyolite, pumice, and occasionally basaltic fragments with a maximum length of 30 cm are included in the unit, which is high to highly welded medium tuff.

2.4. Geologic structure

The MER contains two main fault systems: a N30E to N40E trending fault system that mainly characterizes the rift margins, and an N-S to N20E trending fault system known as the Wonji Fault Belt (WFB) (Boccaletti, et al., 1998). In general, these are the two major orientations in the MER: NNE-SSW and NW-SE. The lithologic units invariably have fundamental layering structures that form during rock formation. Layering is often continuous and characterized by color and textural variety (Furi et al., 2011). Similarly, two different fault networks are visible along the MER, according to (Tesfaye et al., 2003).

Faults and other large fractures running NNE-SSW and NW-SE on the either side of researched area are important lineaments. The lineament that are subparallel to the rift axis are NE-SW trend because of extensional tectonics. But according to (Bonetto et al., 2021) at least three sets of faults—the NNE-SSW, N-S, and NNW-SSE trending faults—have been identified in the region. WFB is a tectonically active fault system, the axis of the first two sets, which are dominant and stretch across considerable distances. Additionally, cross-rift oblique-slip fault systems with an E-W to NW-SE trend have been identified locally.

The MER is dominated by brittle deformation, which includes fractures, joints, and faults. These formations are divided into two primary fracture systems, each of which mostly consists of joint sets and a few faults (Abebe et al., 2005). The first orientations are most dominant system and are part of the WFB traversing the rift. The other trend is a transverse structural discontinuity presumably formed earlier than the main rift faults.

2.5. Hydrogeology

2.5.1. Groundwater potential

The types of volcanic rock that are there and the structures that have an impact on them dictate the characteristics of the aquifer in this basin. The primary porosity of these volcanic rocks varies greatly based on lava flow type and condition under which it occurred (MoWIE, 2015). Over the time, tectonic activity has caused this rock to whether and fracture, resulting in the development of secondary porosities. Because of this, the volcanic aquifers in this area are regarded as secondary porosity media, and the fracture is crucial to the movement and storage of groundwater (Yitbarek et al., 2012). The fractured ignimbrite and rhyolitic ignimbrite are regarded as medium permeability groups and are also good water-bearing units. The alluvial deposits, basaltic flows, and domes are significant permeable units. Massive ignimbrites and lacustrine deposits are among the remaining geological units that are regarded as being low-permeable.

Combination of fractured ignimbrites, quaternary Scoraceous basalts, and fractured basalts, as well as quaternary alluvial and lacustrine aquifer unit in the region form aquifer unit (MoWIE, 2015; Bedane, 2008). Which can be classified into two main groups (Furi, et al., 2011). Those are the volcanic rock that includes weathered and fractured Ignimbrites, Scoria, Scoriaceous basalt, and basalts.

Volcanic rock

Those types of rock include a material having a wide range of hydrogeological properties such as Ignimbrite, trachyte, rhyolites, basalts, scoria, and pyroclastic rocks. Rhyolites and trachyte can be considered practically impervious as groundmass even if intersected by frequent tectonic or secondary discontinuities. Since uppermost trachyte dome and rhyolite flow is weathered, the size of fractures and other openings is reduced. That causes a decrease in the permeability of complex rock bodies.

Alluvium and lacustrine deposit

A portion of the study region is covered by alluvial unit outcrops in the NW west which extends to Debrezeit Lakes (Maneti et al., 2005). Alluvial sediments are porous and permeable due to their loose nature. The majority of this research area is taken up by sediments of alluvial and lacustrine origin. Sandy clay and silty clay with gravel in the lower bed make up the alluvial deposits. The Koka lakes are surrounded by lacustrine deposits. The transport and storage of groundwater are slightly favored by this structure. Upper basalt aquifers are connected to alluvial aquifers, which prevent them from forming distinct aquifers.

2.5.2. Ground water flow direction

The terrain and heavily faulted and fractured rocks of the region control groundwater flow. It's flow parallel and subparallel to the main faults affect the subsurface hydraulic connection between the rift and the river-groundwater relationship (Bonetto et al., 2021). These encourage profound percolation through the rock's main pores and fractures. Distinction in groundwater flow direction is influenced by both the terrain and the kinds of structures that are present in the region.

2.5.3. Groundwater Recharge

Precipitation appears to effect porous pyroclastic and lacustrine sedimentary aquifers as well as fractured volcanic rock aquifers such as strongly weathered and fractured ignimbrite. Butajira and Arsi mountains or highlands are replenishment channels from the mountains and hills that favor deep infiltration of rainfall, runoff and streams (MoWIE, 2015).

Chapter Three

3. Theoretical Background Geophysical methods

3.1. Electrical Resistivity methods

The most effective and important method of groundwater exploration is the resistivity technique of geophysical prospecting (Kearey, 2002). An electric potential field in the earth's crust is created using artificial current sources for DC resistance approaches (Reynolds, 1997). ER methods have a number of benefits, including control over the depth of penetration, equipment mobility, availability of related software, access to a choice of simple and elegant interpretation tactics, etc. (Ahmad, 2017). It helps to determine bedrock depth in engineering sites, defining aquifers in groundwater surveys, locating geothermal fields, and mapping giant ores in mineral exploration (Bayewu et al., 2018).

The ER principle shown in Fig. 3:1 was utilized to map the geological environment of the existing aquifer and understand the thickness of stratified media. This technique successfully applied to groundwater due to its effectiveness and non-destructive behavior in creating subsurface images compared to the traditional method. Depending on the local area's resistivity readings, ER method can be used to assess the aquifer's depth, stratigraphy, and water quality (Mohamaden, 2016). To determine the spatial resistance distribution in the ground, potential field is created and measured (Aubert et al., 1984). Depth measurement (Samouelian, 2005; Reynolds, 1997) and horizontal profiling (lateral resistivity variation) are two main ways of using electrode arrays (Milson J., 2003).

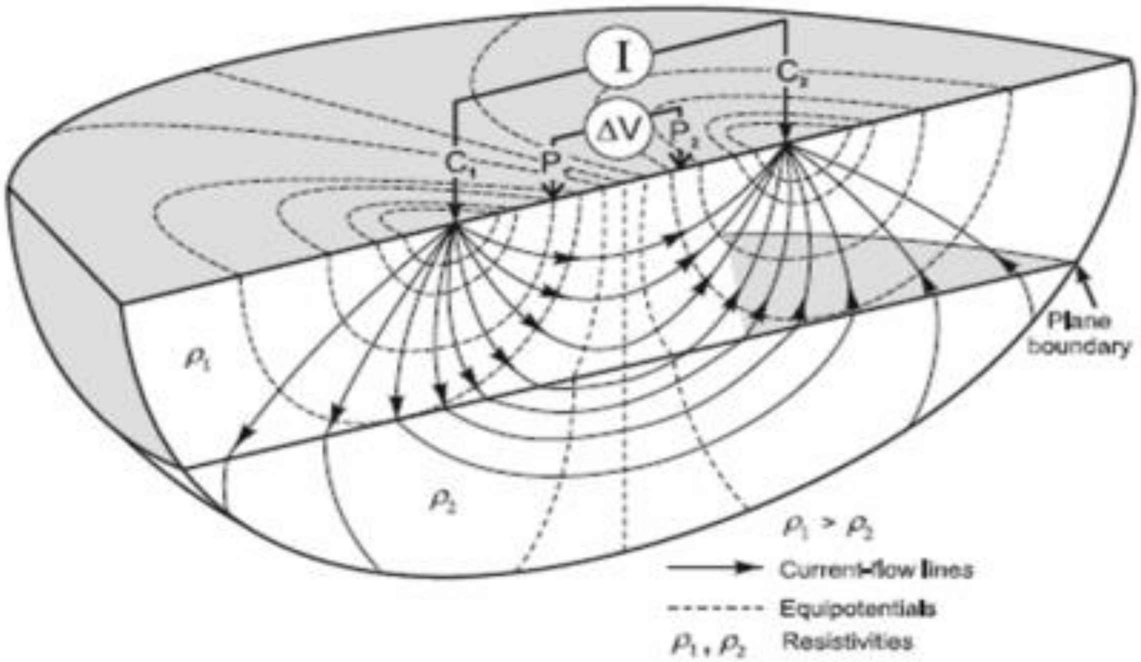

Figure 3. 1. Current and equipotential lines produced by a current source and sink

3.1.1. Vertical Electrical soundings (VES).

It is one of electrical resistivity approach that can be used in various investigations in which the center and orientation of the potential configuration remain constant. Deep probing is accomplished through a series of resistivity measurements with steadily increasing electrode spacing (Haile & Atsbaha, 2014). The characteristics of the investigated geological sections are recorded using this method depend on the kind of arrays that are employed (Bayewu et al., 2018). It is a 1D resistivity approach that uses the least number of equipment and workers to deliver detail information of subsurface rocks (Aubert et al., 1984). To produce the apparent resistivity values, the resistance values from the resistivity m were multiplied by the corresponding geometric factor (K).

$$Resistivity\ (ohm.m) = Rho = K \times \frac{Vmn}{I} \qquad (3.1)$$

In this arrangement, the current electrodes are positioned symmetrically at gradually increasing intervals about a center point (probing point), while the potential electrodes are close together (Heigold, 1979). Several resistance measurements are carried out at different electrode distances. When the electrodes are separated, the electric field penetrates deeper and affects more underlying layers and readings (Asta, 1920). Electrical

Sounding is used to estimate the depths and resistivity of the strata present by determining how resistivity varies with depth below a specific location on the ground surface and by correlating the geophysical information with the available geological data (Griffths and King, 1981). The potential electrodes are hardly ever increased in the Schlumberger VES while the current electrodes are usually moved outward in steps AB > 5 MN.

3.1.2. Principles of VES Survey

According to (Griffths and King, 1981) current electrodes is used to send electric current into the ground while measuring the resulting potential difference and resistivity value. VES is commonly used in ER measurements to determine the vertical variation of the earths apparent resistivity and potential field generated by the current (Mohamaden, 2016). VES measurements are very useful to understand distribution and quality of groundwater (Mengistu et al., 2019).

As noted by Telford et al, (1990) the vertical resistivity variation of the subsurface soil is expected to be result of up of horizontally stacked media. Various factors like; Porosity, salinity, liquid content, fractures and faults all affect subsurface resistivity (Furi et al., 2011).

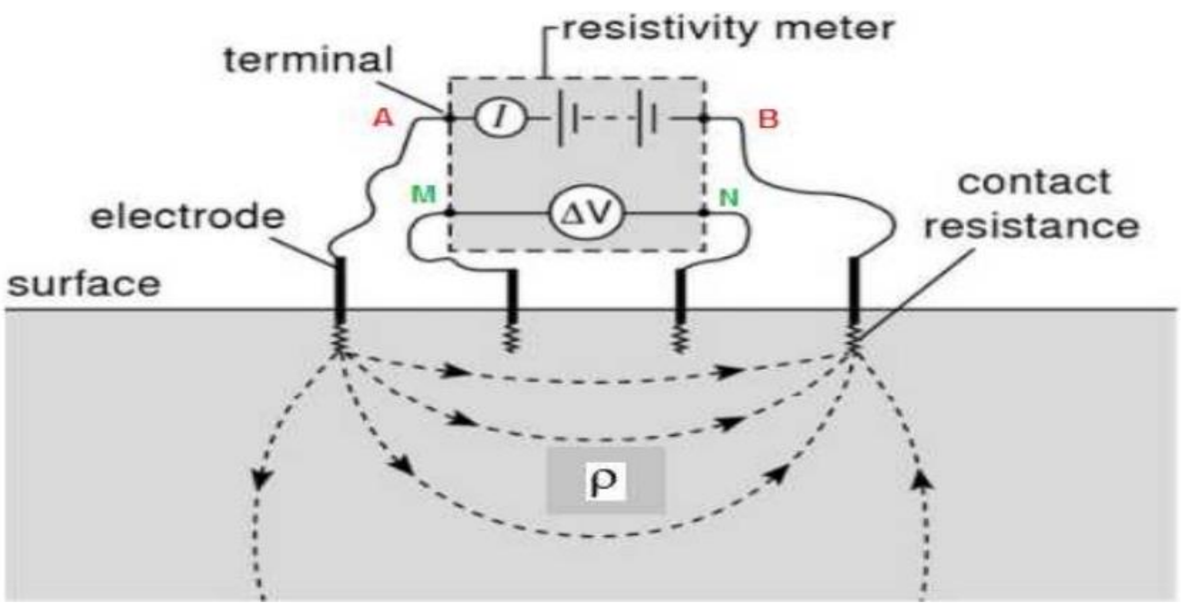

Figure 3. 2. Electrical resistivity equipment

As shown in the Fig (3.2) the procedure comprises retaining the potential (MN) electrodes in place while gradually extending the spacing between current electrode around the sounding point. This generates a curve that illustrates the relationship between apparent resistivity and depth. Additionally, the depth of penetration increases with the primary electrode spacing, providing for greater awareness of the geological strata and structures (Grifffths and King, 1981).

3.1.3. Basic principles of the DC resistivity method

The electrical investigations serve to determine the resistance distribution under the earth's surface through measurements on the earth's surface. These measurements can provide an estimate of the actual subsurface resistivity (Amarachi and Ako, 2012). The physical principle underlying resistance measurements is Ohm's Law, which controls the flow of electricity in the earth (Grifffths and King, 1981). If a constant current flow is taken into account in a large medium, as seen in (Fig. 3.3), the current flow is determined by the rules of energy conservation;

$$(I_c)_s = -\frac{dQ}{dt}, \qquad (3.1)$$

where $(I_c)_s$ is the current flow brought on by charges flowing out, and Q is the charge contained in's'.

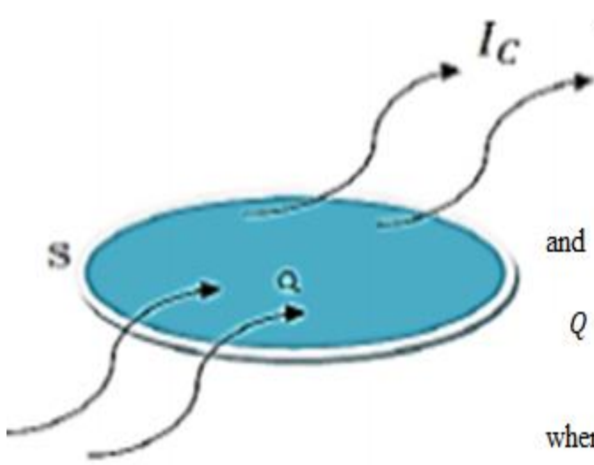

With respect to current density and charge density;

$$(Ic) = \oint \vec{J}.ds \qquad (3.2)$$

and

$$Q = \int q.dv \qquad (3.3)$$

wherever V is the surface bounded volume.

Figure 3. 3. Current flow in continuous medium

by introducing equations (3.2) and (3.3) in equation (3.1) we can obtain equation (3.4) below.

$$\oint \vec{J}.ds = -\frac{d}{dt}\int q.dv \qquad (3.4)$$

Using the divergence theorem of left side of, Eqn (3.4), and interchanging the order of differentiation and integration on the right-hand side of the equation

$$\oint_s J.ds = \int_v (\nabla.J)dv \qquad (3.5)$$

$$\int (\nabla.J)dv = -\int \left(\frac{\partial q}{\partial t}\right) dv$$

$$\int \nabla.J + \frac{\partial q}{\partial t})dv = 0 \qquad (3.6)$$

Equation (3.6), which must be accurate for any volume, provides

$$\nabla.J + \frac{\partial q}{\partial t} = 0 \qquad (3.7)$$

Equation (3.7) is the continuity equation. At a given current electrode spacing, rising of normalized current flow indicates the existence of a conductive body in the current flow path (Griffths and King, 1981). Furthermore, the presence of subsurface conductive structures is supported by a similar current flow observed with increasing current electrode spacing (Aubert et al., 1984). For homogeneous isotropic medium, Kirchhoff's law applied, like electric charge conservation law and its continuity: -

$$\nabla.J = 0 \qquad (3.8)$$

Where, J is current density

The amount of electric current entering and leaving the bulky material must be the same unless there is a source or a leak. Ohm's Law: In a differential form.: In a differential form Ohm's Law is expressed as:

$$J = \sigma E \qquad (3.9)$$

Where, current density j correlates inversely with the resistivity of the medium (ρ), but directly related with the electric field strength (E) and the conductivity (σ).

Relationship between electric field strength (E) and potential function (U) is

$$E = -\nabla U \qquad (3.10)$$

U must meet two requirements: At greater distances from the source, the potential must converge to zero. The potential field should be uninterrupted between two different media. The potential difference along the boundary would be finite over a small (De Almeida et al., 2021). According to Ohm's law, this would produce an endlessly high current density, which is impossible.

$$U_1=U_2 \qquad (3.11)$$

$$\sigma 1 \frac{\partial U1}{\partial n} = \sigma 2 \frac{\partial U2}{\partial n} \qquad (3.12)$$

σ_1 and σ_2–are electrical conductivity of the subsurface layer and $\partial U_1/\partial n$ & $\partial U_2/\partial n$ – normal potential component.

At the boundary between two media, the normal components of the current flow are the same. Combination of Ohms law and divergence condition results in eqn (3.13),

$$J = \sigma E \text{ and } E = -grad\ U$$

$$J = \frac{1}{\rho} E = -\frac{1}{\rho}(-gradU)$$

$$J = \frac{1}{\rho}\ Grad\ U \qquad (3.13)$$

From the eqn (3.8) div J=0

So,

$$\frac{1}{\rho}\ Grad\ U = 0 \qquad (3.14)$$

In isotropic media ρ is a scalar function of the observational point and **J** lies along similar direction to **E**.

For this case, from combination of equations (3.8) and (3.14)

$$div\left(\frac{1}{\rho}\ grad.V\right) = 0$$

$$div\frac{1}{\rho}.grad\ V + \frac{1}{\rho}\ div.grad\ V = 0 \qquad (3.15)$$

The basic formula for electrical prospecting is given as equation (3.15) above. Because, Resistivity value (ρ) of homogeneous medium does not dependent on the coordinate axes. Therefore, the equation above reduces to Laplace Equation.

$$div.grad\,V = 0$$

$$\nabla^2 V = 0 \qquad (3.16)$$

This indicates that the potential dispersion of direct current in a uniform surface satisfy Laplace equation. Similarly, the expression of electric field strength for the homogeneous area is given by;

$$E = \frac{\rho I}{2\pi r^2} \qquad (3.17)$$

According to Ohm's law, the electrical field strength (E) produced by the current flow (I) or the measured potential difference (U) are used to calculate the resistivity.

$$J = \sigma E$$

This implies that $E = \frac{J}{\sigma} = J\rho$ and $E = -grad\,U$ were, $\frac{1}{\rho} = \sigma$

$$J = \sigma E = -\frac{1}{\rho}\frac{dU}{dr} \qquad (3.18)$$

In a homogeneous semi-spherical media

$$J = \frac{I}{A} = \frac{I}{2\pi r^2} \qquad (3.19)$$

The electric field strength is $E = J\rho = -\frac{dU}{dr} = -\frac{\rho I}{2\pi r^2}$ this eqn is re arranged to

$$dU = \rho I \frac{dr}{2\pi r^2} \qquad (3.20)$$

The Potential field at Each point is

$$U = \int du = \frac{\rho I}{2\pi}\int_0^r \frac{dr}{r^2} = \frac{\rho I}{2\pi r} + c \qquad (3.21)$$

Since I=0 when r→∝; we take as C=0. If so

$$U_m = \frac{\rho I}{2\pi r} \qquad (3.22)$$

The potential at sites M and N, which are separated from source electrode A by $r_1 = r_{AM}$ & $r_2 = r_{AN}$ is calculated as follows to generalize this equation:

$$U_N = \frac{\rho I}{2\pi AN} \quad (3.23)$$

Similarly,

$$U_m = \frac{\rho I}{2\pi AM} \quad (3.24)$$

By using the eqn (3.23) and (3.24) the potential difference is evaluated as

$$\Delta U = Um - Un = \frac{\rho I}{2\pi}\left(\frac{1}{AM} - \frac{1}{AN}\right) \quad (3.25)$$

Potential due a dipole source

$U_{AM} = \frac{\rho I}{2\pi x}$ is potential at M due to A, $U_{BM} = \frac{\rho I}{2\pi(l-x)}$ is potential at N due to A

Now the potential at M due to A & B is: -

$$U_m = U_{AM} - U_{BM} = \frac{\rho I}{2\pi}\left(\frac{1}{x} - \frac{1}{l-x}\right) \quad (3.26)$$

the potential difference between A and B will be;

$$\Delta U = U_M - U_N = \frac{\rho I}{2\pi}\left(\frac{1}{AM} - \frac{1}{AN} - \frac{1}{BM} + \frac{1}{BN}\right) \quad (3.27)$$

Now the resistivity of the medium is calculated by

$$\rho = \left\{\frac{\Delta V}{I}\left(\frac{2\pi}{\frac{1}{AM} - \frac{1}{AN} - \frac{1}{BM} + \frac{1}{BN}}\right)\right\} \quad (3.28)$$

Where, $K = \left(\frac{2\pi}{\frac{1}{AM} - \frac{1}{AN} - \frac{1}{BM} + \frac{1}{BN}}\right)$ is array coefficient or geometric factor.

Now the apparent resistivity is,

$$\rho_a = \frac{K\Delta U}{I} \quad (3.29)$$

From this resistivity value is derived by multiplying with a geometric factor because resistivity measurement devices typically provide a resistance value, R=V/I.

$$\rho_a = KR \quad (3.30)$$

The subsurface strata can be identified based on the characteristics of electrical method because, different geological materials have different electrical properties (Bayewu et al., 2018). Physically, it indicates how evenly the current lines are distributed in the area around the receiving electrodes or how uneven the soil is, and it is influenced by the array's design.

3.1.4. Electrode configuration

The electrodes placement used to assess electrical resistivity depends on where the potential and current electrodes are placed (Griffths and King, 1981). There are numerous electrode configurations that the resistivity method can uses. Wenner, pole-pole, and Schlumberger arrangements as well as the dipole-dipole, pole-dipole, gradient, and etc. are some of the examples. Most of them uses two current electrodes and two potential electrodes except Lee partition electrode arrangement which uses five electrodes (Aubert et al., 1984). The Schlumberger electrode spacing design was used in this work.

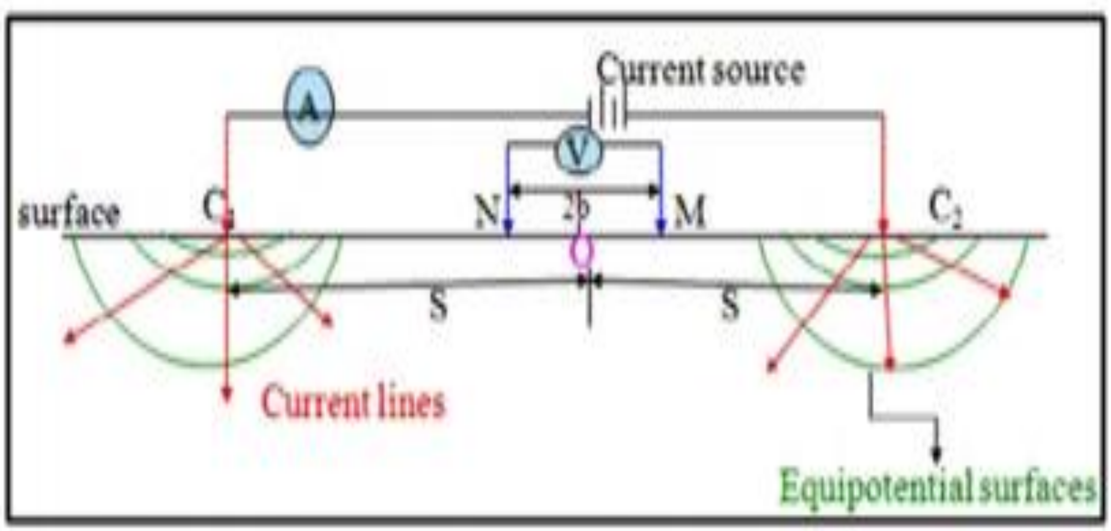

Figure 3. 4. Schlumberger electrode arrangement

As shown in (Fig 3.4) it is a symmetrical configuration are arranged symmetrically around the center by C1, N, M, and C2 lying in a straight line. For detecting changes in subsurface layer resistivity, Schlumberger approach was developed (Oladunjoye et al., 2019). To do this, current electrode spacing is symmetrically extended around the sounding point

(Abera, 2020). The technique is used to draw lines separating stacked media's horizontal horizons.

3.1.5. The resistivity of earth material

Electrical examinations often aim to detect liquid-saturated zones because the resistivity range is essentially a function of liquid content. The flow of charged ions in pore fluids mostly regulates the observed resistivity in earth material (Furi et al., 2011). The type and quantity of pore space-filling solutions and degree of fracture affect the resistivity of fractured rocks. Similarly, resistivity of the mineral grains that fill the structure of the rock influence the resistivity values (Reynolds, 1997). Rocks that have been fractured exhibit lower resistivity than their unaltered equivalents. For completely saturated rocks, resistivity varies approximately as the inverse square of porosity (Griffths and King, 1981), and the relationship between resistivity and porosity is explained by Archies' law:

$$\rho = a\rho w p^{-m} \qquad (3.31)$$

p is a parameter of porosity (it mostly depends on the porosity and structure of pore spaces), w is the resistivity of the water contained in the pore structure, and is the bulk resistivity of rock. For non-clayey formations, the Archie formula is

$$Rock\ resistivity = F \times water\ resistivity \qquad (3.32)$$

Where, F= formation factor= $\frac{a}{porosity(N)}$ (3.33)

The Variation in resistivity of typical rocks and sediments from about 1 ohm-m to over 10,000 ohm-m, so at least 4 orders of magnitude **Fig** (3.5).

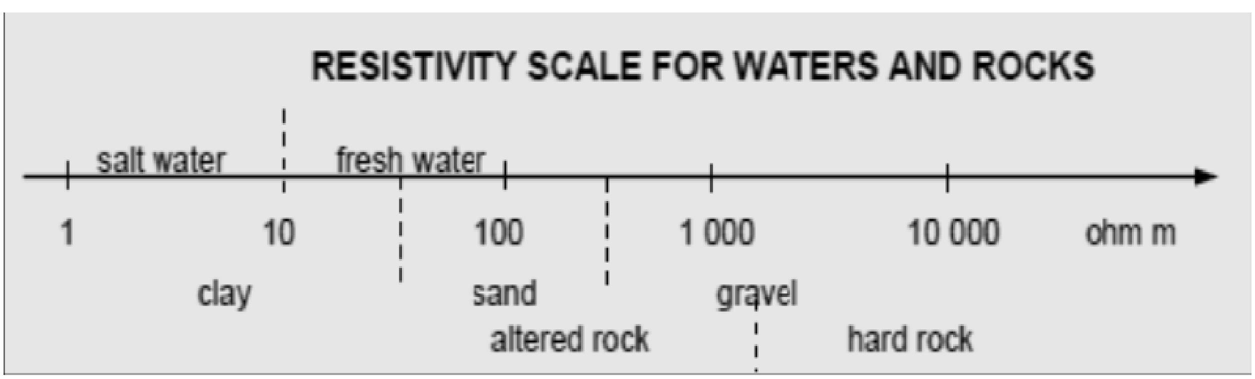

Figure 3. 5. Resistivity variation of Water and rock material

Water-bearing rocks become less resistant as the amount of water in their pores rises. To conduct electricity, the rock needs its pores to be connected and filled with water (Furi et al., 2011). The investigation of horizontal and vertical discontinuities in the electrical characteristics of the soil also employs the resistivity approach (Zohdy et al., 1974). A fundamental and diagnostic physical characteristic that may be assessed using a variety of methods is electrical resistance. It is quite helpful to employ many assessments of a single characteristic since some are more appropriate or desirable than others in particular circumstances (Reynolds, 1997).

3.2. Dar Zarrouk Parameter

The Dar Zarrouk parameters (DZP), defined by the longitudinal unit conductance in Ω^{-1} (C, layer thickness versus resistivity) and the transverse unit resistance in $\Omega \cdot m^2$ (R, layer thickness times resistivity), are two of the most important parameters in electrical prospecting (Utom, Odoh, & Okoro, 2012). As shown in (Fig. 3.6) equations (34) and (35) show that R stands for the electrical transverse resistance perpendicular to the soil layers and C for the conductance provided to current lines parallel to the soil layers. In porous aquifers, C and R are frequently related to K and T because they can indicate the aquifer's ability to defend itself from contamination and its transmissivity, respectively.

$$R = \rho h \tag{3.34}$$

$$\boldsymbol{C} = \frac{\boldsymbol{h}}{\boldsymbol{\rho}} \tag{3.35}$$

where h is the layer thickness in meters and q is ER of the layer in ohmmeters.

At each of the 16 VES locations, several metrics, including hydraulic conductivity, permeability, and coefficient of anisotropy, were determined in order to explain the hydraulic characteristics of the aquifers and the groundwater potential. Using the approach of, the aquifer's hydraulic conductivity and Transmissivity or permeability (Tr) were estimated (Heigold, 1979; Niwas, 1981) as shown in eqn 36 and 37 respectively.

$$K = 368.4\rho^{-0.93283} \tag{3.36}$$

$$T = Kh \tag{3.37}$$

While, ρ represents aquifer resistivity.

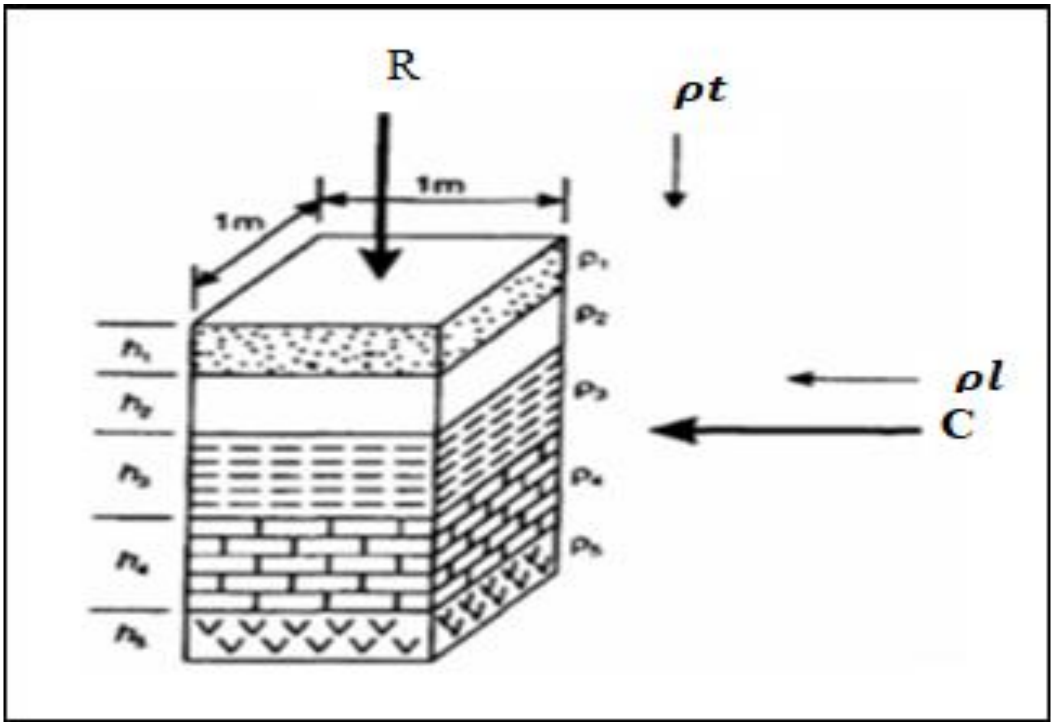

Figure 3. 6. 3D electro stratigraphic model with total longitudinal conductance (C) and transverse resistance (R)

Two fundamental properties are established for uniform, level, and equally diffusing stratum: its resistivity (ρ) and its thickness (h) for particular layer. Similarly, Other parameters such as C, R, ρ_l and anisotropy (λ) were calculated from the corresponding resistivities and thicknesses for the aquifer layer.

3.2.1. Longitudinal conductance (C)

The longitudinal unit conductance (C) is utilized to identify target regions with groundwater potential and characterize the salinity of aquifer. When considering groundwater potential, areas with high C values are typically those with a reasonably dense succession. It is suitable for assessing the groundwater flow potential in aquifers and estimating the hydraulic conductivity of subsurface materials.

3.2.2. Traverse Resistance (R)

It is a measurement of a geologic formation's electrical resistivity along the transverse section that is parallel to flow path of current. It is frequently employed to establish the width and depth of underlying strata as well as to identify geological features like faults and fractures. It organizes materials according to their various electrical properties. Low transverse unit resistivity materials like sand and gravel, which are more conductive (Henriet, 1976).

3.2.3. Longitudinal Resistivity ($\boldsymbol{\rho l}$)

With the help of series resistivity measurements, the ER of a geologic formation is calculated along the direction of current flow. It is also employed to differentiate between fresh, brackish, and salt water. The lithology, porosity and fluid content of geological formations can be revealed and this information is useful to identify, locate and classify aquifers, mineral deposits and hydrocarbon reserves. That is valuable for groundwater management, (Abiola & Enikanselu, 2009). It's calculated by the

$$\rho l = \frac{H}{C} \qquad (3.38)$$

Where, H is the depth of the layer below the aquifer.

3.2.4. Hydraulic conductivity(K)

The longitudinal conductivity and porosity of the subsurface are both factors that affect hydraulic conductivity, a measurement of how easily water can pass through a porous material. By measuring the conductivity of a geological formation, likely evaluation of hydraulic conductivity is possible, which is important for understanding the movement and availability of groundwater resources.

3.2.5. Transmissivity (T)

Transmissivity is the ability of materials to transfer groundwater horizontally at a specific hydraulic head. It is essential to groundwater analysis because it determines the flow rate of groundwater and the viability of extracting groundwater from an aquifer. Transmissivity, which is similar to hydraulic conductivity (K), controls groundwater flow inside an aquifer (Utom, Odoh, & Okoro, 2012). It is also a tool for groundwater management and modeling as it helps predict how groundwater will behave under different conditions. The ability of a substance to pass water through it, or its permeability, is a metric that characterizes an aquifer's hydraulic conductivity. It can be stated that regions with high transmittance values have a high potential of groundwater, and the materials used for aquifer construction are very permeable (Okonkwo & Ugwu, 2015).

3.2.6. Coefficient of Anisotropy ($\boldsymbol{\lambda}$)

The electrical conductivity or resistivity properties of a material is measured by the coefficient of anisotropy. When a geologic material exhibits an ideal orientation of its structural features, such as mineral grain or fracture, which affect the electrical properties, electrical conductivity or resistivity of the material can vary (Henriet, 1976). This may represent the direction of flow path along the research area. It is calculated by the ratio of maximum electrical resistivity to minimum electrical resistivity.

$$\boldsymbol{\lambda} = \sqrt{\frac{\boldsymbol{\rho t}}{\boldsymbol{\rho l}}} \qquad (3.39)$$

3.2.7. Aquifer protective capacity

The sum of longitudinal conductance (C) of overlying layer obtained from the VES were useful in examining the aquifers protective capacity. The longitudinal conductivity map was calculated from Equation 3.35 for all VES sites and used in the overburden protection capacity assessment. Because the ground acts as a natural filter for seeping liquids. Therefore, its ability to retain and filter seeping liquid from the ground surface is a measure of its protective capacity (Okonkwo & Ugwu, 2015). Similarly, (Abiola & Enikanselu, 2009) suggest that the underlying aquifers receive protection from materials with high longitudinal conductivity.

3.3. Magnetic method of prospecting

This type of geophysical investigation comprises determining the direction, gradient, and strength of the magnetic field as well as interpreting changes in these parameters throughout the survey area (Henkel & Guzmán, 1977). The liquid outer core of the Earth, which has a high concentration of iron, is thought to be the primary source of the magnetic field that surrounds the planet (Owono, 2018). Magnetic anomaly field measurements can be used to find structures. It measures the residual magnetic field associated with a geological formation or man-made item (Henkel & Guzmán, 1977).

The magnetic approach is widely utilized in engineering and geotechnical investigations for mapping subsurface structures, discontinuities, and weak zones (Tigistu H., 2014). The technique is frequently used for subsurface research to identify geological formations that could store groundwater in the studied area (Blakely, 1995). The variance in rock magnetization is used in magnetic surveys. Minor components, whose distribution might vary greatly and make them less indicative of the formation, are responsible for the magnetic characteristics of rocks (Griffths and king, 1981).

It is a passive geophysical method that assesses the strength of any anomalies produced by the Earth's magnetic field by examining the magnetic properties of deep rocks. (Kearey, 2002). It can be used for a variety of tasks, from modest engineering or archaeological investigations to extensive investigations of local geological systems to uncover concealed metallic remnants (Kearey, 2002).

At the magnetic equator, magnetic field strength is at a minimum of about 26,000 to 30,000, and it reaches a maximum of 65,000 to 70,000 towards the magnetic poles (Abera, 2020). The most common use of magnetic data in groundwater studies is to map the depth of magnetic bedrock. Finding of faults and geological connections requires the data interpretation to reflect variations in the local abundances of magnetization (Christensen & Sørensen, 1994).

Applications of magnetic methods include studying fault zones, minerals and geothermal areas, mapping buried utilities, and studying archaeological sites. Locating faults and geological connections makes use of data interpretation that takes into account variations in local abundances of magnetization (Blakely, 1995).

The lithological variations, differences in magnetized body thickness, faulting, folding, and topographical relief could all contribute to the magnetic anomalies (Owono, 2018). The aim of geophysics in groundwater resource mapping is not the groundwater itself, but rather the geological setting in which the water is found (Phillips, 2002). When two magnetic poles are separated by r, a force F develops between them with strengths m and M. The force pushes the poles away when they have the same polarity, and it attracts the poles together when they have the opposite polarity. The equation for F is the following.

$$F = \frac{mM}{4\pi\mu r^2} \qquad (3.40)$$

Where μ is the magnetic permeability; m and M are pole strengths and *r* are the separation distance between them. Local magnetic anomalies, are the result of disturbances caused mostly by variations in concentrations of ferromagnetic material in the vicinity of the magnetometer's sensor.

3.3.1. Principles and elementary theory

The starting point of the magnetic methods is based on the observation that a ferrous substance is exposed to an induced magnetic field when exposed to magnetic field of the earth (Blakely, 1995). At this point, the earth's field is superimposed by the induced field, resulting in a magnetic anomaly. The amount of magnetic material present and how close it is to the sensor affect detection (Milson J., 2003). The anomalies are normally presented as profiles or as contour maps (Abera A, 2020).

The magnetic intensity field, measured by a magnetic sensor above the earth's surface, is the sum of the magnetic fields generated by different sources. The magnetic approach detects abnormal fields that are caused by buried targets or geological features that are mineralized underground. Qualitative interpretations of magnetic anomaly indicate the existence or absence of subsurface geological features /buried targets and is converted to a constrained geological mode (Abera A, 2020).

3.3.2. Earth's magnetic field and susceptibility

The magnetic field of the earth is produced by the churning of liquid metals in the core, which also generates electric currents and a magnetic field. True north and magnetic north are not the same direction. The earth's rotating axis passes via the geographic North Pole, which is located 11.5 degrees distant from the magnetic North Pole. The Earth's core and its surrounding areas are where the majority of the geomagnetic field is generated. The three parameters declination, inclination, and total force vector can characterize the earth's magnetic field. Its direction changes at about every 200,000 years.

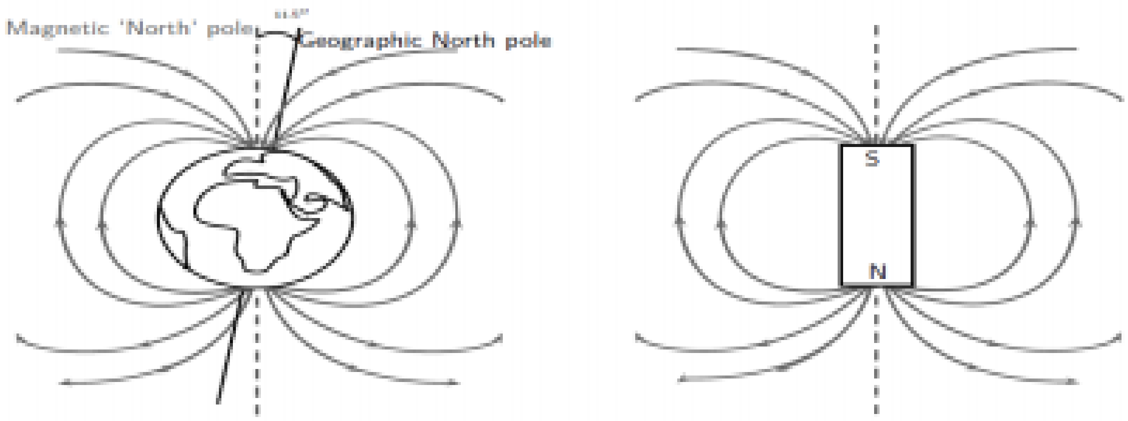

Figure 3. 7. magnetic direction of the earth

In addition to the mineralogical composition, other characteristics, such as the orientation and form of the magnetic particles spread throughout the rock, can be used to determine the susceptibility of the entire rock (Table 2). In general, since magnetite is oxidized to hematite, rock weathering lessens vulnerability. The typical rock weaknesses listed below can typically vary by an order of magnitude or more. A weak magnetic field is observed over the conductive zones, believed to be subterranean fractures. A basic description of their use can be found in (McCarthy, 2002). The magnetism of minerals that make rocks is connected to rock magnetism. Additionally, basement faults and zones of weakness that represent preferred fluid flow pathways were located using magnetic surveys (Aubert et al., 1984).

Table 3. 1. Susceptibility range of different rock materials

Materials	**Susceptibility**
Altered ultrabasic rock	$10^{-4} - 10^{-2}$
Basalt	$10^{-4} - 10^{-3}$
Gabbro	10^{-4}
Granite	$10^{-5} - 10^{-3}$
Andesite	10^{-4}
Rhyolite	$10^{-5} - 10^{-4}$
Shale, shiest and other	$10^{-3} - 10^{-4}$

Most sedimentary rock	$10^{-4} - 10^{-5}$
Limestone and chert	$10^{-6} - 10^{-5}$

3.3.3. Correction of Magnetic Data

Correcting the magnetic data is crucial to cancel out just those sources of magnetic anomalies resulting from the effects of the subsurface on the observations (Kearey et al., 2002). The difference between daily corrected observed value and the normal field (IGRF) gives the magnetic anomaly. The magnetic field varies with time and the necessary corrections must be made to determine anomaly due to various geological sources lying down to the depth where the temperature reaches the Curie point. Magnetic data correction include; -

3.3.3.1. Diurnal variation correction

Different strategies can be used to eliminate the impacts of daily changes. By repeatedly taking the base reading during the magnetic survey, this can be fixed. The readings at stations that are occupied during the day are distributed in accordance over the observed variances in the base readings. The base values are only used to correct for time-based fluctuations (Kearey et al., 2002). The raw data must be modified to exclude any anomaly source that aren't coming from underground magnetic sources because noise components are present in every magnetic data collection. The daily correction is the most important correction. It is easier to calculate the daily correction using the measured values of the base stations that were recorded over a measurement period.

$$\delta d = \left(\frac{BS2 - BS1}{T2 - T1}\right)(Ti - T1) \qquad (3.41)$$

Were, $\boldsymbol{\delta_d}$ = Diurnal correction

BS_1 reading of base station at first time

BS_2 =Reading of base station at second time

T_1 = Observation time of first base station

T_2 = Observation time of second base station

T_i = Observation time of each measurement

The data must be adjusted to account for the impact of latitude and longitude, in order to attain anomalies. The rise in intensity with latitude must be taken into account because the earth's magnetic field intensity varies from 25000nT at equator to 69000nT at the poles (Reynolds, 1997).

3.3.3.2. Geomagnetic correction

An impact of the geomagnetic reference field on the survey data is removed by the geomagnetic adjustment. Survey data at any specific area can be fixed by deducting the theoretical value, obtained from IGRF, from the actual value (B_{ob}). As a result, TMA (ΔB), which is produced by removing the diurnal correction (δB_D) and IGRF correction (B_{th}) is given by

$$\Delta B = BT - \delta BD - Bth \qquad (3.42)$$

where B_T is the total field, is diurnal correction δB_D and B_{th} is IGRF correction.

3.3.4. Qualitative interpretations

Magnetic data were interpreted qualitatively depending on the magnetic anomaly, analytic signal, directional derivatives, vertical derivative and etc.

3.3.4.1. Total magnetic field anomaly

The TMA give evidence on the subsurface geology of the surveyed area. This is because several rock types having different magnetic properties, which can affect magnetic field intensity at the Earth's surface. Geological features such as faults, folds, and regions with a high mineral content can be mapped using this information. It contains the combined impacts of deep-seated, long-wavelength source effects as well as shallow depth, short wavelength source effects.

3.3.4.2. Reduction to equator

According to (Oni et al., 2020) separation of magnetic anomalies from their underlying causes at low and high magnetic latitudes are challenging. Reduction of magnetic anomaly to the equator converts all vertical components in a field into horizontal lines by eliminating the tilt effect from the data. The Earth's magnetic field and the magnetization of the magnetic sources are made to seem horizontal by using this technique at low latitudes and it aligns the top center of magnetic anomalies over their sources. Furthermore, it is used to eliminate the asymmetry of the anomaly caused by non-zero magnetic tilt. This makes it easier to interpret the data, especially with regard to the destination. In addition, it is important to call off the effects of a strong residual component and greatly improves the anomaly pattern's consistency with known geology (Hayatudeen, 2021).

3.3.4.3. First order Vertical derivative

FVDR improves resolution of both lineament and anomalies due to its short wavelength. Edge detection and source depth estimation are two examples of contemporary first vertical derivative applications (Yusuf, 2022). The first order VDR often has a zero over the edge, positive over the source, and is negative outside of a vertical sided source.

The filter operator is what makes minor feature-induced anomalies more prominent while suppressing longer-wavelength regional trends. This means that VDR is particularly effective at detecting smaller area size anomalies, but may lose the ability to detect deeper anomalies in favor of near-surface sources. It emphasizes the short-wavelength features of the anomaly field while reducing the emphasis on the long-wavelength features or enhance the lineament and anomaly due to their short-wavelength character and attenuate the long wave length components (Hayatudeen et al., 2021).

VDR was calculated as

$$VDR = \sqrt{\frac{\partial \Delta \boldsymbol{B}}{\partial x}} \qquad (3.43)$$

The high slopes occur along the edge of the horst while highest value occurs directly over the top part of the sources.

3.3.4.4. Total horizontal derivative

THDR provide more details on the differences in the general magnetic field's directions. It displays anomalous textures and emphasize discontinuities in anomalous patterns (Oni et al, 2020). If the local magnetic field and source magnetizations, among other things, are vertical, then this function has peaks above the source for the thin dyke and at edges for the thick dyke (Phillips, 2002). The isolated edges of horizontal plate-shaped magnetic entities or the peaks of isolated vertical contacts from the reduced to equator magnetic field can be precisely located using this method. THDR of anomaly field is calculated by

$$THDR(x, y) = \sqrt{\left(\frac{\partial \Delta B}{\partial x}\right)^2 + \left(\frac{\partial \Delta B}{\partial y}\right)^2} \qquad (3.44)$$

Where, THDR is total horizontal derivative, $\frac{\partial \Delta B}{\partial x}$ is X_ directed horizontal derivative, $\frac{\partial \Delta B}{\partial y}$ is Y_ directed horizontal derivative, and ΔB is total magnetic anomaly grid.

According to (Christensen & Dransfield, 2002) the X-directed horizontal derivative is filter that suppresses the East west (E - W) oriented anomalies while enhancing the N -S oriented anomalies generated by shallow sources. Similarly, Y-directed horizontal derivative suppresses N – S and enhancing the E -W oriented anomaly. It offers further insights into directional variations of the complete magnetic field.

According to (Mamo, 2010) it is possible to extract relevant details from magnetic data before modelling it using various data enhancement/filtering approaches. We can find near surface discontinuities using horizontal derivative (HDR).

3.3.4.5. Analytic signal (AS)

AS is a mathematical technique that extracts the amplitude and phase information from the original magnetic data. It is filtering technique which generates maximum amplitude directly over discrete bodies or magnetized geologic bodies in contact which implies that horizontal locations and depths of magnetic contacts is simply determined (Nabinghan, 1972). This technique highlights shallow sources including the edges and boundaries of magnetic anomalies (Rajagopalan, 2003) and but not the dip information. The AS is commonly used in magnetic interpretation to locate the anomalies directly over their sources.

According to (Mono, et al., 2018) regardless of their geomagnetic latitude or geologic dip, the analytical signal applied to the TMA produces good horizontal sites of contact. The amplitude of AS is essentially fully independent of the magnetization direction when the sources are vertical. One advantage of the analytical signal is the ability to locate sources in both the horizontal and vertical planes (Owono, 2018). It reveals high analytic signal values that depict magnetic anomalies results from various of anomalous bodies in vertical and horizontal contact (Abera A, 2020).

Mathematically its calculated by

$$AS = \sqrt{\left(\frac{\partial \Delta M}{\partial x}\right)^2 + \left(\frac{\partial \Delta M}{\partial Y}\right)^2 + \left(\frac{\partial \Delta M}{\partial z}\right)^2} \qquad (3.45)$$

Where AS is amplitude of analytic signal and $\Delta M$is observed total magnetic anomaly.

Analytic signal is considered for the investigation of subsurface anomalous geologic sources occurring at shallow depths. The analytical signal maximizes over the edge of the magnetic structures in general. The centers of two-dimensional structural features and the boundaries of lithological units were identified using this map.

3.3.4.6. Tilt derivative

Mono, et al., (2018) introduces that tilt derivation is used to map shallow bedrock structures. A common application of slope filter is for feature and causal body edge recognition in potential field images. While negative values are farther away from the sources, positive ones are directly above them. Peaks in the slope derivative tend to coincide with the local peaks in the original input grid. The original omnidirectional dip derivation highlights local anomalies, including those of low amplitude. For the purpose of enhancing features and detecting causal body, the tilt filter has also grown in popularity (Owono et al., 2018).

The tilt derivative of magnetic anomaly is calculated by

$$TDR = \tan^{-1}\left(\frac{VDR}{THDR}\right)$$

which is similar to

$$TDR = \tan^{-1}\left(\frac{VDR}{\sqrt{\left(\frac{\partial \Delta B}{\partial x}\right)^2 + \left(\frac{\partial \Delta B}{\partial y}\right)^2}}\right) \qquad (3.46)$$

Were; TDR= tilt derivative, VDR=vertical derivative, THDR= total horizontal derivative.

The TDR map shows geological features, such as faults, represented as magnetic lines. The zero-contour line of the TDR_TMI-RTE map is believed to be where magnetic susceptibilities abruptly shift between high and low anomalies, particularly in the sharp gradient (Owono et al., 2018). According to (Miller & Singh, 1994) by concentrating on the tilt derivative's vertical to horizontal derivative ratio, which will be mostly unaffected by the depth of the source, should resolve the effect of the depth for both shallow and deep sources in the tilt angle derivative enhancement technique.

This function is very helpful for highlighting structural trends and features in magnetic grids, and it is non-directional in the sense that it performs well on trends and anomalies with all geometries and spatial orientations (Stewart & Miller, 2018).

Chapter Four

4. Data Acquisition and processing

The current study was conducted to map the subsurface stratigraphic units and geological structures and characterize the groundwater aquifers of research area using geophysical methods, namely ER and magnetic technique. The transverse used for the geophysical investigations were shown clearly in Figure 4.1.

4.1. VES Data acquisition and instrumentation

4.1.1. Data Acquisition

The VES survey was conducted within the area along three approximately north East-southwest oriented transect and observations were made at sounding point intervals of 2 to 4 km. A total of 16 VES points were collected using Schlumberger array, with a maximum half- electrode spacing (AB/2) of 500 m. To give control during interpretation, few VES points were placed next to boreholes. VES observation points were mostly spaced 3 km apart along the profiles. However, due to site conditions, station spacing is varies by 0.8-1.3 km along the line at some points, and stations are sometimes relocated from the transect lines to find a suitable survey site.

The instrument used for VES is the earth resistivity meter. In the field, the apparent resistivity was recorded at various electrode spacing. By simultaneously plotting and reviewing the VES data in the field, data quality was managed. This was followed by data analysis using a range of software programs including IPI2Win, Surfer and Win Resist to interpret and present the VES data in various forms.

4.1.2. VES data Processing

The electrode spacing (AB/2) is shown on the abscissa and resistivity value is shown on the ordinate when processing the gathered data. In order to achieve a relatively substantial increment in the depth of penetration the current electrode spacing (AB/2) gradually increased for the resistivity measurements, but the potential electrode gap (MN) was not. This allowed the effect to be measured and corrections to be made to give a single smooth curve, which was computed using IP2WIN and then the WIN RESIST software were used to produce the curve (Velpen, 1995).

4.1.3. VES data Presentation

Both qualitative and quantitative methods were used to label the field data. The form of the field curve is carefully analyzed to ascertain the number and resistivity of the layers when evaluating data qualitatively. Results from this interpretation method comprised geo-electrical pseudo-sections and layers of resistivity maps. The IP2WIN software were used to evaluate the on-site VES data and establish the preliminary model parameters of potential strata. These parameters, determined using the IP2WIN software, have been organized using the lithological units of prevailing boreholes and analyzed to be used as the first model in the RESIST inversion software, resulting in layers' electrical properties that are reliable and have tolerable error levels of between 1.5 and 5.0%.

Using the Surfer 16 software, the geo-electrical parameter, or actual resistivity and layer thickness, were derived in the quantitative interpretation. The stacked strata map shows the lateral variation in resistivity at a specific depth for various values of AB/2. In relation to the current electrode spacing, these maps display the distribution of resistivity in the local area. The Schlumberger method's maximum penetration depth ranges from 1/4 to 1/3 of the maximum distance between current electrodes (Frohlich et al., 1996). The resistivity distribution versus electrode spacing values is qualitatively reflected by pseudo-section (AB/2). Similarly, geo-electric sections generally represent the distribution of bed resistivities and thicknesses which are intended to provide a more accurate approximation of the actual subsurface geo-electric situation. In practice, most quantitative interpretations depend from these. The final model parameters are obtained by the inversion software RESIST to produce geo-electric sections. The pseudo depth and geo-electric intervals of all profiles are shown in next chapter accordingly.

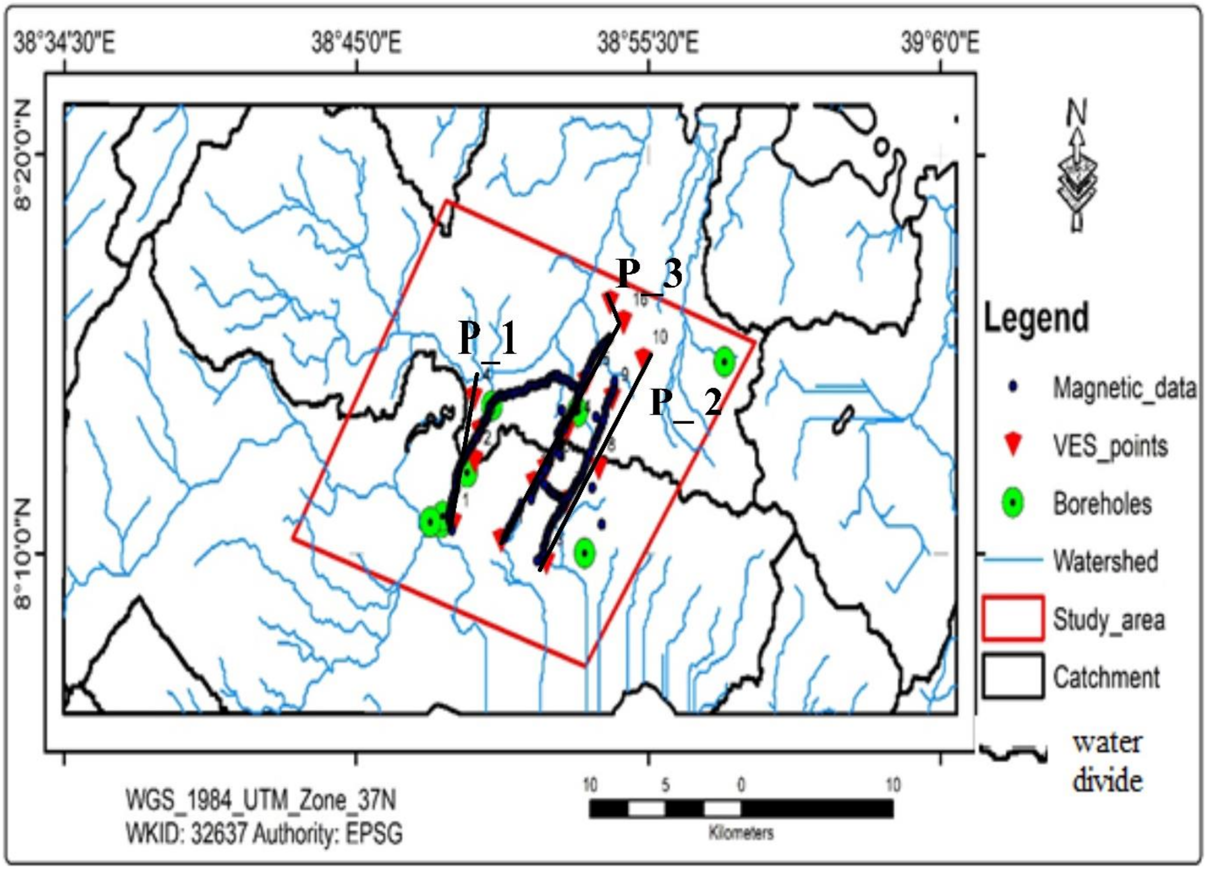

Figure 4. 1. Location map of Electrical survey profiles, boreholes and magnetic data.

4.2. Magnetic data acquisition

The Proton Precession Magnetometer -600 was used to conduct the magnetic survey; it is a convenient and reliable tool for this work. The time of measurement and location were recorded with a handheld GPS. This kind of magnetometer measures the entire magnetic strength of the earth at a certain observation point with a manufacturer-specified accuracy of one gamma and

Complete magnetic field survey was carried out along the VES lines and observations were taken at every 150 m. A total of 225 data points were collected with transect spacing similar to VES, with transect distance varying between 2 km to 3.4 km. During the data collection total magnetic field intensity, time, date, and location of the data points were all noted. The profiles were roughly oriented northeast-southwest to explore relationship between surface watershed and possible subsurface structures that could also function as a subsurface watershed. Only a small portion of this magnetic data was gathered close to previously drilled boreholes.

Data quality was kept under control by averaging all three measurements at each station and Base station readings taken throughout the magnetic survey was used to correct for diurnal variation. In addition, data was collected from early morning to 12:30 p.m. to minimize the influence of daily fluctuations.

4.2.1. Data Reduction and processing

4.2.1.1. Magnetic data reduction

It is a set of procedures used to eliminate data signals and noise that are unrelated to the site's geology. which prepares dataset for clarification by condensing the data to only include the signals necessary for the purpose. Below is a list of these actions:

i. **Data checking and editing: -** entails cleaning up erratic noise and spikes in the data that is generated by high tension power line and wind.
ii. **Diurnal removal: -** removes the base magnetometer's time-synchronized signal from the survey data to account for the Earth's main field's temporal variance. A diurnal correction formula, which is given in eqn (3.34) was used to calculate the diurnal corrections to the reported total magnetic field strength at all of the observation stations.
iii. **IGRF removal: -** It removes the main field of the earth's strong effect. To do this, a primary field calculated with Oasis Montaj was subtracted from the daily corrected survey data.

The TMA map generated using the continuation filtering methods used in Oasis Montaj was used for the basis for majority of the subsequent processing and enhancements. The magnetic data distribution was along three different lines as shown on (**fig**.4.1).

The regional anomaly map (Fig.5.19), the residual anomaly map (Fig.5.20), and the TMA map (Fig.5.18) were produced from using the constructed TMA map.

4.2.2. Magnetic Data Processing

A number of approaches, including the residual map, analytical signal, VDR, horizontal derivative, TDR of the total magnetic anomaly map, RTE, 3D Euler deconvolution, upward continuation map at 1000 m to a depth of 500 m and 2D modelling were used to process the total intensity map. The TMA map (Fig. 5.18) represents the sum of the effects of shallow depth, short wavelength and deep-seated, long-wavelength source effects. The methods used in the magnetic data processing phases were used to perform additional filtering approaches and enhancements after separating the regional from the residual magnetic anomalies.

4.2.3. Magnetic data presentation

Magnetic anomaly totals have been produced as after removing the effects of core field (IGRF) and diurnal changes (daily correction) from the measured (observed) magnetic intensity anomaly totals. Using Geosoft Oasis Montaj (V 7.0.1), the IGRF-corrected anomaly values were utilized as the final and baseline anomaly values to create the IGRF-corrected anomaly map. Which served as the foundation for subsequent adjustments, filtering, and interpretation.

The magnetic maps that have been analyzed are used for qualitative and quantitative interpretations. The aim of the qualitative interpretation of the produced magnetic maps is to get a clear overview of the underground structures and estimating the relative locations of the magnetic anomaly sources. However, quantitative interpretation was employed to estimate the depth of the examined area's fractures, contacts, and shallow subsurface structures. This interpretation technique uses 2D magnetic modelling and 3D Euler deconvolution. The particular computer software utilized for the analysis and processing was Oasis Montaj V.7.0.1. Each stage of magnetic data processing is illustrated in the next chapter. The variation in overall magnetic anomaly indicates the presence of prominent anomalous features or contacts along the anomaly. The presentation of magnetic data can take the form of profile or contour maps. Magnetic profile and contour map shows the anomaly of the magnetic data.

Chapter Five

5. Result and Discussion

5.1. Introduction

The results of the resistivity measurement were presented in this chapter as an interpreted VES curve, slice stack map, pseudo depth map, and geo-electric slices for quantitative interpretations. All data, except slice stack map for VES and magnetic maps, are shown and discussed per profile. Only drill hole data from holes nearby the research area were used to interpret geophysical data, particularly electrical resistivity data. It was applied in the investigation of the aquifer system and helps to clearly interpretate the data geologically.

The borehole data helps to correlate the lithological section with the various resistivity units of the geo-electric section. For qualitative and quantitative assessments, the findings of the magnetic survey are shown in a number of maps, including total anomaly, analytical signal, TDR, total horizontal, first vertical, RTE map and etc.

5.2. Interpretation and Discussion of VES

5.2.1. 1D modeling of VES data

The initial model parameters which are subsequently put into the inversion software (RESIST) were determined using IP2Win. The Win Resist software works through utilizing input models, comparing the field data to the model, and iteratively determining which match is most accurate. The % RMS error shown by the software indicates a satisfactory match between model and field data quality. The current data has an RMS error of 1.2 to 2.5%. Fig. 5:1 shows interpreted VES curves, each of the curve is selected from survey transverse. Five to seven subsurface strata are found in those three sounding curves (using the AB/2 of 500 m for the survey). The rest of the interpreted VES curves listed in the appendix.

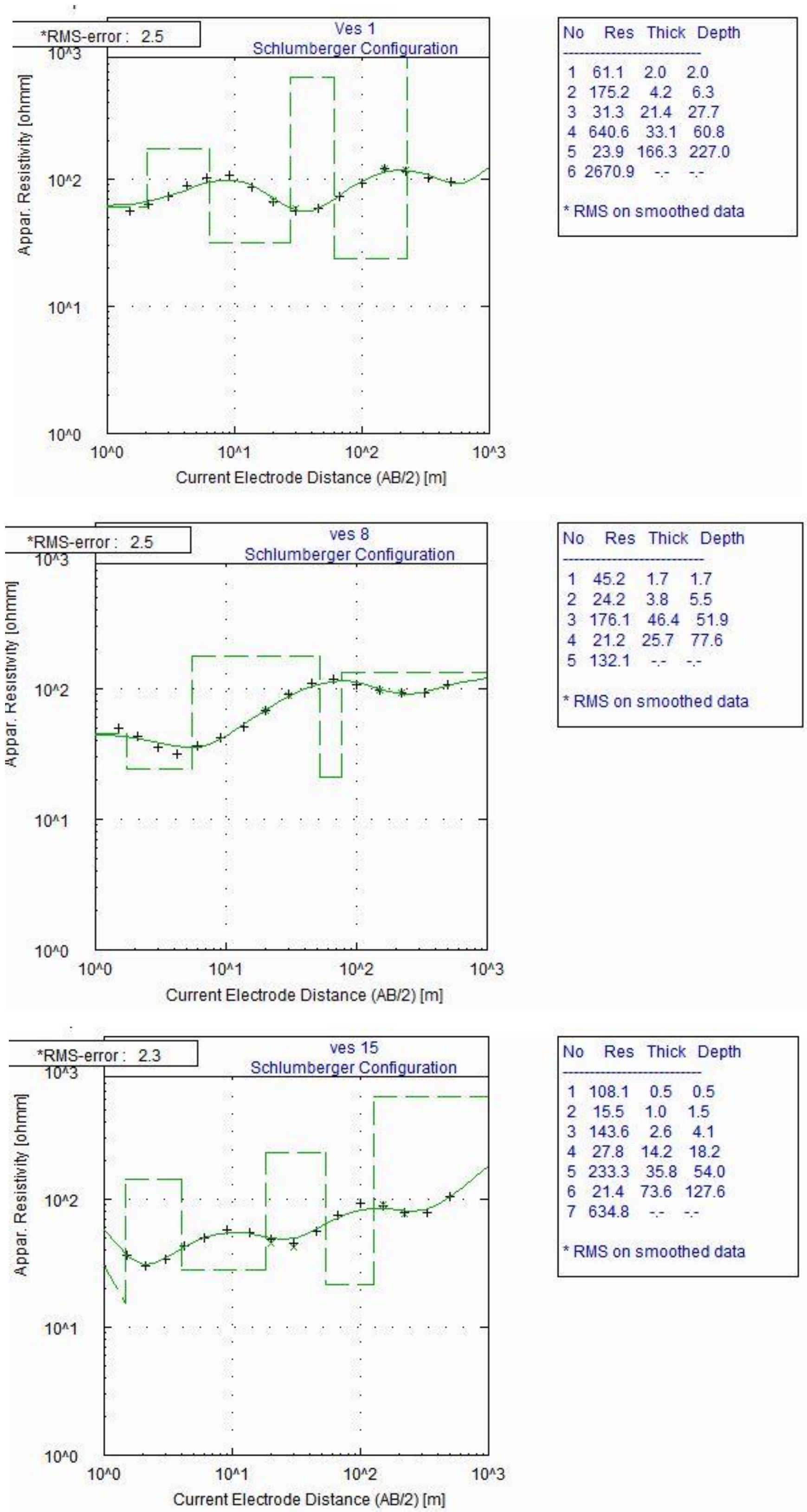

Figure 5. 1. Interpreted VES curves of the three sounding points.

Table 5. 1. the curve nature and type of all VES data

VES station	Curve nature	Curve type
VES 1	$\rho1 < \rho2 > \rho3 < \rho4 > \rho5 < \rho6$	KHKH
VES 2	$\rho1 > \rho2 < \rho3 > \rho4 < \rho5 > \rho6$	HKHK
VES 3	$\rho1 > \rho2 < \rho3 > \rho4 < \rho5 > \rho6$	HKHK
VES 4	$\rho1 < \rho2 > \rho3 < \rho4 > \rho5 < \rho6$	KHKH
VES 5	$\rho1 < \rho2 > \rho3 < \rho4 > \rho5 < \rho6$	KHKH
VES 6	$\rho1 < \rho2 > \rho3 < \rho4 > \rho5 < \rho6$	KHKH
VES 7	$\rho1 < \rho2 > \rho3 < \rho4 > \rho5 < \rho6$	KHKH
VES 8	$\rho1 > \rho2 < \rho3 > \rho4 < \rho5$	HKH
VES 9	$\rho1 > \rho2 < \rho3 > \rho4 < \rho5$	HKH
VES 10	$\rho1 < \rho2 < \rho3 > \rho4 > \rho5 < \rho6$	AKQH
VES 11	$\rho1 < \rho2 > \rho3 < \rho4 > \rho5 < \rho6$	KHKH
VES 12	$\rho1 > \rho2 < \rho3 > \rho4 < \rho5 > \rho6 < \rho7$	HKHKH
VES 13	$\rho1 < \rho2 > \rho3 < \rho4 > \rho5 < \rho6$	KHKH
VES 14	$\rho1 < \rho2 > \rho3 < \rho4 > \rho5 < \rho6$	KHKH
VES 15	$\rho1 > \rho2 < \rho3 > \rho4 < \rho5 > \rho6 < \rho7$	HKHKH
VES 16	$\rho1 > \rho2 < \rho3 > \rho4 < \rho5 > \rho6 < \rho7$	HKHKH

5.2.2. Sliced stacked section

The apparent resistivity slice stack map shown in Fig: 5-2 was generated for listed AB/2 values of 1.5, 20, 66, 100, 220, and 500. Properties of geological media are assessed qualitatively using all VES points. The evenly spaced sounding stations are intended to provide a good picture of the terrain. The lateral differences in resistivity at various depths are reflected in slice stack maps. Low resistivity zone (<120m) which occupies most part of investigation area is the most prominent feature of this section. With increased investigational depth, the area of high apparent resistivity shrinks. Another important feature is the northeast-southwest trend that exists between the high resistivity in the east and southeast and the low resistances in the west and northwest. This trend may be related to faulting.

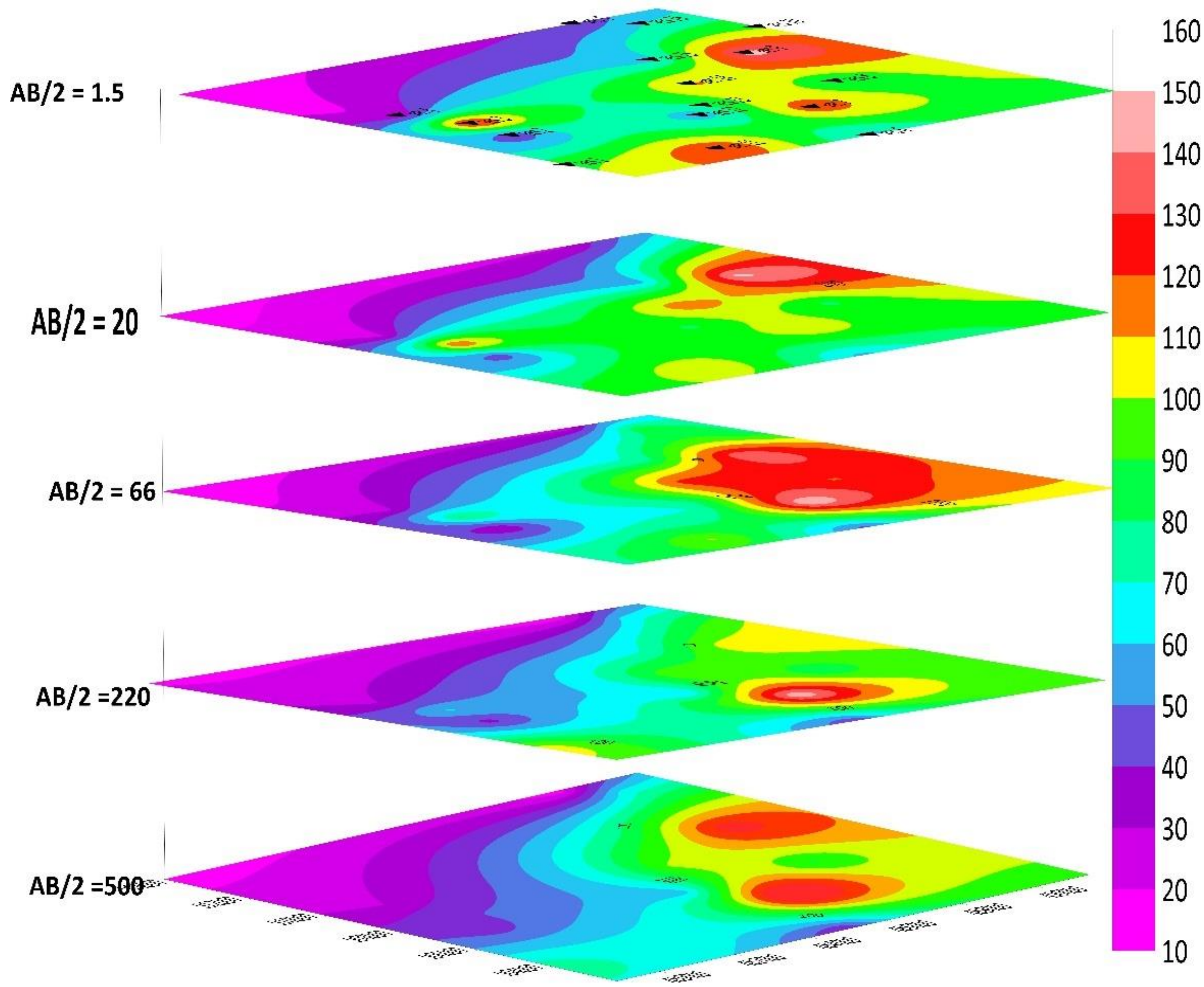

Figure 5. 2. Sliced stacked apparent resistivity plot

5.2.3. Pseudo depth and Geo-electric section

Pseudo-sections were constructed from the VES data along survey lines to recognize distribution of different resistivity values both horizontally and vertically. The pseudo-section was produced using the surfer 16. A preliminary suggestion for identifying a high groundwater potential is provided by the qualitative interpretation of the pseudo-section. Geo-electric sections were constructed using the concluding result of 1D inversion of VES data along all survey lines. To identify the relative resistivity changes used in the construction of these geo-electric intervals, the pseudo-depth intervals along the survey lines were investigated.

5.2.3.1.Profile One

Pseudo depth section

Fig. 5-3 demonstrates the produced pseudo-depth section for VES-1, 2, 3, and 4, which are located on profile one. Lateral resistivity variation is observed between VES 1 and 4. Compared to the other the uppermost portion of VES-3 on the map shows clear center zones exhibiting high resistivity. But all the other VES shows low resistivity top layer. Similarly, there is high resistivity zone exists below VES 1. To generalize the vast region across the profile shows wide coverage of the medium resistivity zone.

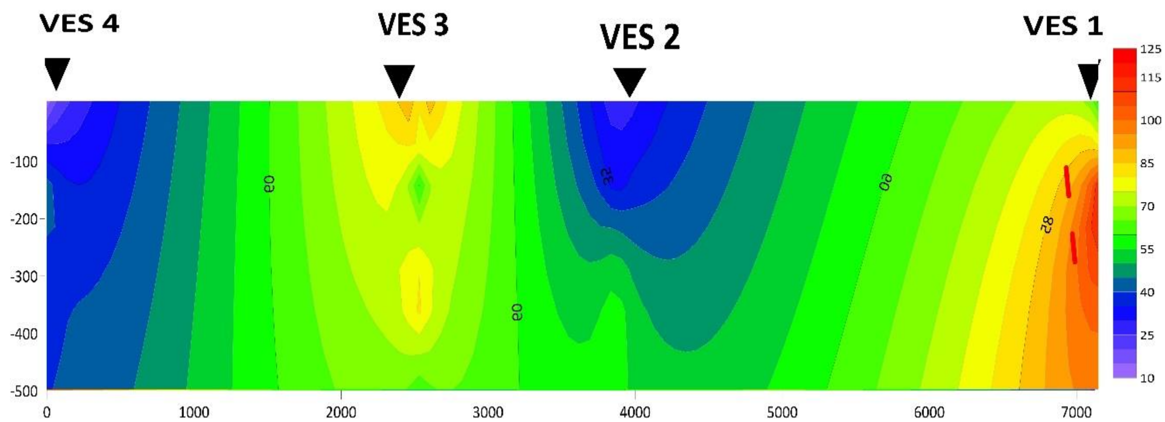

Figure 5.3. Pseudo depth section of first transverse

Geo-electric section

Geoelectric section was produced using the 1D inversion of VES data along the lines. The distribution or arrangement of sub surface layer in vertical dimension was identified using this information. Different elements like grain size, material type, and the degree of fracturing beneath the measuring point are credited for the variation in resistivity results. This profile contains four VES points oriented nearly in the NE –SW direction. As indicated in Fig. 5.4, the near-surface geoelectric layer has a resistivity range between 13.3 and 120 ohm-m and this layer is interpreted as topsoil. The thickness of this layer is from 1.3 to 2.4 m. Resistivity values of the second layer ranges between 10.5 – 37.9 ohm-m and a thickness range of 2.8 – 5.6 m. This layer is interpreted top clay soil mixed with sand or sandy clay material. Third layer of the profile is interpreted as pumice material with resistivity variation of 117 to 538 ohm-m. the thickness of this layer is 3 to 7 m.

The fourth layer with resistivity variation between 5.9 and 31ohm-m and with a thickness of 9 to 27 m. This layer is interpreted as Alluvial deposit, and clay material. Due to its thick layer and low to medium resistivity range, the layer is interpreted as a saturated zone and a probable perched aquifer zone. The fifth layer of the profile has lithologic units with resistivity values of 173 to 500, and 640 Ohm-m respectively. Lithology of this layer may be represented by, pumice and mixture of pumice with massive Ignimbrite and also it may be Rhyolite due its high resistivity range respectively. Below VES 1 high resistivity values is observed which may be result of the mixture of pumice with rhyolite. This layer has thickness range of 33 to 76 m beneath the overburden layers.

Layer six is indicated by lightly weathered and heavily fractured or weathered ignimbrite and sand (alluvial deposit) deposits. Due to its thick stratum and low resistivity range, the stratum is interpreted as a low resistivity zone with a resistivity range of 3.2 to 47 ohm-m, and this stratum is also interpreted as a heavily fractured and weathered ignimbrite and alluvial deposit. Compared to the layer above, it is a saturated zone and a probable aquifer zone. This horizon has a low resistivity portion with a larger thickness. Therefore, structures with such resistivity and large thickness could be considered zones of good groundwater potential. This layer is probably the main aquifer zone (MoWIE, 2015). The last layer which is found only beneath the VES 2 and 4 is interpreted as high resistivity zone with resistivity value of about 1805 to 2670 Ohm-m which is interpreted as fresh ignimbrite.

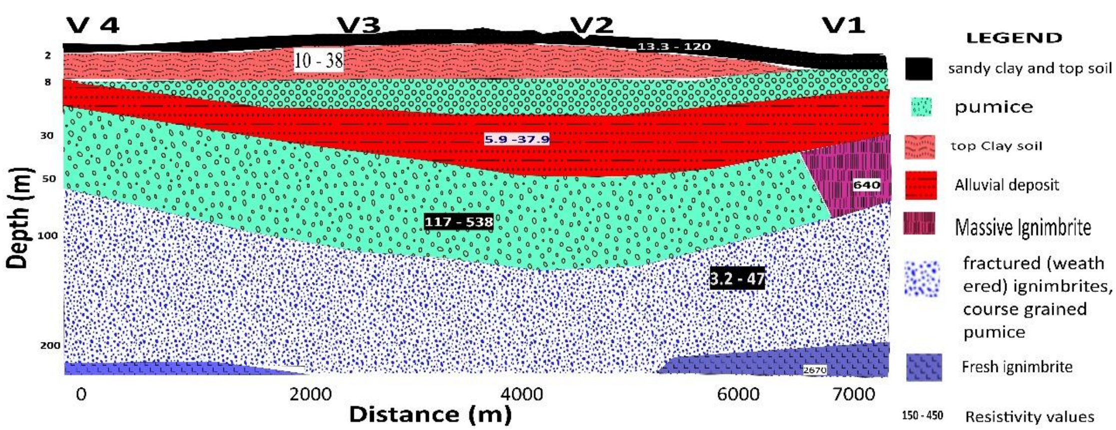

Figure 5. 4. Geoelectric section of first transverse

The comparison of the VES result with the closest borehole data of the Meki area is shown in Fig 5.5.

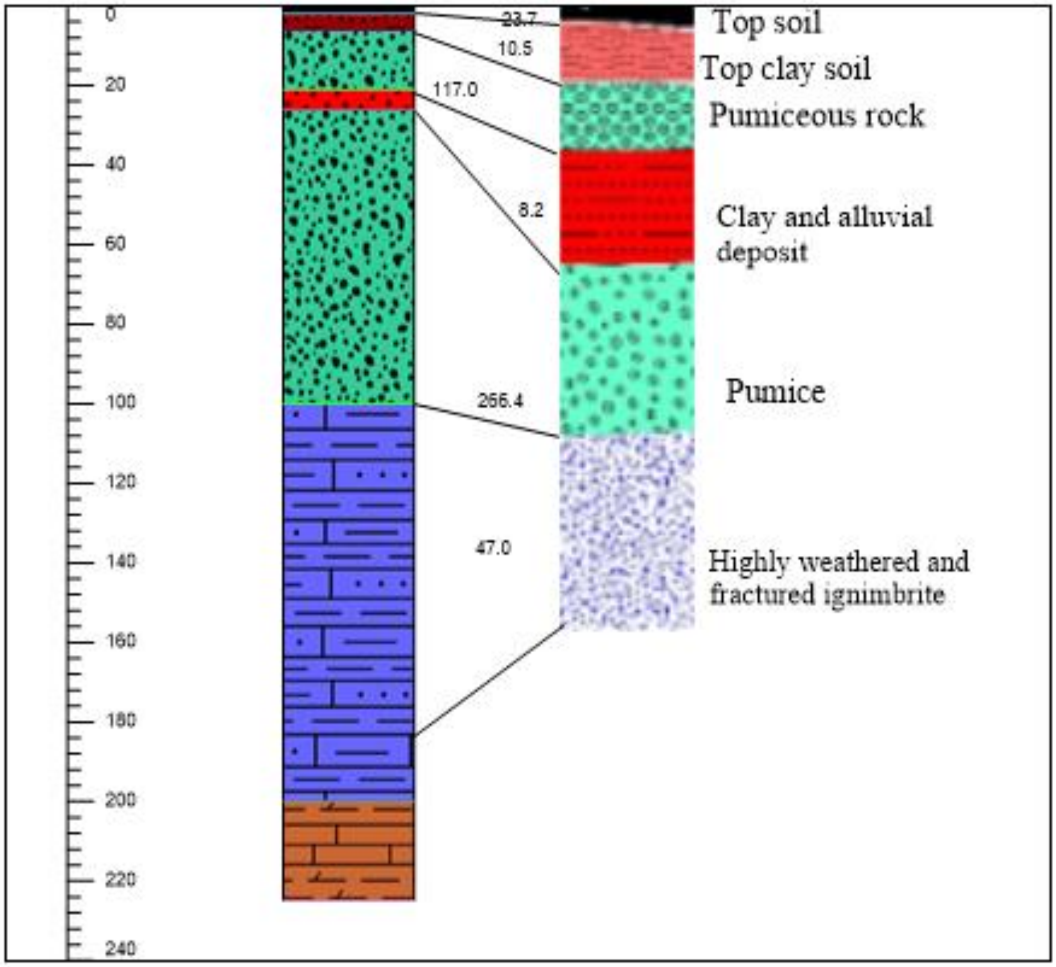

Figure 5. 5. VES 2 and lithology log at Sera Wakele Borehole

5.2.3.2. Profile two

Pseudo depth

Along the profile two Pseudo depth is constructed using VES 6 to VES 10 that lies on the survey line. As shown in Fig. 5.6 low resistivity zone was observed at the shallow to a deep below VES 6, and middle depth 8 respectively. But, only at shallow depth below VES10, this implies the area is expected as groundwater saturated zone. The high resistivity zone is observed at large depth below VES-7 to VES 9. A significant portion of the VES 7 and 10's has medium resistivity, with values ranging from 85 to 135 Ohms. A low to moderate resistivity zone dominates the vast area beneath the section, indicating prominent coverage across the area.

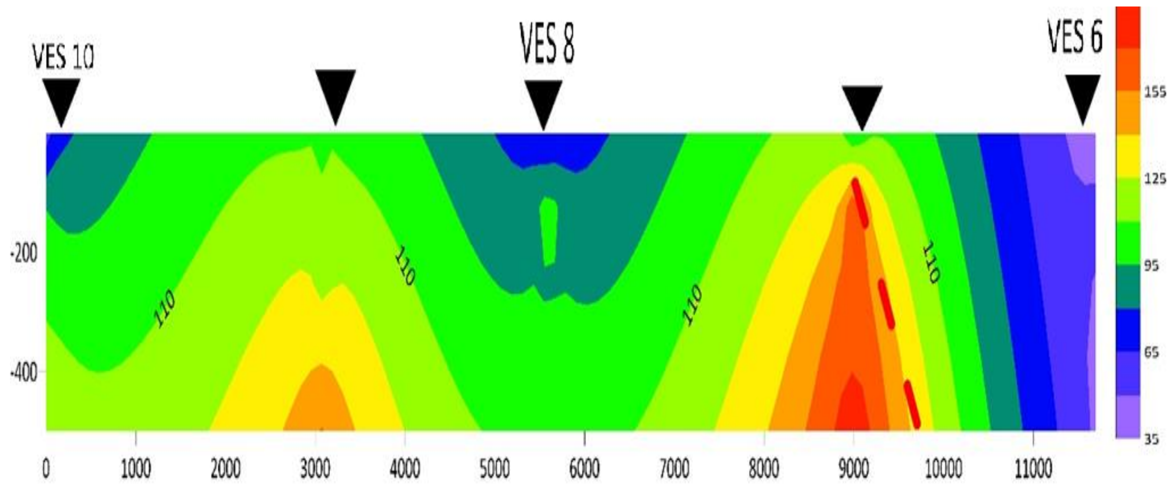

Figure 5. 6. Pseudo depth section along profile two

Geoelectric section

Figure 5-7 illustrates the geo-electric section that has been constructed from interpreted curves derived from five Vertical Electrical Sounding (VES) points located along this traverse. Prescence of Tuchi Sumeya borehole (MoWIE, 2015) near profile-2, specifically in close proximity to VES-7 and VES-8, was utilized to further constrain the depth and facilitate the identification of lithological units beneath these VES points during the modeling phase. The uppermost geoelectric layer, characterized by resistivity ranging from approximately 39 to 95 Ohm-m, exhibits a thickness variation of 1.5 to 2.2 meters. This layer is likely attributed to the topsoil. The second geo-electric layer manifests two distinct regions of resistivity value ranging from 24 – 53.3 and 87 to 141 Ohm-m respectively. This layer likely reflects pumice below VES 6 and 7, and alluvial deposit and clay soil beneath the other sounding points. The range of thicknesses is 1.6–4.8 and 5.3–5.6 m, respectively. The third geo-electric layer is also combination of two different lithological unit which manifests resistivity value of 131 – 209 Ohm-m with a thickness of 14 to 46.5, and resistivity value of 26.8-53.30 Ohm-m with thickness varying from 20 to 30m below the VES 6 and 7. This may be understood as sandy clay soil, and mixture of pumice and fine sand respectively.

The fourth layer of VES 6, and VES 7, corresponds with the third layer below VES 8, 9, 10. It has the resistivity range of 141.9 to 495 Ohm-m which may represent the pumice mixed with fine sand. The thickness of this layer ranges between 34 and 38.6 m. Similar to the fourth layer, fifth layer of the VES 6, and 7 is related with the fourth layer of VES 8, 9, and 10. It has two prominent lithology along this profile. The resistivity range of this layer is between 21 and 50.3 Ohm-m. The thickness of these layer is 60 -114.4 m at the western side of Derba query site, and 15.7 – 54m from Derba to Jerme Bora. These layers were interpreted as highly fractured and weathered ignimbrite and alluvial deposit. This a low resistivity horizon with a large thickness which is the result of groundwater saturation in the study area (MoWIE, 2015).

The last layer of VES 6 to 9 of profile survey possesses resistivity values varying from 80–299 Ω-m. which is interpreted as un-fractured ignimbrite mixed with pumice. Beneath the VES 10 there is other aquifer layer with resistivity value 35.3 and depths extends from 250m. this may represent highly fractured and weathered ignimbrite. The large thickness of these aquifer is may be indication of the amount of water potential.

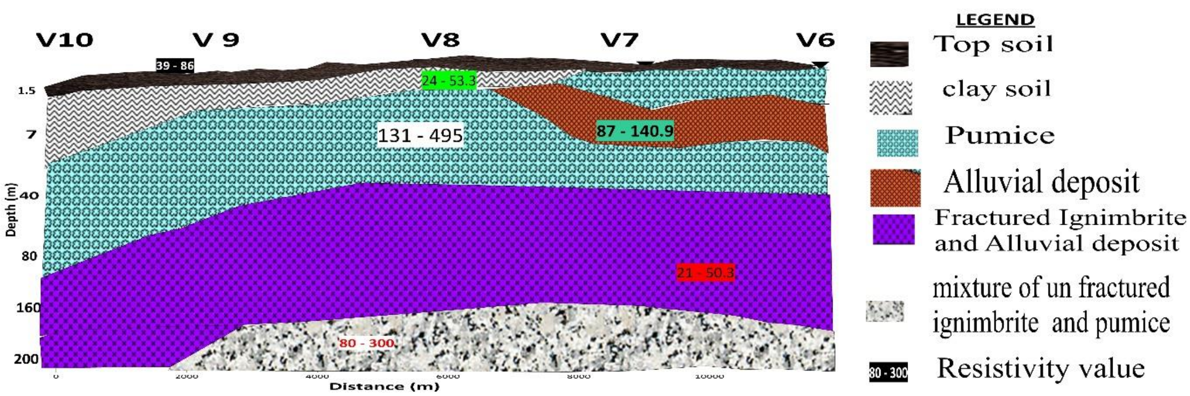

Figure 5. 7. Geoelectric layer section along profile two

As shown in the fig 5.8 the lithologic correlation of the VES 10 and Bite Dhaba borehole shows almost similar lithology with geo-electric cross section. The existence of the small variation may be due to the lateral distance between the borehole and the survey point.

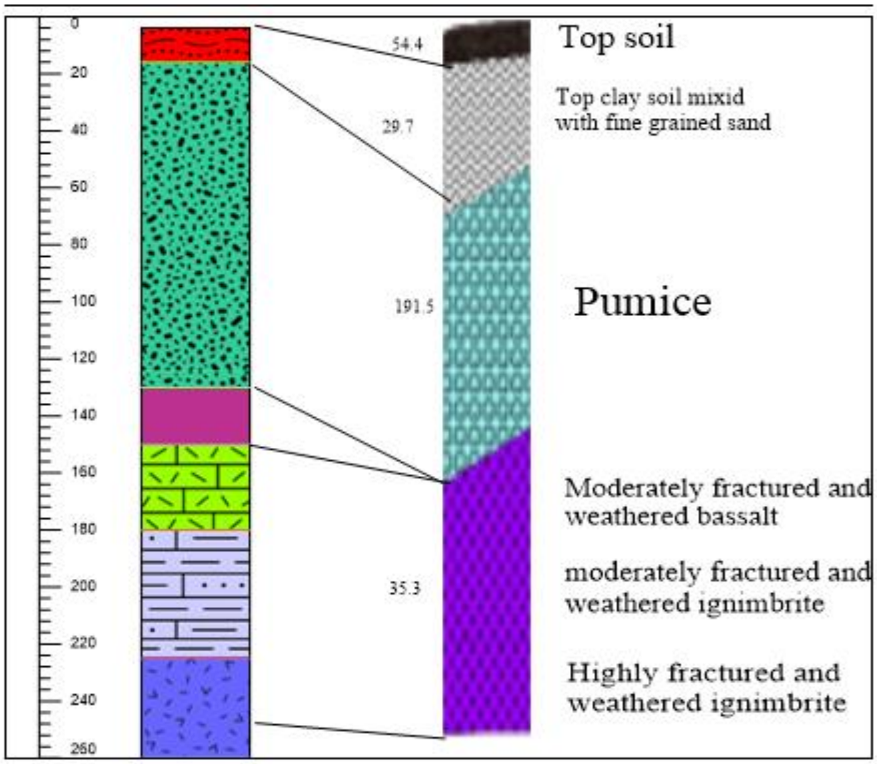

Figure 5. 8. VES 10 and lithology log at Bite Dhaba Borehole

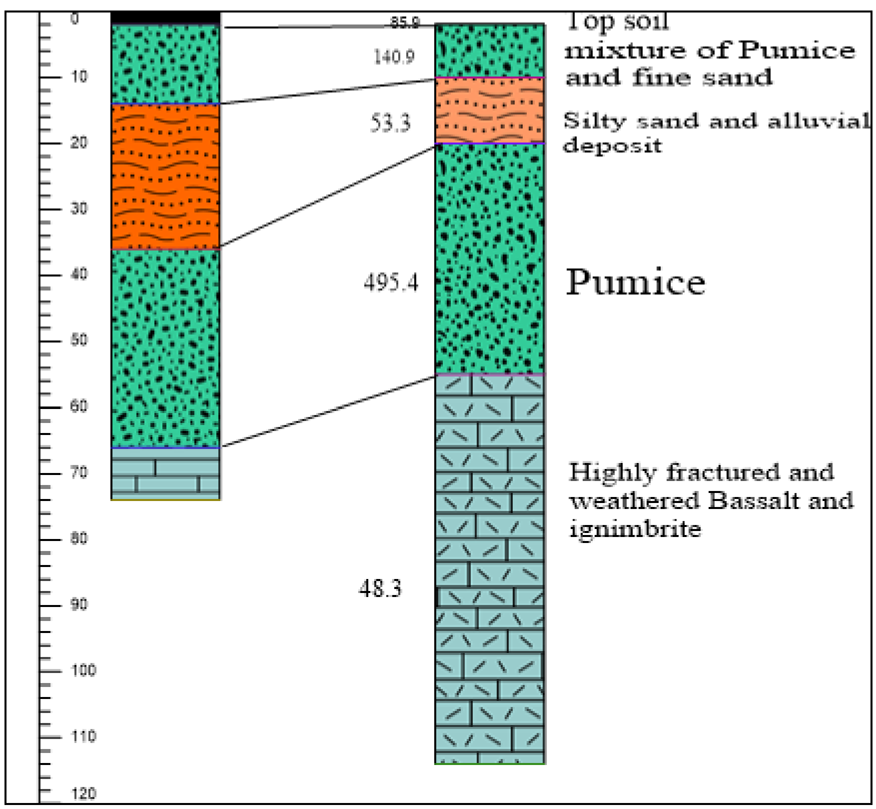

Figure 5. 9. VES 7 and lithology log of Tuchi Sumeya Borehole

5.2.3.3. Profile three

Pseudo depth

The pseudo-depth section map is constructed from VES-11, 12, 13, 14, 15, 16 and 5 that lie on the profile three are given in **Fig.** 5-10. Except for at VES 14, there is no lateral variation in resistivity in these pseudo depth sections. The resistivity value of the section increases toward VES-14 from both sides. Similarly, it increases with depth very slowly. Between VES-13 and VES-14, especially, middle sector has a comparatively higher resistivity than the surrounding regions. This suggests that the area beneath the section has a material with a high resistivity. However, areas with low resistivity and resistivity ranges between (5 and 95 Ohm-m) are a good indication of a saturated groundwater resource.

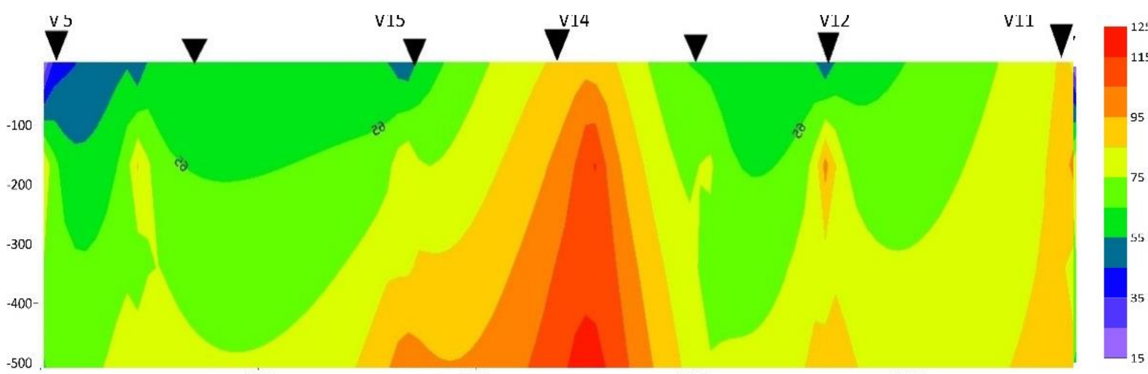

Figure 5. 10. Pseudo depth section of third Profile.

Geoelectric layer

Using the interpreted layer parameters collected from seven VES points located along this traverse, the resulting geoelectric section has been constructed. The presence of the Berta borehole near Profile 3, particularly in close proximity to VES-14 and VES-15, was used to generate correlations in depth and to identify lithological units among all VES points along this traverse during the modeling process. To produce the geoelectric section shown in (Fig. 5.11), the lithological description and resistivity parameters of the drill depth section were coupled with the interpreted VES data. This integration helped with the representation of the geoelectric features in the section and allowed for a more detail understanding of the underlying characteristics. The uppermost geoelectric layer exhibits variable resistivity ranging from approximately 14.6 to 108 Ohm-m, with a thickness variation of approximately 1.5 to 2.7 meters. This layer is commonly attributed to the topsoil, considering its characteristics and depth range. The second geo-electric layer is identified by the resistivity value ranging from 78.7 -237 Ohm-m. The thickness variation of this layer is from 2.5- 6.21 m. This layer likely interpreted as pumice. The third geoelectric layer reveals resistivity value varying from 10.9 – 67.5 Ohm-m with thickness variation from 7.9 – 23.7m and may be represented sandy clay soil and alluvial deposit. The fourth geo-electric layer of this profile manifests resistivity value vary from 80.8 – 265.8 Ohm-m. with thickness variation of 25 – 51 m. This layer may be represented as course grained pumice and slightly weathered ignimbrite.

The fifth geo-electric layer which we call aquifer layer has resistivity value from 5.1 – 30.2 Ohm-m and thickness varying from 52 - 83.3 m. The lithology's type of this layer may be highly fractured ignimbrite and alluvial deposit. From a geo-electrical perspective, this layer within the sequence appears to hold greater promise for its high groundwater potential. The resistivity signature observed in this section is supposed to be a result of a conductive ignimbritic rock that is intercalated with clay. This combination of materials contributes to the conductivity and suggests the likelihood of groundwater presence. The last layer of this profile contains resistivity value of 117 to 634.8. The bottom resistive layer most probably represents slightly fractured ignimbrite in combination with pumice. These layers' thicknesses are considered to be infinite.

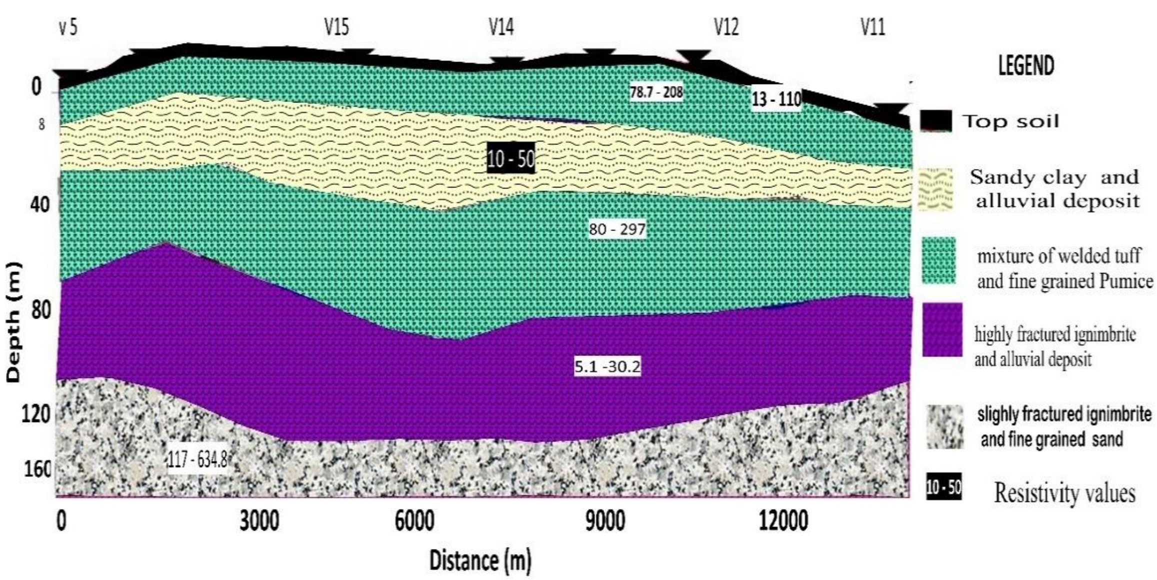

Figure 5. 11. Geoelectric cross section of Profile three.

5.3. Aquifer Characterization Using Dar Zarrouk Parameter

The Dar Zarrouk Parameters (DZP) defined by the longitudinal unit conductance in Ω^{-1} (C, layer thickness over resistivity) and transverse unit resistance in $\Omega \cdot m^2$ (R, layer thickness times resistivity) are also two of the most important parameters in electrical prospecting (Utom et al., 2012). The examination of D-Z parameters longitudinal unit conductance (C), transverse unit resistance (R), and longitudinal resistivity ($\boldsymbol{\rho l}$) provides a very convincing and easily applicable solution in understanding the geophysical behavior of saline and fresh water aquifers (Singh et al., 2004).

It is defined as product of transmissivity of an aquifer and storage coefficient (measure of amount of water that can be stored in aquifer). It provides information about hydrogeological characteristics of an aquifers. It is often used in ground water modelling and management.

Table 5. 2. Summary statistics of the VES variables for the entire data set considered in the Dar Zarrouk parameter.

Ves station	Resistivity	Thickness of aquifers (h)	Longitudinal conductivity (C)	Transverse resistance (R)	Hydraulic conductivity (K)	depth to layer beneath (H)	Longitudinal resistivity (pl)	Transverse resistivity(pt)	Anisotrophy	Protective capacity
1	23.9	166	6.945606695	3967.4	19.07693973	227	32.68253012	13.95053742	0.653337572	2.104166667
2	47	108.6	2.310638298	5104.2	10.15164861	173	74.87108656	6.372653406	0.291744771	0.055692459
3	3.2	37.5	11.71875	120	124.4802831	150	12.8	31.12007077	1.559248386	0.15010211
4	9.4	126	13.40425532	1184.4	45.55717292	181.9	13.57031746	31.55692022	1.524938405	0.029288703
5	5.1	77.7	15.23529412	396.27	80.58921662	137.5	9.025096525	45.54023368	2.246320392	0.259642521
6	21.2	116.2	5.481132075	2463.44	21.33407121	184.8	33.71566265	13.41460538	0.630773008	0.220419202
7	48.3	59.2	1.225672878	2859.36	9.896536245	114	93.01013514	5.13925391	0.235063338	0.006293611
8	21.2	25.7	1.212264151	544.84	21.33407121	77.6	64.01245136	7.06553647	0.332231144	0.096305125
9	50.3	55	1.093439364	2766.5	9.528969964	95.7	87.522	5.47641952	0.250143797	0.002673082
10	30.3	46.2	1.524752475	1399.86	15.28922579	160	104.9350649	4.414763947	0.205113113	0.434782609
11	18.8	51.3	2.728723404	964.44	23.86420412	112.5	41.22807018	10.88207708	0.513758944	0.084152072
12	17.3	83.7	4.838150289	1448.01	25.78891526	150.3	31.0655914	14.36149173	0.679923362	0.18924003
13	23.5	62	2.638297872	1457	19.37967045	122.9	46.58306452	9.776562797	0.458119807	0.115838248
14	30.2	56.9	1.88410596	1718.38	15.33644653	131.4	69.74130053	6.641124869	0.308585704	0.034552846
15	21.4	73.6	3.439252336	1575.04	21.14802141	127.6	37.10108696	12.19823178	0.573396614	0.153450493
16	13.5	67.3	4.985185185	908.55	32.50202143	110.2	22.10549777	19.84923813	0.947592842	0.114555256

5.3.1. Longitudinal conductance (C)

The longitudinal conductance (C) is the geo-electric parameter used to define target areas of groundwater potential. It clearly defines the saline, Brackish and the freshwater region in the area. The greatest C value in the area represents portion of saline water in the area. Similarly, it is intermediate for Brackish and lower values in the fresh water area below 3 Ω^{-1}. High longitudinal conductance allows more current to flow, while low conductance indicates that material is more resistive and allows less current to flow. This implies that the high conductance value is related with high ground water potential in the area.

- ✓ C values < 3 suggest that the south-eastern corner of the investigation area is mostly where the fresh groundwater is concentrated.
- ✓ C values 3– 6 demonstrates the area of brackish water that lies between freshwater and saltwater in the center of area of investigation, across the NW-SE line.
- ✓ C values >6, the center to northern portion of the research region is covered by the saline aquifer, which is depicted on the map as being roughly green to red.

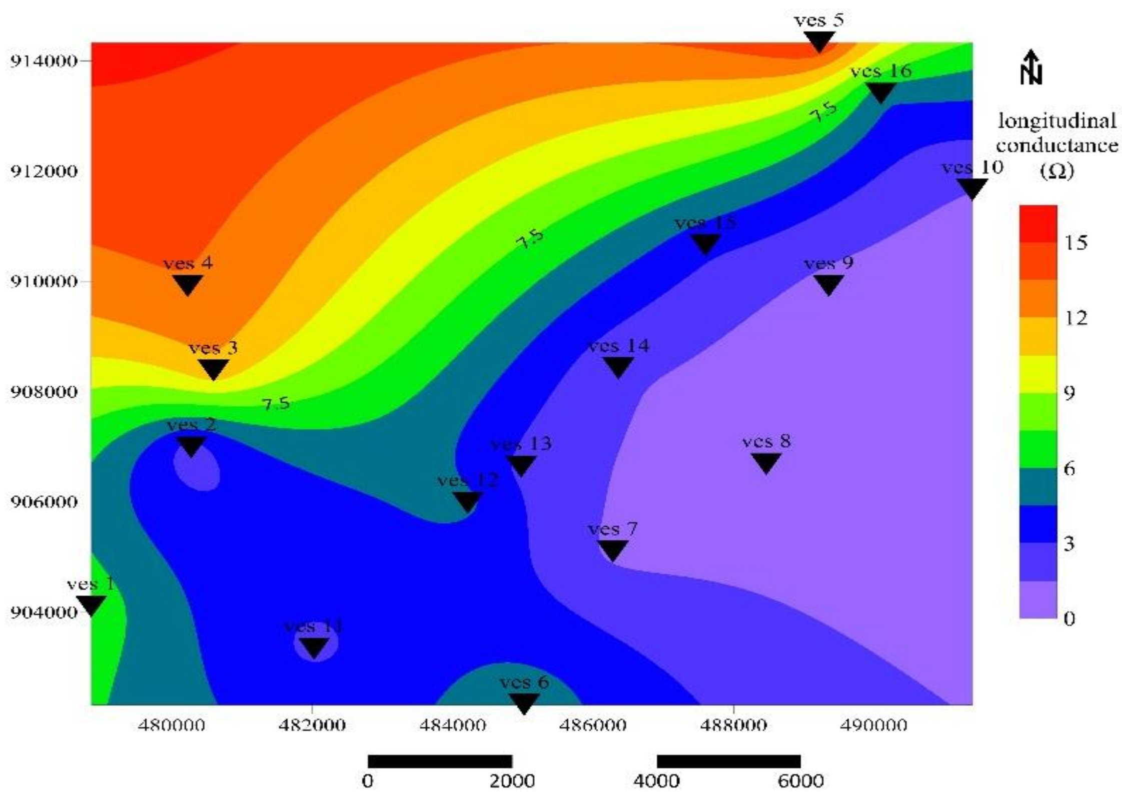

Figure 5. 12. Longitudinal conductance contour map

To generalize freshwater (VES 7, 8, 9, 10, 13 and 14); brackish water (VES 6, 11, 12, 15 and 16); and salty water group (VES 1, 3, and 5) are the three groups of the aquifers in the shown in the **Fig.** 5.12. In addition, highest priority should be given to areas with high longitudinal conductance values in terms of groundwater potential because they often imply rather thick succession.

5.3.2. Traverse Resistance (R)

Similar to the longitudinal conductance this technique also identifies the aquifer in to three different classes based on their salinity. As shown in Fig. 5.13 the transverse resistance map, R, with contour interval of 400 Ωm2, distinguishes remarkably between the three areas of the brackish, fresh, and saline aquifers.

1. For $0 < R < 1,200\ \Omega m^2$, it is possible to locate the saline aquifers.

2. R values from 1,200 to 2,400 Ωm^2 show brackish group of aquifers.

3. $2,400 < R < 5,600\ \Omega m^2$, possibly represents the aquifers of freshwater. The contours of freshwater and brackish saltwater are not similar, as can also be seen on the map.

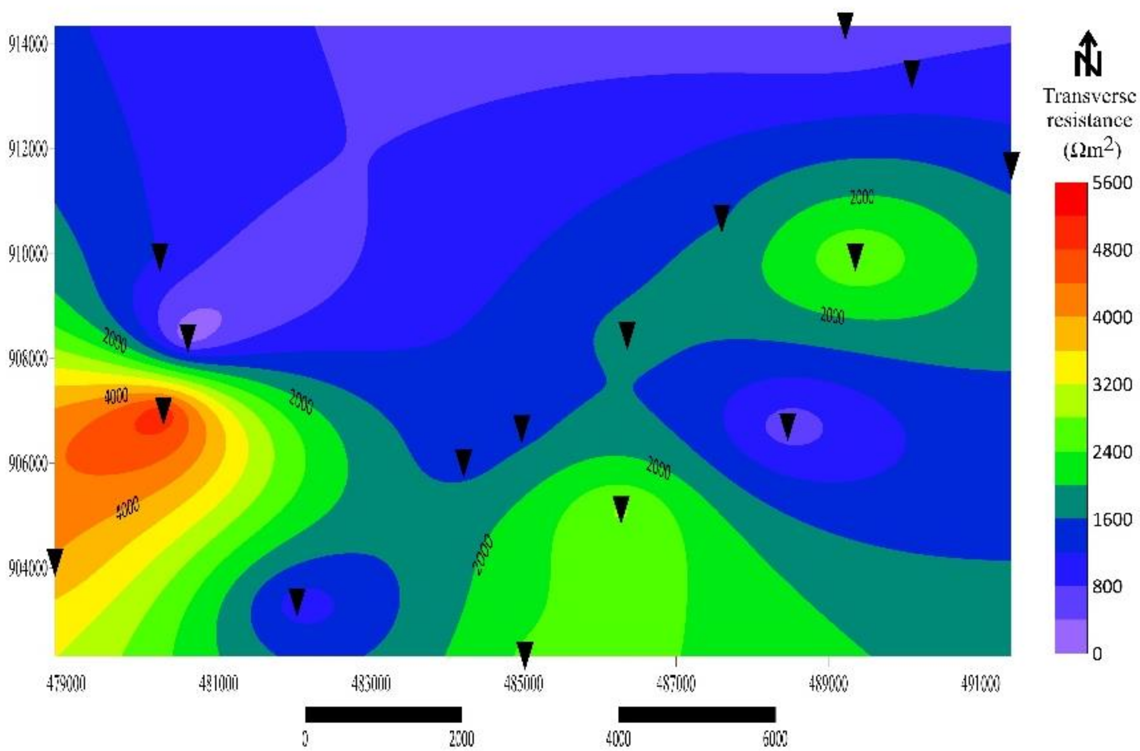

Figure 5. 13. Traverse resistance contour map

Aquifers in the area consists saline water below the sounding points in the northern area. Such as; VES 3, 4, 5, 8, and 11; brackish aquifers are observed at the sounding points of VES 6, 7, 9, 12, 13, 14, and 15; and freshwater aquifers are identified by the sounding numbers VES 1, 2, 6, and 7, which clearly show a marked change in behavior. The region with strong transmissivity and low transverse resistance that has been reported here has high yield of aquifer units.

5.3.3. Longitudinal Resistivity($\boldsymbol{\rho l}$)

Similar to the other Dar Zarrouk parameter, the ρl has also been used to distinguish between freshwater, brackish water, and salt water. As illustrated in Fig. 5.14, the ρl for saline water is 0 – 32, brackish water aquifer ranges from 32 to 72 m, whereas it is above 72 m for freshwater aquifers. Specifically (VES 3, 4, 5, and 16); (VES 1, 6, 8, 11, 13, 14 and 15); and (VES 2, 7, 9 and 10) shows sounding points from saline water; brackish water and freshwater respectively according to the finding of the research.

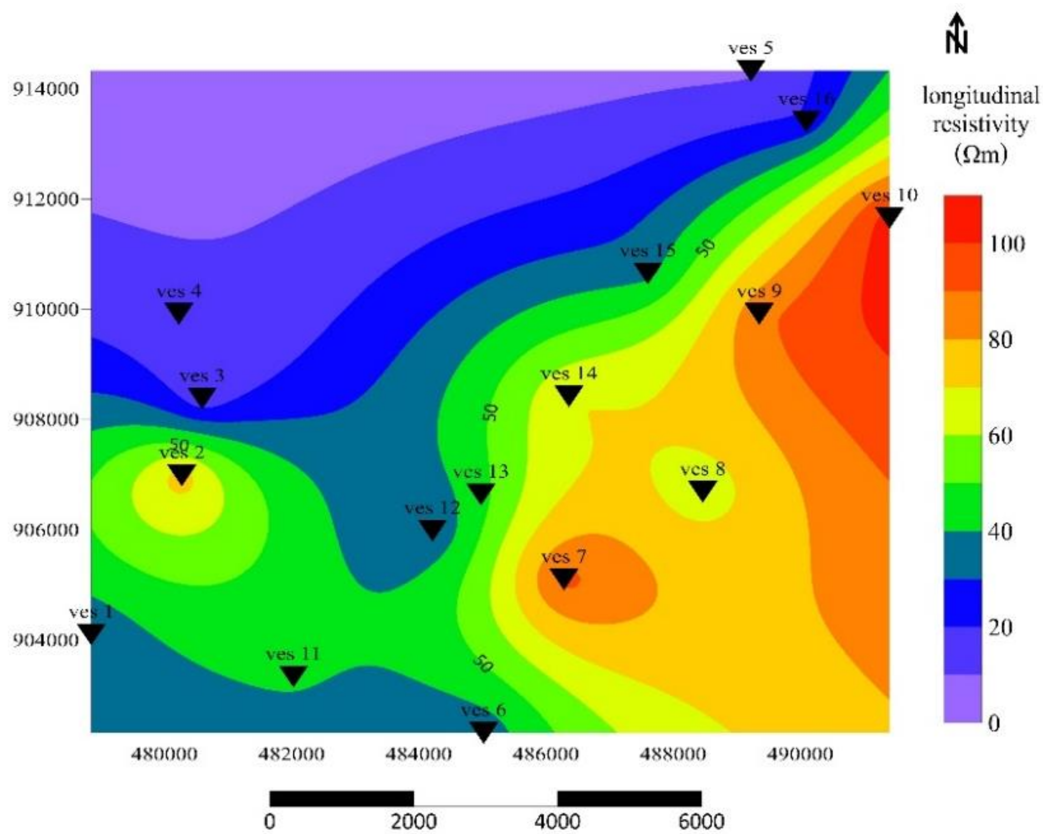

Figure 5. 14. Longitudinal Resistivity contour map

5.3.4. Hydraulic conductivity (K)

Hydraulic conductivity of the aquifer (K), which varies from 5 to 135 m/day shown in Fig. 5.15. It was discovered that low hydraulic conductivity values predominated in the majority of the investigation region, indicating that the area's groundwater flow is complicated by the geologic constraints of the area's semiconfined aquifers. High hydraulic conductivity can be found in the northern sides of the survey area. This suggests that the movement of water through this part is more valuable.

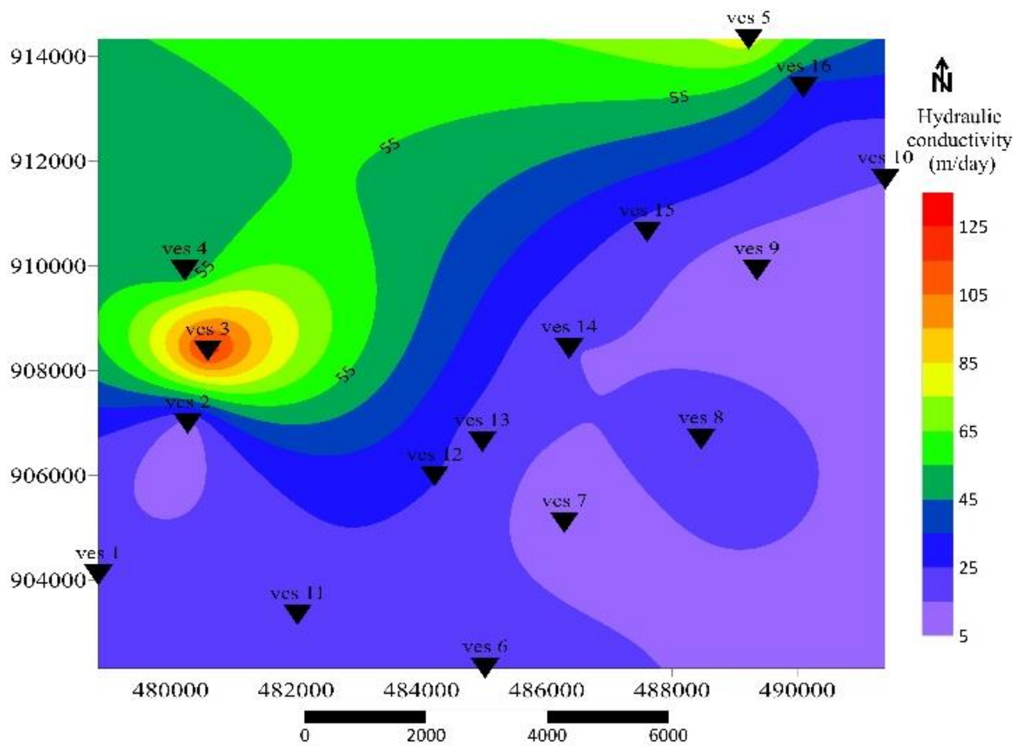

Figure 5. 15. Distribution of aquifer hydraulic conductivity contour map

5.3.5. Transmissivity (T)

Transmissivity is parameter that characterizes an aquifer hydraulic conductivity, which is the materials ability to transmit water through it (Utom et al., 2012). Similar to the above techniques north western and some of the northern part is categorized under the high transmissivity (781 m^2/day) (MoWIE, 2015) values which indicate the high potential of water bearing aquifers and highly permeable to enable to fluid movement (Okonkwo & Ugwu, 2015). But the south eastern and southern part is considered as low transmissivity around 47.07 m^2/day (MoWIE, 2015) values which is not easily permit the movement of water through it.

The potential for groundwater flow and availability inside the aquifer is indicated by a greater transmissivity. Higher transmissivity aquifers are typically more effective in storing and transferring higher volumes of water. From this information we can say that high transmissivity value in the northern and north western direction indicates high potential of water. The existence of Pumice fragments is mostly angular that reduce the permeability of the deposit and pumiceous lappli tuff and silty clay reduce the vertical permeability.

5.3.6. Coefficient of Anisotropy (λ)

The anisotropic contour map in (Fig. 5:16) can discriminate the flow path of aquifers by using the other Dar Zarrouk parameters. According to (Singh & Singh, 1970) areas with a high capacity of aquifers are represented by lower values of anisotropy. This suggests that as compaction and rock durability rise, the anisotropy coefficient (λ) does as well. The high anisotropy value indicates the presence of subsurface heterogeneity or preferential flow paths. Similarly, anisotropy suggest that the separation between high and low value of anisotropy indicates subsurface contact.

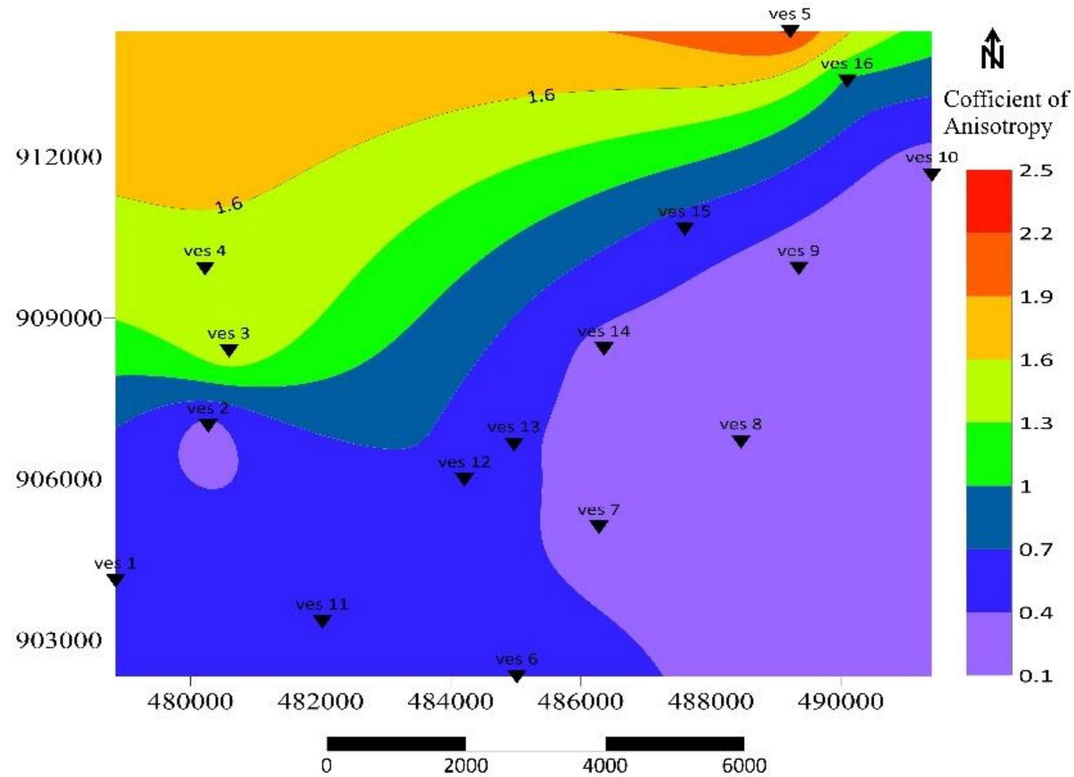

Figure 5. 13. Coefficient of Anisotropy contour map

5.3.7. Aquifer protective capacity

According to (Oladabo & Akintorinwa, 2007) the protective capacity of aquifer overburden was classified into different zones including excellent, very good, good, moderate and weak based on the range of C values. Areas with conductance greater than 10 Ω^{-1} were classified as zone of excellent protective capacity, while zones with C value ranging from 5 – 10 Ω^{-1} were classified as zone of very good protective capacity. ranging from 0.8 -4.9 Ω^{-1} were classified as good protective capacity, and those ranging from 0.2 to 0.79 Ω^{-1} were categorized into moderate protective capacity and areas below 0.2 is in the category of weak protective capacity. The values of longitudinal conductance(C) obtained from the VES data ranges from 0.2 to 4.4 Ω^{-1} were used to generate the longitudinal conductance map (Fig. 5.17).

The protective capacity in the study area is divided into two categories: moderate and good protective capacity. So, the recommended protective capacity is located at the north-eastern, east central part around Sera wakele and Tuka Langano kebele. How ever, the high protected area at west central part of the aquifer may be saline water so the only recommended area is at north eastern area.

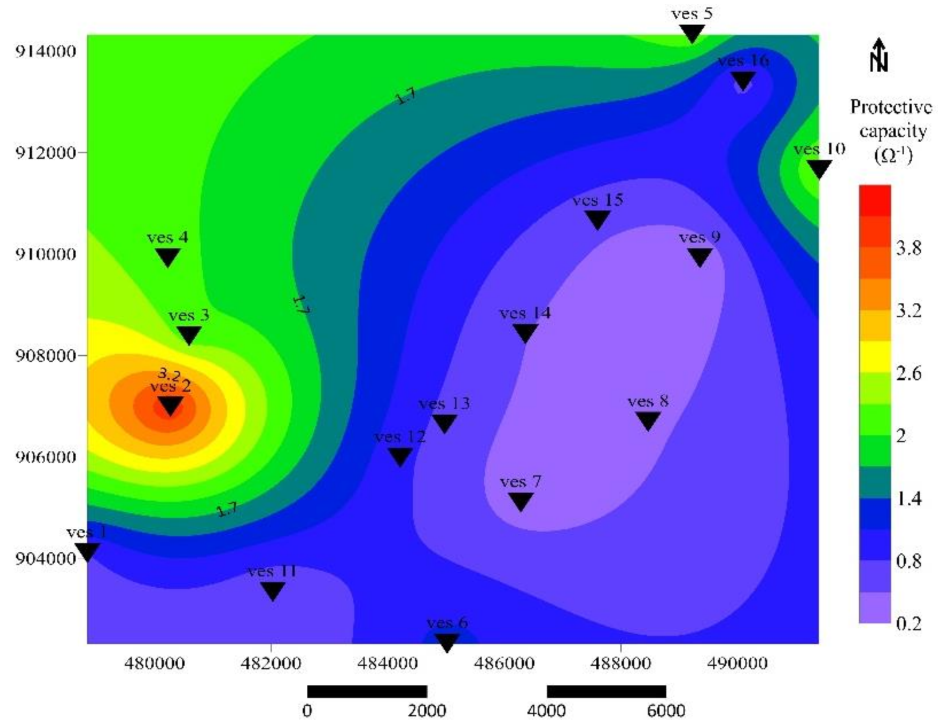

Figure 5. 17. Aquifer protective capacity map

5.3. Interpretations and Discussions of Magnetic Data

5.3.1. Total magnetic field anomaly

The change in the magnetic anomaly indicates magnetic influences from underlying rocks, as demonstrated in the TMA map (Fig. 5:18). The majority of the surveyed area reveals very low to moderate anomaly values of the overall magnetic field anomaly. The map shows two prominent negative features of elliptical and broad shape, respectively distributed in the central and south-western parts, showing the maximum negative value of 803 nT. These anomalies trend east-west.

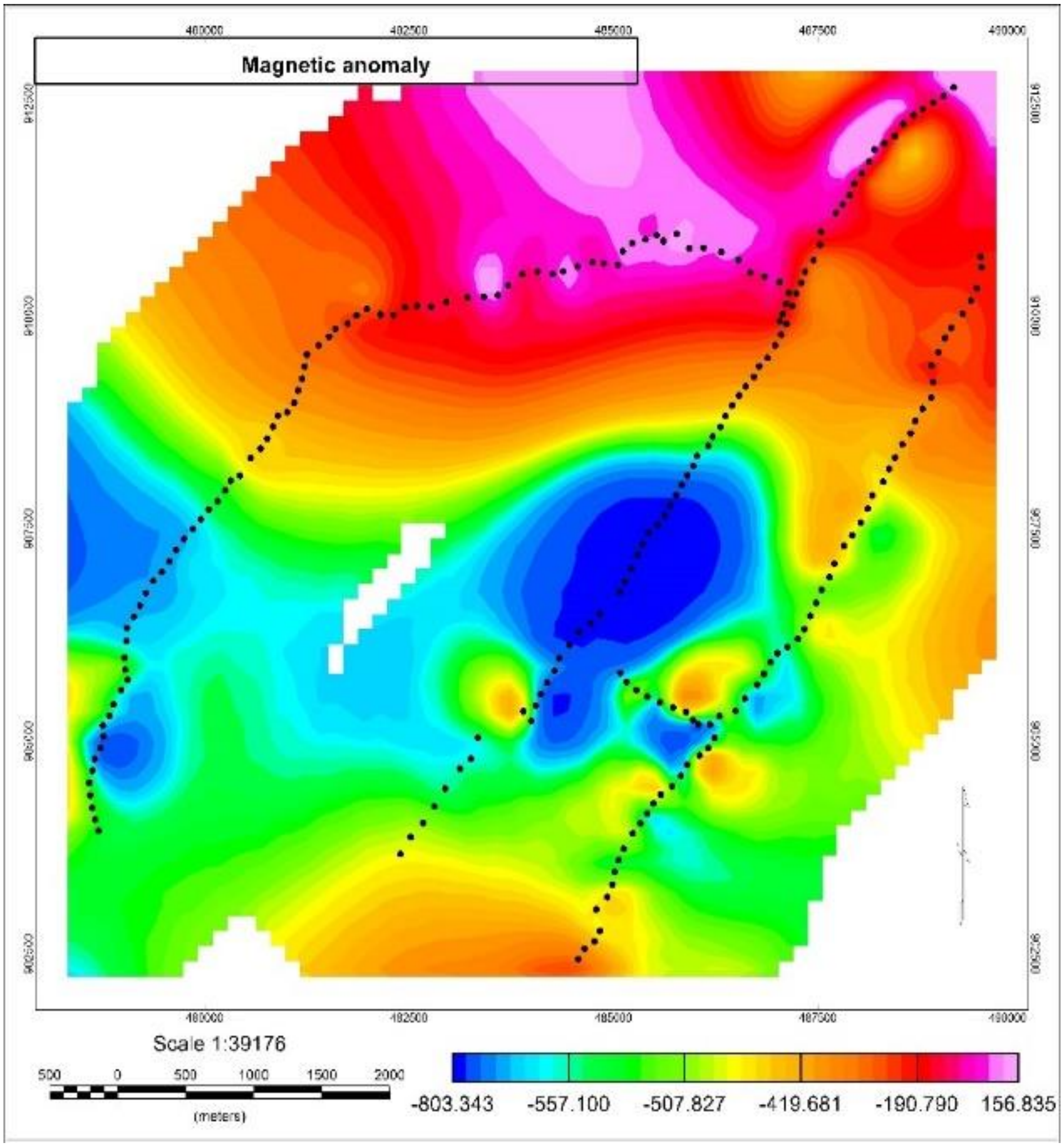

Figure 5. 18. Total magnetic anomaly map of Meki to Alemtena area

We also observe cylindrical features with high anomaly values trending northwest-south with central magnetic trends in excess of 100 nT. These large cylindrical trends indicate the presence of strongly magnetized subsurface intrusive bodies. which reaches an amplitude of 100 - 166 nT. and trends along the NW-SE position. It is noted that the negative anomalies trend from the west side of the study area to the east side through the central area over the water-divide between Awash and the Rift Valley Basin, with a gentle dip increasing intensity and showing the overlapping geological formations.

High anomaly values in the northern of the research area's may be caused by mineralized silty clay and deep-seated fractured ignimbrite. It may be result of the influence of nearby linear features such neighboring faulting and fracturing filled by magnetized source. However, the TMA map shows very low anomalies in the middle and western part of the investigation area, low level magnetic anomalies due to the cross ridges in the area, and high-level magnetic anomalies observed in the south-eastern part of the map is recognizable because of the presence of fault-like structures in southwestern part and volcanic ash deposits in the central parts along the transverse ridges.

5.3.2. Reduction to equator

According to (Leu, 1982) next to the equator, the magnetic figures will appear horizontal after RTE. Three magnetic zones, each with a different magnetic anomaly pattern, may be observed on the TAM-RTE map (Fig. 5.19). The primary cause of this magnetic zoning is the magnetic properties of underlying rock types. Pumiceous rock that suggests a basement may be found along the ridge in the first zone, which is found in the western and central parts of the area. This is characterized by a very low magnetic intensity. The second zone is within the portion underneath the sand deposits. Low to moderate magnetic abnormalities are noticed. In this region, the magnetic intensity amplitudes range from -5 to +50 nT. The third zone occupies the north and north-central portion of the area. It is based on the old metamorphic series. It shows high (positive) anomalies: the amplitudes of magnetic intensity in this zone are between +50 and +174 nT.

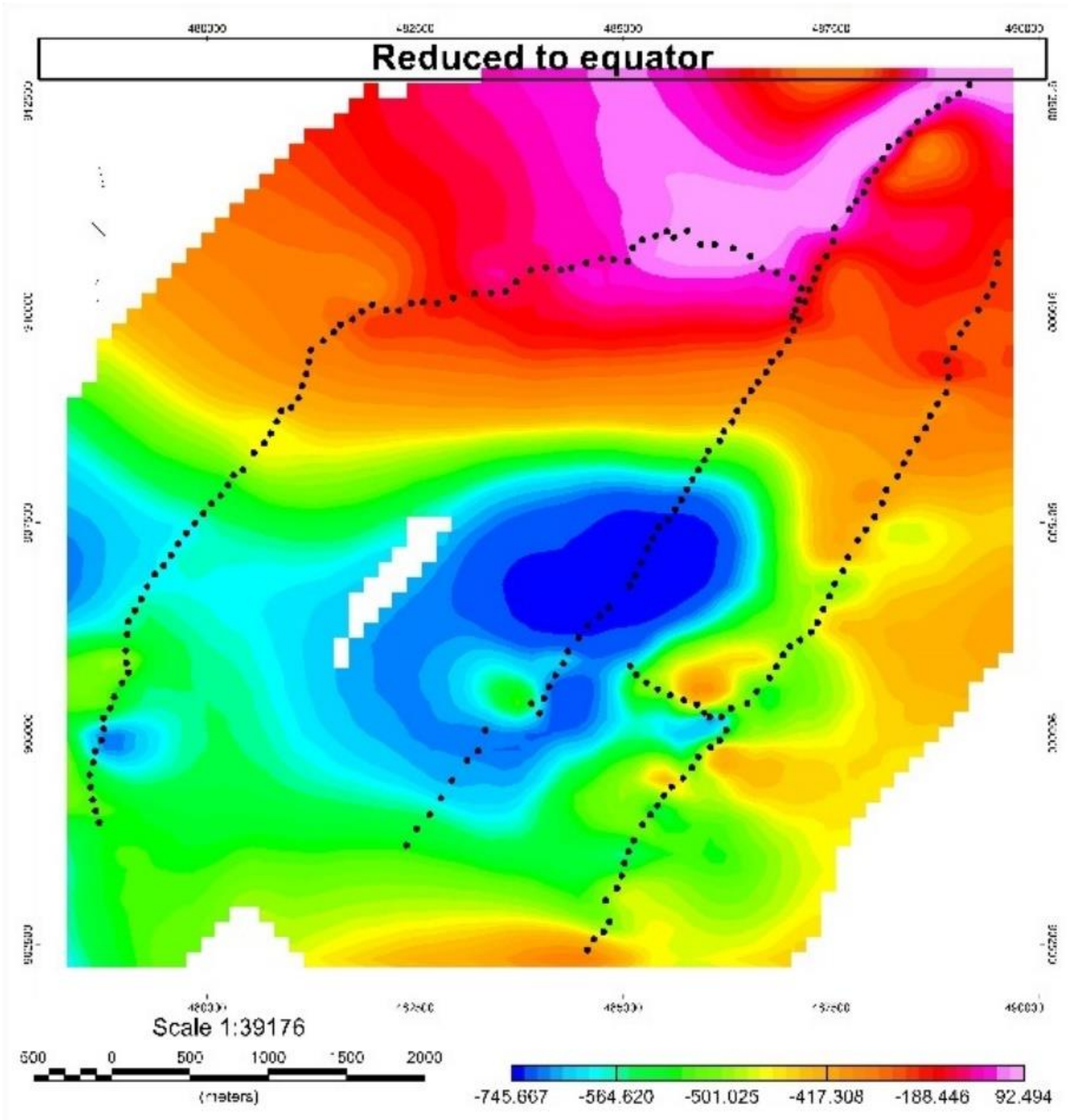

Figure 5. 169. Reduced to the equator anomaly map of Meki to Alemtena area

5.3.3. Residual magnetic field anomaly

After separating the regional anomaly from the data for the entire magnetic field, the demonstrated map in (Fig. 5:20) was generated. The map illustrates shallow subsurface features in detailed manner better than those revealed by the observed TMA map. The Eastern, Southern, as well as Northern portions of the research area have high to very high residual anomalies. The majority of the areas and elongated structures that form the area's extremely high residual anomalies are observed.

Low to extremely low magnetic anomaly values predominate practically all of the research region, which extends from the south-west through the center and into portions of the eastern sections, as indicated on the map. Volcanic ash and fragmented Quaternary sediments form the majority of central to northern sections.

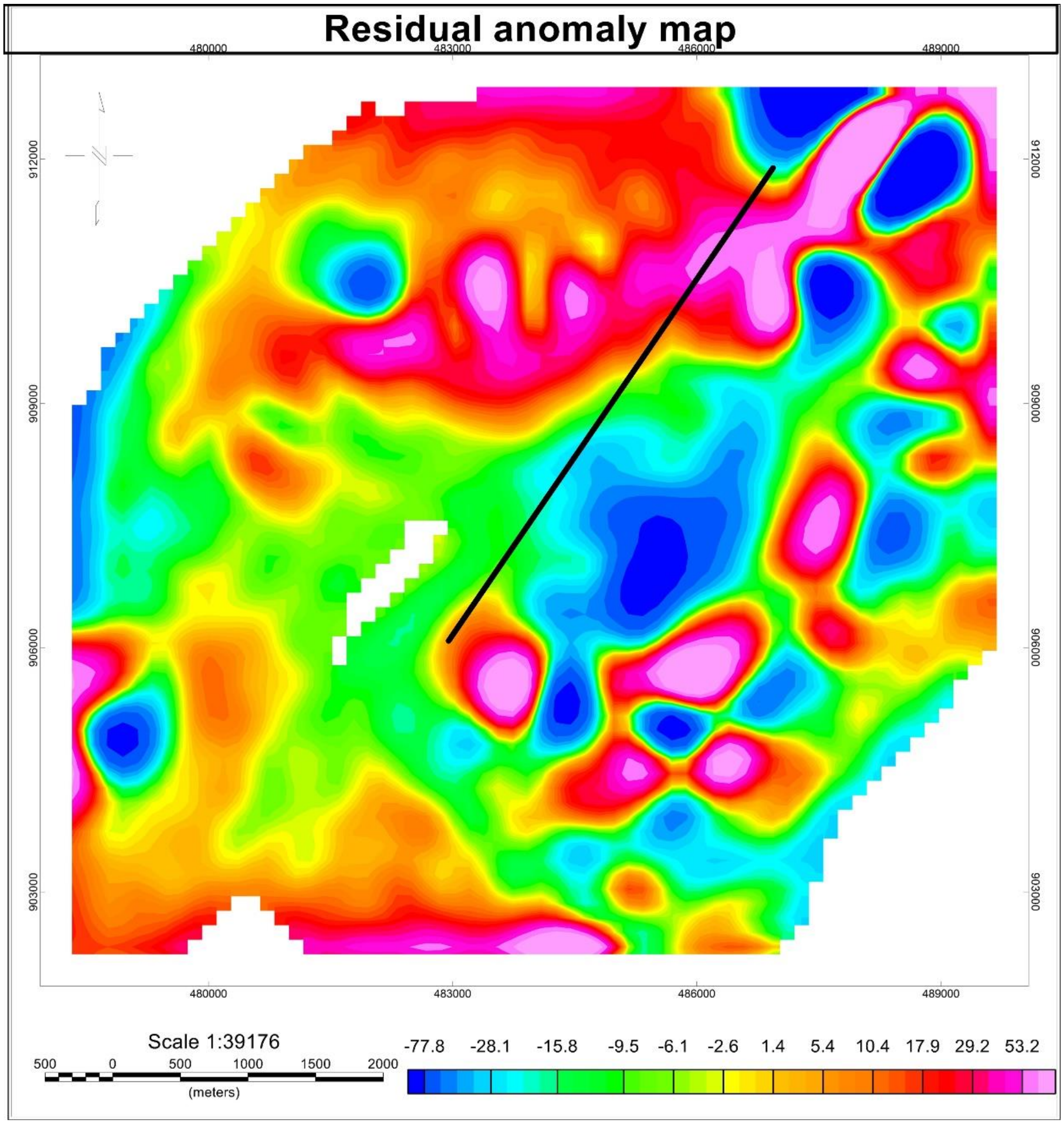

Figure 5. 20. Residual Magnetic Anomaly map of Meki-Alemtena area

5.3.4. Upward continuation

The upward continuation is technique that removes the effect of shallow sources of magnetism from the data. This is done by mathematically moving the data to higher elevation, which suppresses and enhances signal from shallow and deeper sources respectively. As the continuation height increases the effect of shallower features disappears. Particularly, at a high continuation height (Fig. 5:21) most of the shorter wavelength are removed. The anomaly profile curve gets smoother as continuation heights increased. Thus, the continuation height chosen characterizes the regional anomaly field in the region under study. As noted by (Jacobsen, 1987) the existing source at and below depth $\frac{z}{2}$ can be represented by the magnetic anomaly if it is extended upward to a specific height. Therefore, by extending the residual anomaly to different heights, one can visualize the buried sources at depth of half the extension height (Z/2).

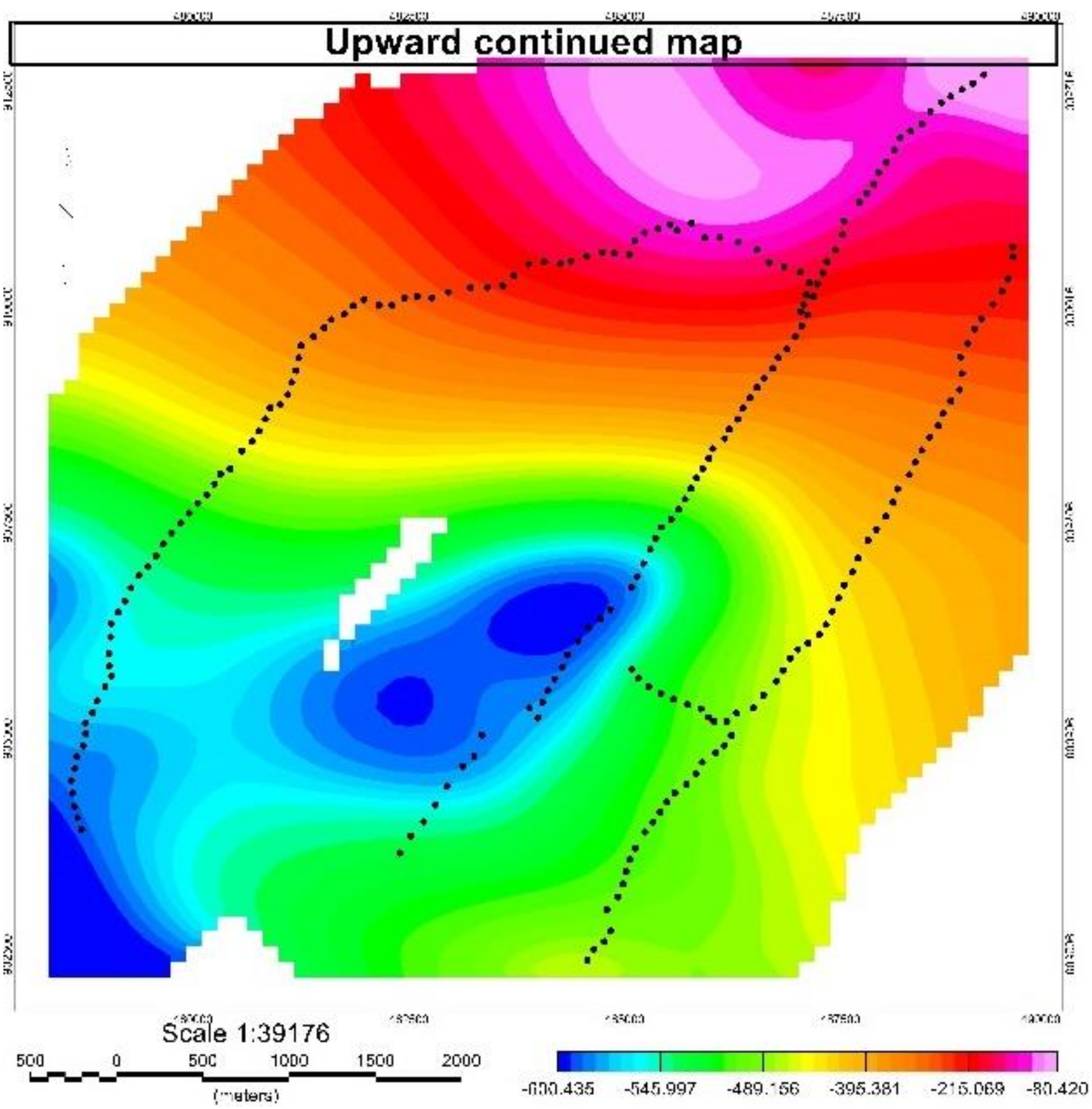

Figure 5. 21. upward continued map of the equator reduced anomaly map

5.3.5. First order Vertical derivative

First vertical derivative was applied on the total anomaly map to enhance the top of the body of the magmatic intrusions (Fig. 5.22). The high magnetic anomalies at the northern, southern and south-central side of the investigation site are due to the short wave-length anomalous bodies that appears at shallow depth. The maximum amplitude at those area shows that the subsurface discontinuity at shallow depth. The maximum amplitude running in the E – W, NE – SW direction.

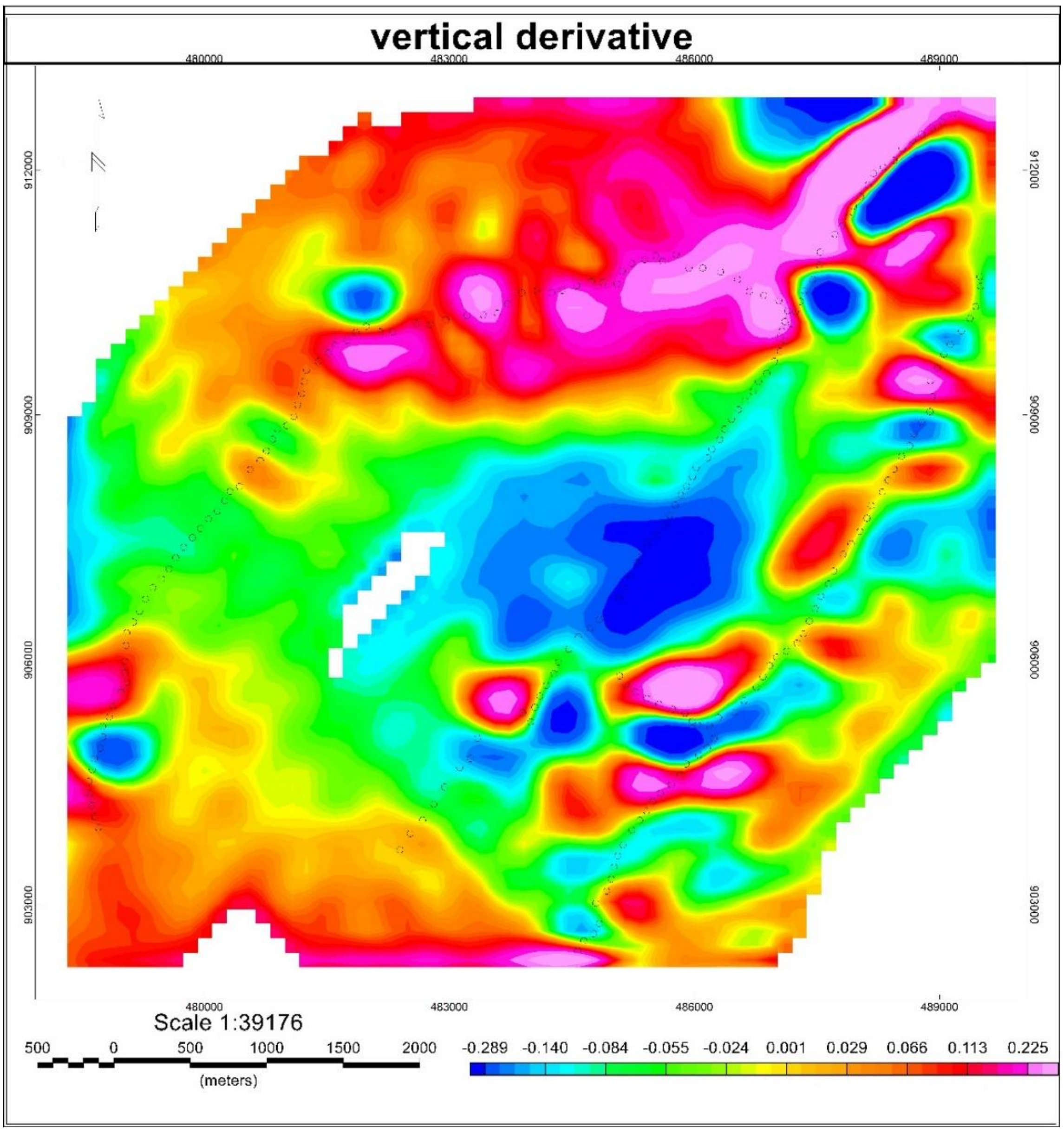

Figure 5. 22. first order vertical derivative map of Meki-Alemtena area

5.3.6. Analytic signal (AS)

It is applied on the low pass filtered total anomaly at cutoff wavelength of 500m to enhance the edge and shape of the intrusive structure's body. It is helpful to provide an overview of the near subsurface conditions because an analytical signal map illustrates how anomalous entities respond from their top regions. In the AS map displayed in (Fig. 5.23), the borders of the intrusive bodies and faults are clearly marked. The maximum amplitude of analytic signal may reveal location of contact.

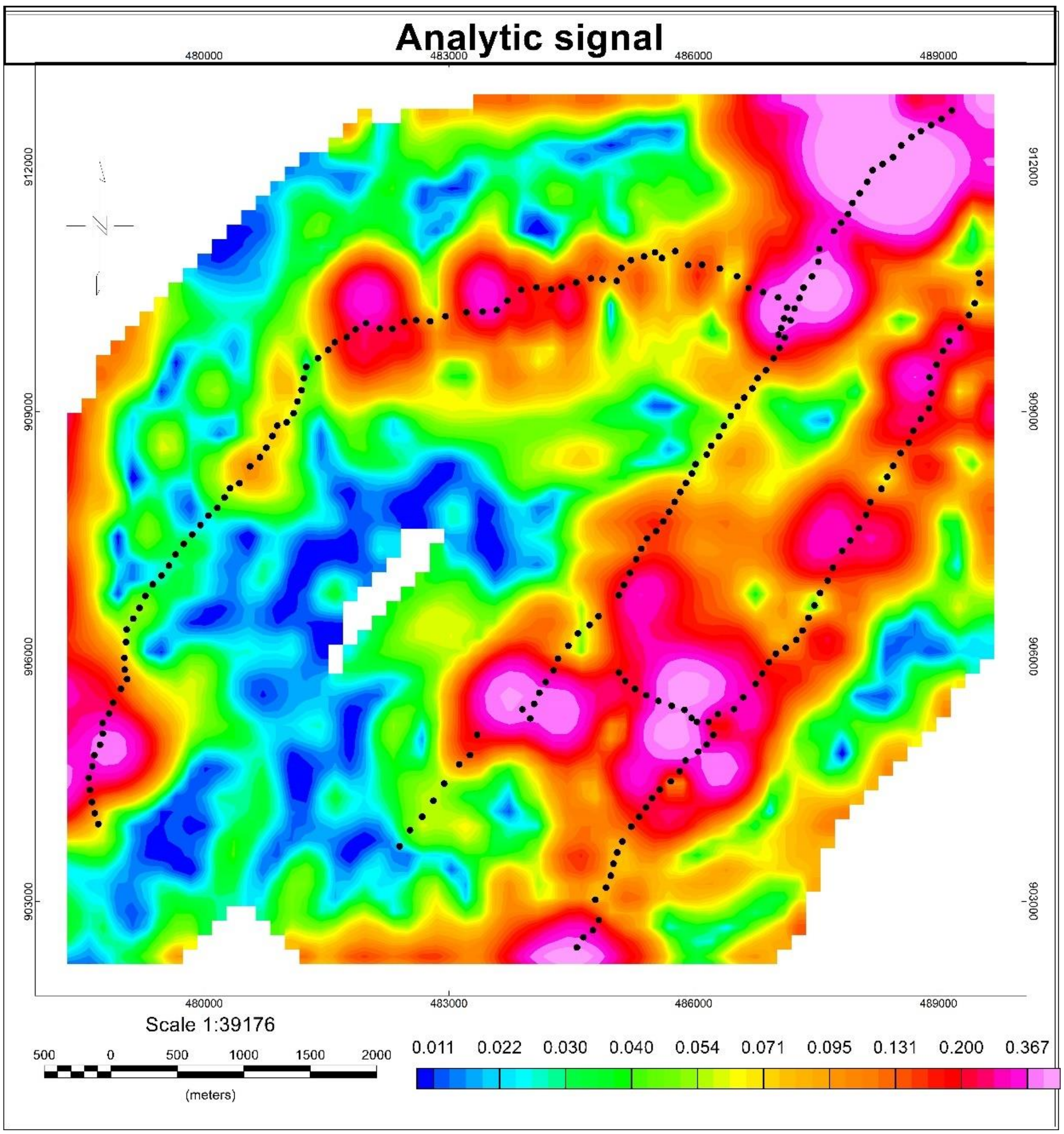

Figure 5. 23. Analytic signal map of Meki-Alemtena area

High amplitude analytic signal appears at the south eastern, western, south central and southern section of the survey area give the idea of presence of anomalous bodies in the area. This is due to the susceptibility contrast in rock unit. The intrusive bodies are concentrated in the south-central part of the area, while the southern and northern parts of the area have a linear structure.

Additionally, it is understood that the maximum amplitudes in the border fall precisely across a magnetic contact. This is influenced by the locations of the source body but not by the magnetization inclinations. The high amplitude of AS in the south, south-west, center, and north-east regions exhibits discontinuities from the north to the south and from the east to the west; this discontinuity may be caused by shearing effect. These highest positive analytic signals are aligned in NE –SW direction which is coincide with general structural trend of the area.

5.3.7. Horizontal gradient

This enhancement technique offers further insights into directional variations of the complete magnetic field. These derivatives create horizontal derivative map shown in (Fig. 5.24) that reveal the texture of the anomaly and highlight any discontinuities in the anomaly pattern. Since the gradients are greatest towards the margins of horizontal bodies, this filtering technique is thought to be the simplest way to estimate the position of contacts. From this we consider that there is magnetic feature like contact that runs from NE - SW trend that, the E – W trend in the southern and south-central part.

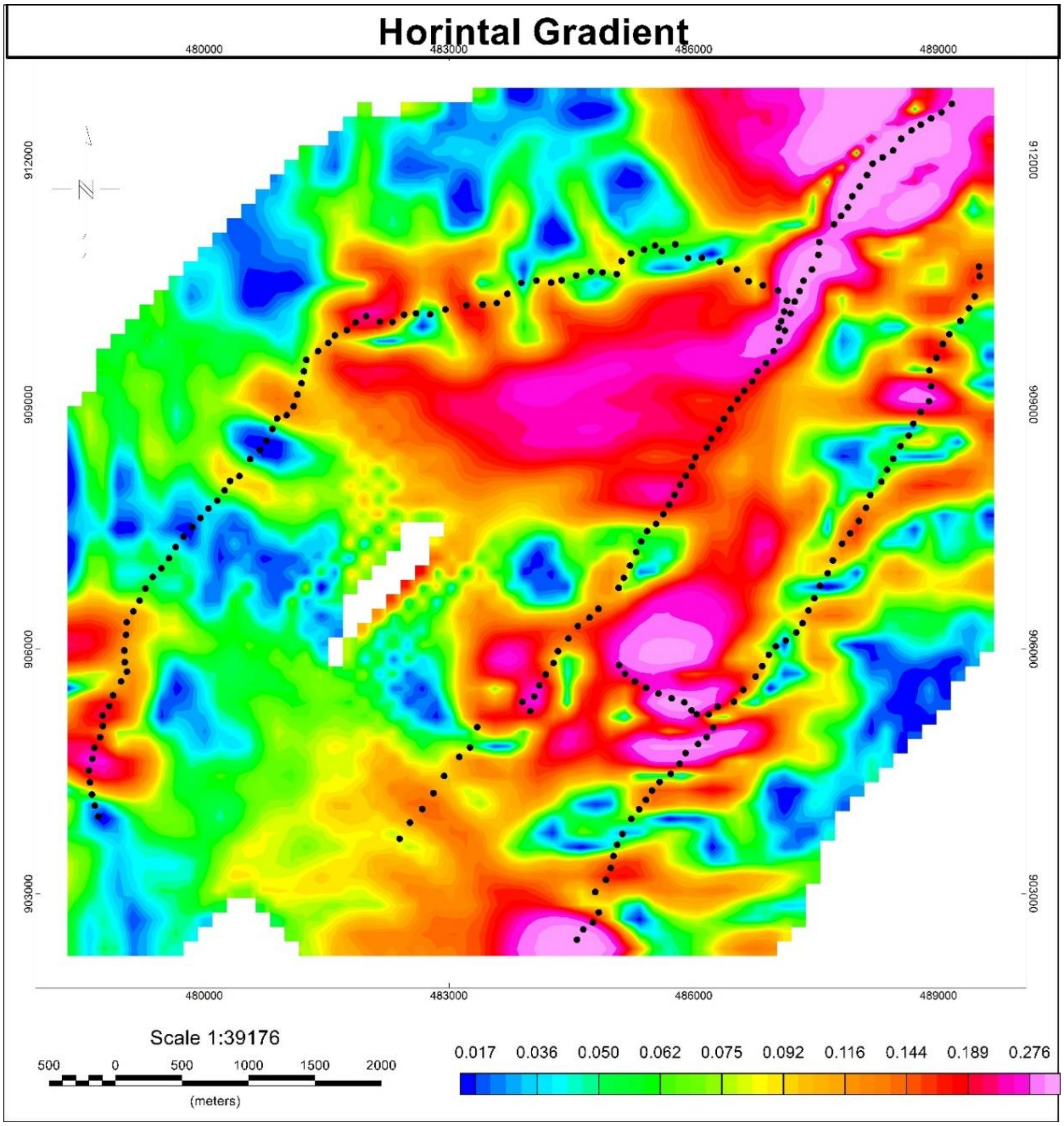

Figure 5. 24. Total horizontal derivative map of Meki-Alemtena area

5.3.8. Tilt derivative

From tilt derivative map, the location of faults and different contacts was simply detected. The nearly E – W trend may be due to the existing water divide. This Tilt derivative map of magnetic data shown in (Fig: 5:25) shows detailed structural contact. Zero contour line given on color scale bar of (Fig. 5.25,26) reflect the position of strong gradients at the contact boundaries of magnetic sources where magnetic susceptibilities between positive and negative anomalies abruptly shift. Which is in the direction of NE – SW, N – S, E - W and NW -SE trend direction. Additionally, the map displays E-W trends in the investigation area's central, southern, and northern regions, and a positive anomaly points to a magnetic source. Depending on this, magnetized objects may cover the northern, western, and eastern portions of the region in large quantities. The contact boundary of magnetic sources is therefore represented by the zero-contour line.

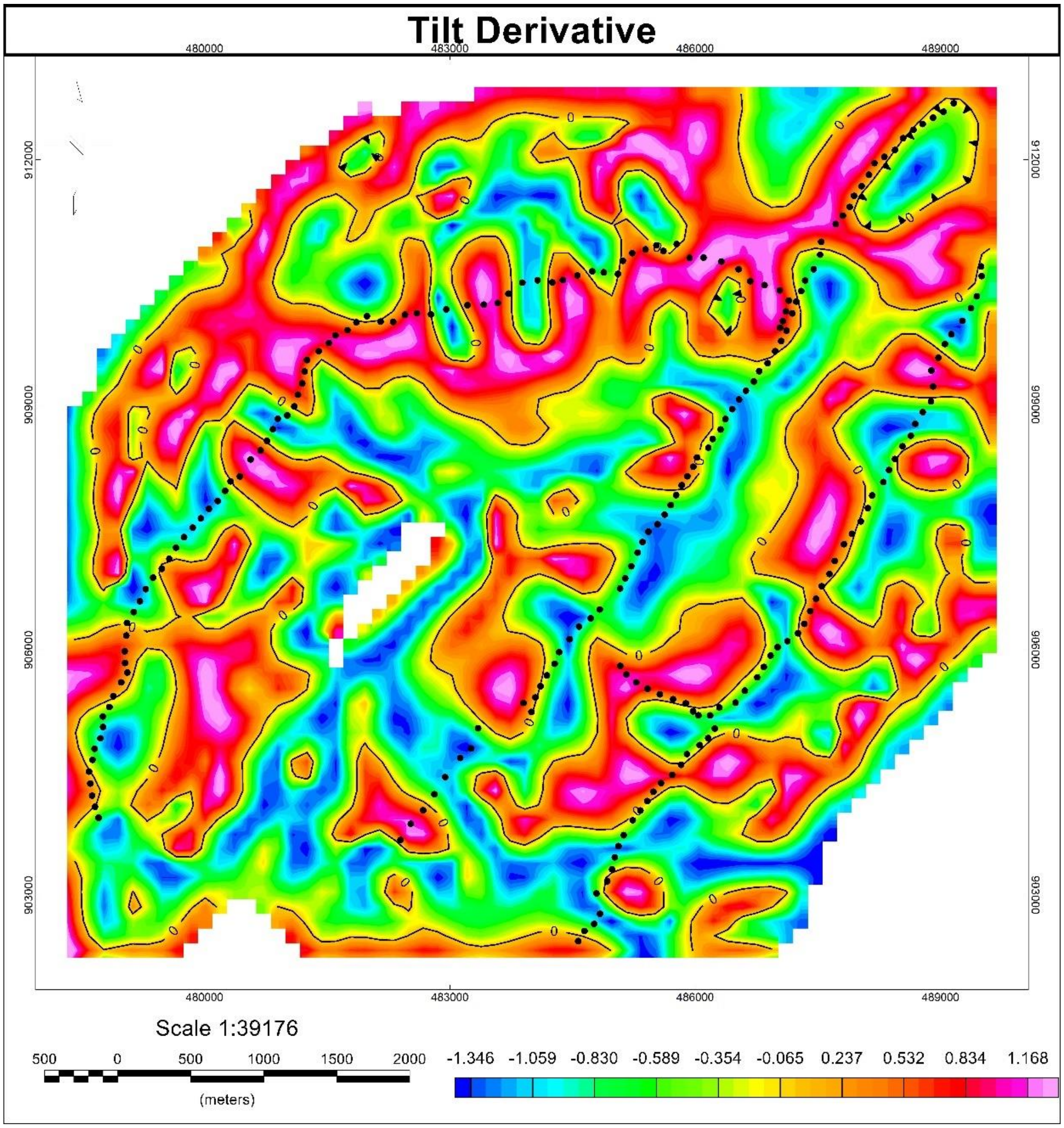

Figure 5. 25. Tilt derivative of Meki-Alemtena area

The magnetic structures are more obvious when it is produced from total horizontal derivative, which has sharper and continuous peaks over source edges. The maxima produced by the tilt derivative are more precise and are centered around the body edges.

The figure shown in (Fig. 5.25 and Fig 5.26) are similar but the second figure shows more detailed features.

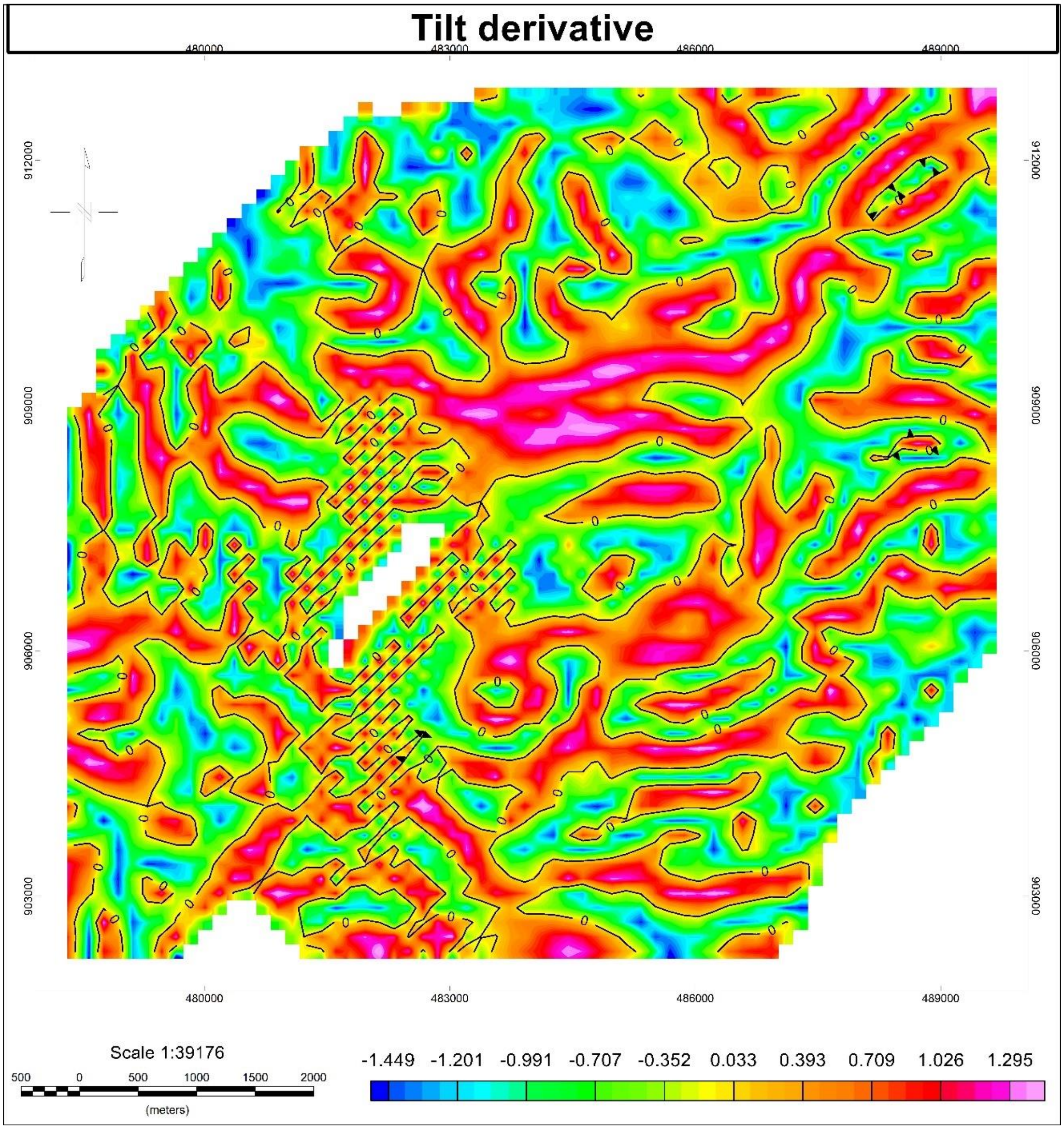

Figure 5. 26. THDR_TDR map of the Meki to Alemtena area

5.3.9. Second order vertical derivative

Anomalies of limited spatial extent are resolved sharpened by the second vertical derivative map. The approximate boundaries of magnetic sources are delineated by zero contours of second vertical derivative anomalies (Fig. 5.24). The zero contour in the research region represents the boundary of the magnetic sources or it is a representation of geological contact, similar to the tilt derivative in (Fig. 5.26). The second order vertical derivative of the field, the calculated edges are closer to its real position (Jaferson & Fransisco, 2011).

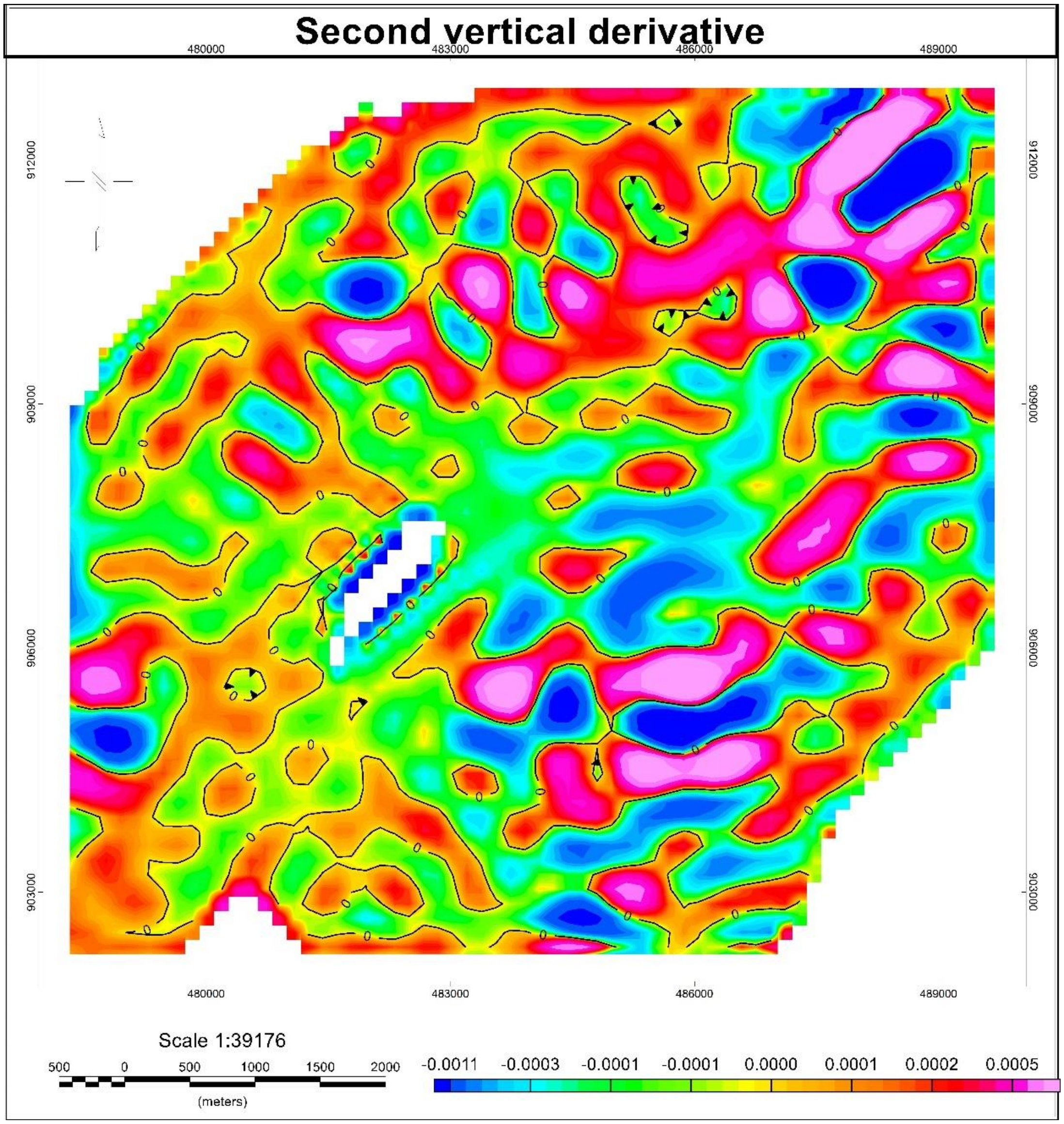

Figure 5. 27. Second order vertical derivative

5.3.10. 3D Euler deconvolution

The main applications of Euler deconvolution are source depth estimation and contact delineation. The accuracy of its depth estimation depends on the choice of the suitable structural index, which is based on the geometry of the causal bodies. Only homogeneous functions can use Euler deconvolution. This characteristic of the magnetic field produced by contacts, dykes, and poles (Keating & Pilkington, 2004). It is used to show the distribution of anomaly source and their location. Location and depth of these magnetic anomaly sources are marked by different color plotted on the map.

As shown in (**Fig.** 5:28) pink color represents source occurring at the <100 m and mostly distributed over the north east central which indicates the anomalous source beneath that point is relatively shallower. The red colored circle represents the source occurring in the depth range of 100 to 300 m. its distributed along the east central and north eastern part of the researched area. Green color indicates the source that occurs at the depth ranges between 300 and 500. Similarly, the blue and light blue color reveals the anomalous source which appears at the depth of 500 to 800, and >800 m respectively.

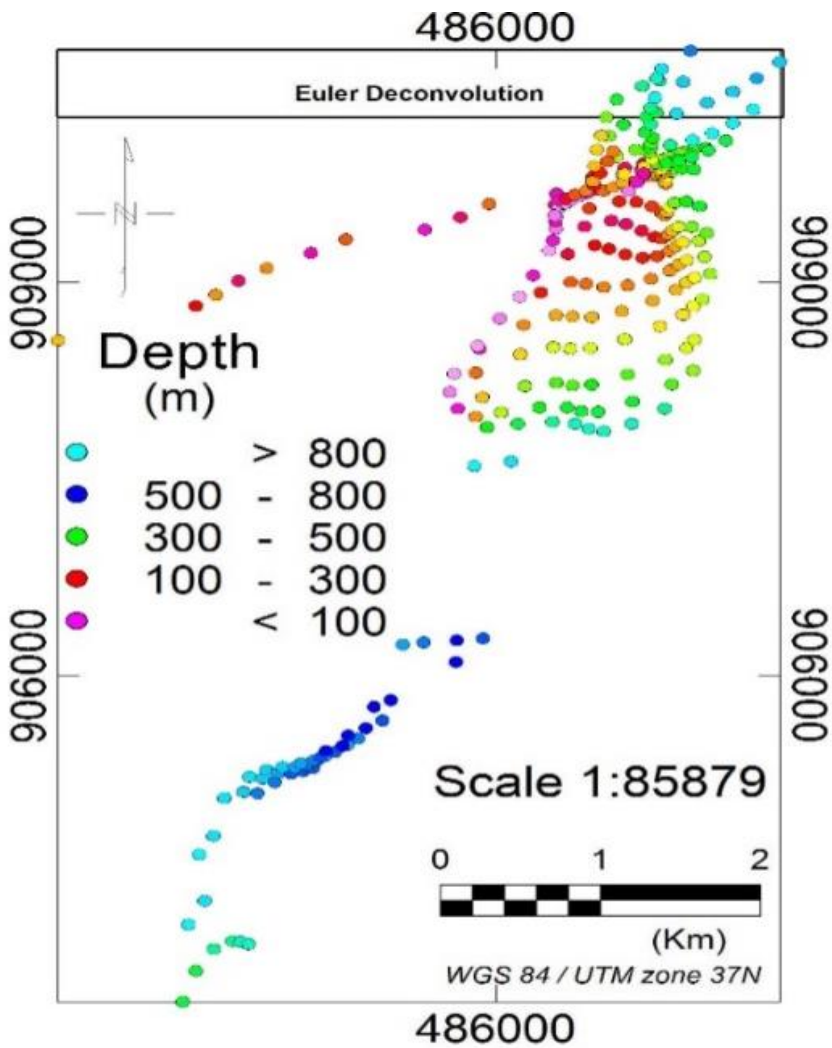

Figure 5. 28. 3D Euler deconvolution map

5.3.11. Geological Interpretation of the Structure

The interpretation of structural map has been drawn from tilt derivative map, Analytic signal map, HDR and Euler deconvolution to highlight the different lineaments in the area of study. This lineament reveals the structural complexity in the basement, characterized by line trends. The analysis of the interpretive structure map shows three dominant structural trends with different intensity and length. The N–S, NE- SW, and E–W are the main trends in the studied area as shown in (Figure 5-29). The relationships among these three trends suggest that the area was subjected to more than a single tectonic event.

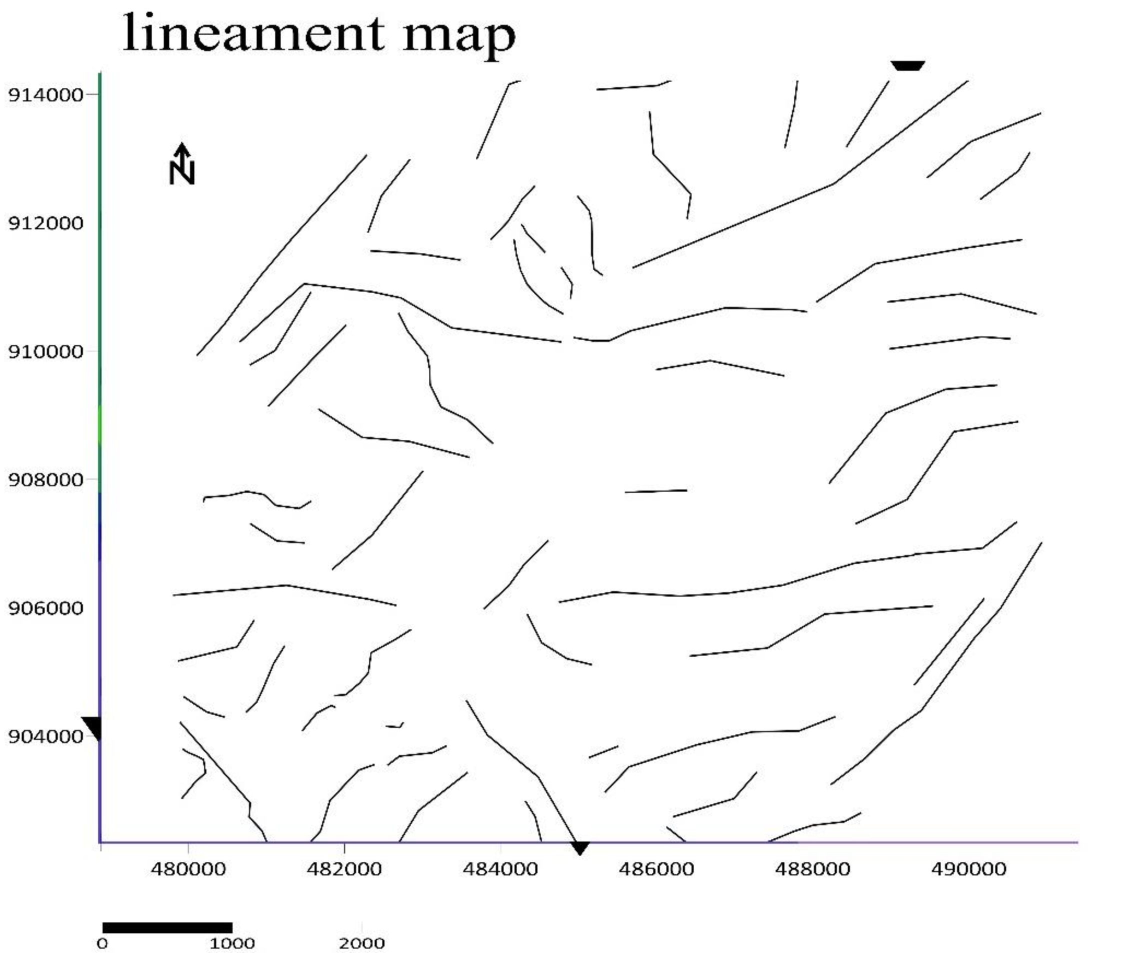

Figure 5. 29. Lineament map of Meki - Alemtena area

The E – W trend is approximately along the direction of water divide which separates the waterflow direction in the region in to north and south. Some of the structural trend in the south section of the major trend is along SE direction. It provides an extensive overview of the underground features that could regulate groundwater flow. Those trends at the South or North of the E – W trends are base for the water flow to opposite direction. They are the dominant tectonic trends which may affects the flow direction of ground water to the lake Langano in the rift valley basin and to the Beseka lake through Koka lakes in the surveyed area.

5.3.12. Magnetic 2D modelling

Geosoft Oasis Montaj GM-SYS 2D modelling software is used to create magnetic 2D-models from the magnetic anomaly data that has been reduced to the equator (Fig. 5.17). To illustrate the lithological changes along the profile, this profile was constructed with a North East–South West alignment and passing over the supposed zone on the map. Positive magnetic anomalies are distinguished by graben structures of the second and third lithologic unit, the negative magnetic anomalies are most likely associated to uplifts. The basement is assumed to be basalt in the model, with a magnetic susceptibility of 0.045 and depths between 300 and 600 meters.

Magnetic 2D modelling shown in (Fig. 5.28) was constructed by using results from magnetic data's qualitative interpretation and quantitative interpretation of VES data by correlating with borehole data. The power spectrum of magnetic anomaly shown in (Fig.5.27) contains three different line different parts with different values of slope. The slope of power spectrum shows that the depth of each layer below the surface. The line spectrum helps to calculate the depth of each layer.

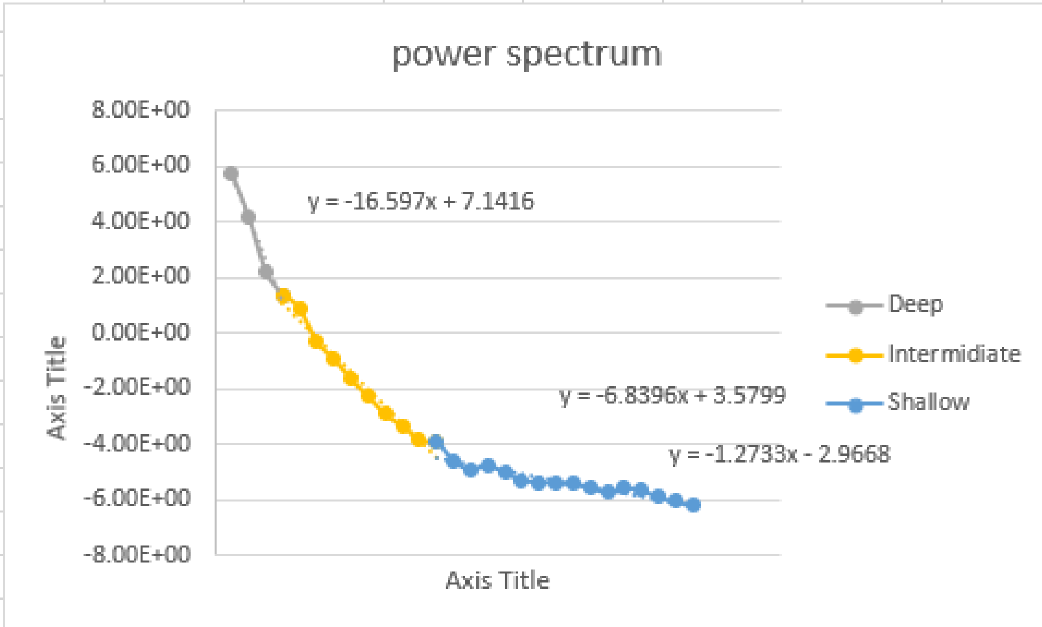

Figure 5. 30. Power spectrum of anomaly map

The magnetic susceptibility values were considered in the initial model while constructing the 2D magnetic map of the research area, as represented in Figure 5.28. These values played a significant role in capturing the magnetic characteristics and variations across the region of interest. The magnetic model of the uppermost layer comprises a near-surface alluvial deposit, followed by a layer of top clay soil, and sandy soil. The sandy soil exhibits a low susceptibility value of 0.00005 cgs (centimeter-gram-second). The second layer represents volcanic ash products and pumice with relatively low susceptibility and an average susceptibility value of about 0.0007cgs. The average thickness of the second layer varies between 50 and 150 meters. The third layer, with an average magnetic susceptibility value of 0.035 cgs, is interpreted as different categories of weathered and fractured ignimbrite. This layer has an average thickness ranging from 150 to 350 meters. The fourth layer consists ignimbrite and basaltic rocks susceptibility value of 0.045 cgs.

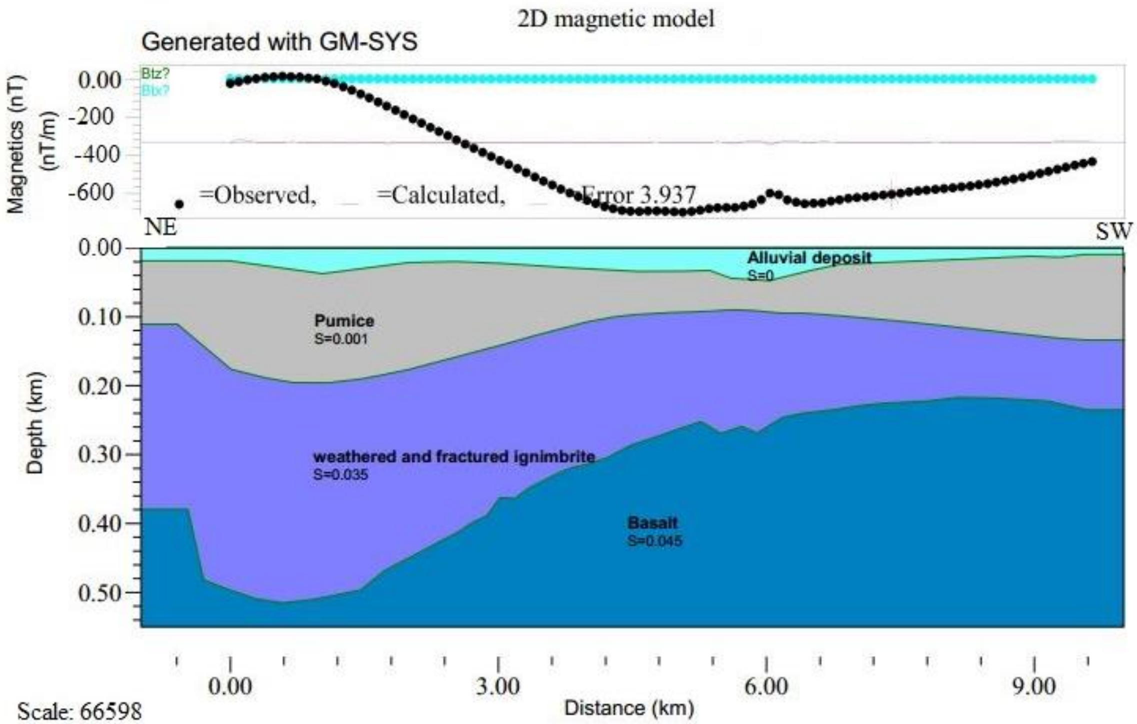

Figure 5. 31. magnetic 2D modelling

5.4. Discussion on Integration of VES and Magnetic method

The method's integration offers more detailed information on the aquifer characteristics and groundwater potential below each VES site. By combining the geoelectric properties derived from VES with the magnetic anomalies found during magnetic surveys, we were able to gain important understandings of the subsurface structure and geological properties. VES, Dar Zarrouk and magnetic data were combined to assess and characterize the groundwater potential.

Six geoelectric layers were delineated from VES data; a thin, very discontinuous, low resistivity stratum representing the top soil, the second layer of geo-electric layer was combination of low and high resistivity stratum representing the alluvial deposit on one side and volcanic pumice with an average resistivity of 5-69 and 117-345 ohm-m respectively. The next resistivity layer represents the alluvial deposit or muddy clay soil which divides the upper high resistivity pumice from the subterranean high resistivity volcanic pumice. The average resistivities of layer 4, represented by the fragmented pumice material, ranges from 250 to 600 ohm-m. The fifth layer of the geoelectric trend consists of thick fractured and weathered low resistivity ignimbrite ranging in resistivity from 5 to 78 ohm-m. This stratum extends to depths of 77 to 250 m with an average thickness of 30 to 100 m. The research area's aquifer layer can be divided into intermediate and deep aquifers. The intermediate aquifer reaches the depth of 50 – 70 m below the surface. But the deep aquifer has a depth of 120 – 250 m. Here very low resistivity anomalies are typical of saline water and the final stratum consists of high resistivity material due to unfractured basalt. These resistivity differences show the presence of distinct lithological units and likely subsurface heterogeneity. This result is very similar to existing drill hole data in the study area (MoWIE, 2015).

The Dar Zarrouk parameter, generated from VES data, is a key indicator of aquifer type. It characterizes the aquifer that occurs in the fifth layer of the geoelectric layer. This variable helps in dividing the water of the aquifer into fresh, brackish and saline water depending on the longitudinal resistivity, transverse resistivity and longitudinal conductivity values. All show that the northern section is covered by salt water (VES 2, 3, 4, 5) and the southeastern section is more or less fresh water (7, 8, 9, 10). But all other sounding points are categorized under brackish water. Furthermore, The Aquifer protection capacity (Figure 5.15) was predicted using the distribution of the longitudinal conductance estimated from the resistivity sounding interpretation of the research area. In terms of aquifers protective capacity, the area with high protective capacity suggests no likely surface or subterranean fluid pollution due to strong protective capacity. In the survey area, the sounding point is more protected in the south-west around (VES 2, 3, 4) and in the north-east at the site (VES 10). The high groundwater potential on the north side of the study area thus falls into the category of good aquifer protection capacity.

The high anisotropy value indicates the presence of subsurface heterogeneity or preferential flow paths. This indicates a clear contrast in hydraulic conductivity. This can result in preferential flow paths along the direction of higher hydraulic conductivity. Groundwater tends to flow more easily and at greater rates toward higher hydraulic conductivity (K) values, resulting in preferential flow along this pathway. This implies a groundwater flow towards a high hydraulic conductivity which occupies northern part of the investigated area. However, the low hydraulic conductivity in the central area prevents groundwater from flowing southwards from the northern area.

Similar to the above, high transmittance values on the north side of the aquifer mean that water movement to the north is easier. This is the cause of groundwater flowing north from the watershed. The presence of a contact along E – W considered in the study area produces the water flow from the water divide in both directions. This allows the flow direction of the groundwater to be controlled. We have been able to enhance our interpretation of the subsurface lithology and hydrogeological conditions, particularly with regard to the anisotropic features, by merging the VES results with the Dar Zarrouk characteristics.

In parallel, with magnetic survey, different intensities and shapes of the anomalies were identified, indicating different subsurface magnetic properties. Evidence for the possible existence of magnetic minerals or geological structures such as fault zones or magmatic intrusions has been provided by the presence of high intensity anomalies in certain areas and the low intensity anomalies indicate the existence of non-magnetic lithological units or regions with consistent magnetic properties. We derive an east-west trending control structure from the tilt derivative and the SVDR of magnetic anomaly, which may be overlaid on the watershed. This can classify the water flow to north and south. Fault zones, fractures, and lithological borders are just a few of the features that magnetic survey might notice. Similarly, the magnetic approach helps in locating structural elements affecting groundwater distribution and flow.

Integration of VES results, Dar Zarrouk parameters and magnetic data provide important insight into the underlying features. The results of the correlation study showed a strong correlation between the regions of high intensity magnetic anomalies and the low resistivity zones identified from the VES data. This raises the possibility of a link between the magnetic minerals causing the anomalies and the clayey/silty sediments detected by the VES. In addition, the VES data showed that the high resistivity zones and the low intensity magnetic anomalies coincided, indicating the presence of non-magnetic lithological units in the fractured rock.

A geological understanding of the research area was developed based on the integrated interpretation. The results of combined Dar Zarrouk, magnetic survey, and VES revealed subsurface lithological diversity and probable mineralization regions. The Dar Zarrouk and magnetic technique shows that the presence of subsurface water divide which is controlled by east west directed contact in the study area. Determine groundwater flow at the site is restricted to the northeast and southwest portions of the site from the watershed.

We also provide a geological classification based on the integrated interpretation. The presence of clayey/silty sedimentary units with magnetic minerals is suggested by the association between low resistivity zones and high intensity magnetic anomalies, likely indicative of areas of potential mineralization. The non-magnetic lithological units within the area could represent pumice formation. Which is known for its high porosity and low bulk density, resulting in a generally high resistivity zones associated with low intensity magnetic anomalies. These comparisons help to identify subsurface lithological variations, structural features and potential areas of mineralization or hydrogeological interest.

Chapter Six

6. Conclusion and Recommendations

6.1. Conclusion

The combination of the data presentation techniques led to the following conclusions, which were based on discussions and interpretations. According to the results of the investigation, there is a close relationship between the primary structural elements of magnetic fields. The result Of VES data shows that: -

The variation of apparent resistivity in the pseudo-depth and geo-electric resistivity indicates the presence of shallow and deeper low resistivity horizons, indicating probable zones of groundwater saturation. This intercept demonstrates the occurrence aquifers at varied depths. The substantial thickness and low resistivity exhibited by these horizons strongly suggest a significant potential for groundwater in the research area. The combination of their extensive vertical extent and low resistivity values implies favorable conditions for groundwater storage and availability within these horizons. The primary geological units that are most likely to contain groundwater, based on the degree of fracture and weathering, include alluvial deposits and highly to moderately fractured ignimbrite mixed with sand. These units possess characteristics that facilitate the storage and movement of groundwater, making them favorable reservoirs for groundwater resources. Comparison of geophysical survey results and the drill hole lithological logging data shows good correlation in the area of study.

Application of the DZP characterizes the aquifers based on the salinity, or degree of freshness of the aquifers, Capacity to protect the aquifers from un necessary infiltration toward the aquifers, permeability of the aquifer. Most of the aquifer are categorized under saline water. In addition to that the aquifers protective capacity is divided into various protection levels "poor/weak", "moderate" and "good" depending on the longitudinal conductance value of the overlying layer. This Dar Zarrouk parameter confirms that the south eastern section of investigation area is set under the category of fresh water.

The tilt derivative revealed E-W and NE-SW trending linear subsurface structural structures. The primary geographic features known as magnetic maps are considered to encourage the flow of ground water from watersheds to low-lying Lake Langano, and similarly, in the Awash Valley, ground water flows towards the north, away from the watershed.

The findings of the resistivity and magnetic measurements also show that the rock units in the study region have localized faulting and fractures at different depths. It is suggested that these faults (contacts) and fractures control the flow of groundwater. The key factors influencing groundwater flow in the region are the fractures. Groundwater development and flow through weak zones and faults depend primarily on the heavily to moderately weathered and fractured ignimbrites and the sand layer. These geological formations provide pathways for groundwater flow, allowing it to recharge and move more freely underground. For all transverse lines, the majority of ignimbritic rocks are highly fractured, indicating the presence of various water-bearing zones at varying depths.

6.2. Recommendations

According to the results of this survey, it is advised that:

To support detailed structural geology and to map lineament orientations, more resistivity, seismic, structural, and magnetic survey data is advised. comprehensive examination of the groundwater flow and underlying structures in the surveyed area also requires the integration of geophysical results with the hydrogeology, geology, and structural geology of the investigation area. In addition to that, it is advised to conduct an additional thorough magnetic survey both inside and outside the area to determine the extent of faults that act as groundwater flow pathways.

In the same case, small-scale characteristics may not be captured by the resolution of the VES and magnetic data, hence additional geophysical techniques or subsurface studies are advised for a more detailed study. Similar to this, a thorough examination of geophysical methods is necessary to ascertain the underlying reasons for structural patterns in the research area. For a detailed examination of the extension of area to outside the study area, and conducting detailed structural geological surveys that identify the orientation of fractures, faults, and weaknesses, as well as their nature in terms of strike, dip, and extension, is highly recommended.

6. References

Abebe, T., Manetti, P., Bonini, M., Corti, G., Innocenti, F., & and Mazarinni, F. (2005). Geological map of the Northern Main Ethiopian Rift (at scale of 1:200,000).

Abera A. (2020). *Principles, practice, and application of geophysical methods to resource exploration and Geohazard studies.* Addis Ababa, Ethiopia: Aster Nega Publishing enterprise.

Abiola, O., & Enikanselu, P. (2009). Groundwater potential and Aquifer protective capacity of overburden units in Ado – Ekiti, Southwestern Nigeria. *Institute of geophysics*, 120 -132.

Ahmad, S. (2017). Assessment of groundwater potentiality using geophysical techniques in Wadi Allaqi basin, Eastern Desert. *journal of Astronomy and Geophysics*.

Amarachi, R. a. (2012). *Groundwater Investigation Using Combined Geophysical Methods.*

Assefa, G. (2007). *Characterization of major sub surface structures in Ada'a plain using the integrated geophysical survey*. Unpublished MS.c Thesis, Addis Ababa, Ethiopia.

Asta, a. A. (1920). *Application of Vertical Electrical Sounding (VES) Method with Resistivity Meter Based on Boost Converter to Estimate the Potential of Groundwater Aquifers in Karang Anyar of Tarakan City.*

Ayenew, T. (1998). *The hydrogeological system of the lake district basin : central main Ethiopian rift.* International Institute for Geo-Information Science and Earth Observation.

Bedane, E. (2008). *Aquifer vulnurability assesment in Modjo river catchment.* Unpublished MSc. thesis, Addis Ababa, Ethiopia.

Bekelu, A. (2020). *Application of integrated geophysical techniques in the investigation of ground water contamination fromtanneries and slaughter houses near Mojo River, Main Ethiopian Rift, Ethiopia.* Addis Ababa: Unpublished.

Belay, G. (2018). *Application of Integrated Geophysical Methods to map Aquifers and Subsurface Geological Structures for the exploration of groundwater Resources:*

at Woldia University and Mechare Meda, North Wollo Zone, North Ethiopia. Unpublished MSc. thesis, Addis Ababa University.

Benvenuti, M., Carnicelli, S., Belluomini, G., Dainelli, N., Di Grazia, S., Ferrari, G. A., . . . Kebede, S. (2002). The Ziway–Shala lake basin (main Ethiopian rift, Ethiopia): a revision of basin evolution with special reference to the Late Quaternary. *Journal of African earth science*, 247 - 269.

Blakely, R. (1995). *Potential Theory in Gravity & Magnetic Applications." Cambridge University Press, Cambridge.* Cambridge: Canbridge university press.

Boccaletti, M., Bonini, M., Mazzuoli, R., Abebe, B., Piccardi, L., & and Tortorici, L. (1998). Quaternery oblique extensional tectonics in the Ethiopian rift (Horn of Africa). *Tectonophysics*, 97-116.

Christensen, A., & Dransfield, M. (2002). Airborne vector magnetometry over banded iron formations. *72nd Annual International Meeting*, pp. 13 -16.

De Almeida, A., Maciel, D., Sousa, K. F., Nascimento, C., & Koide, S. (2021). Vertical Electrical Sounding (VES) for Estimation of Hydraulic parameter in the porous Aquifer. *water 2021*, 170.

EIGS. (1984). *A report on hydrogeology of the Nazret area.* Unpublished report, Addis Ababa, Ethiopia.

Fikre, S. (2006). *Hydrogeological system analysis in Ziway–Shala lakes area using hydrochemistry and isotope techniques, central Ethiopia.* Addis Ababa: Un published.

Gibson, L. (1968). The structure and volcanic Geology of an axial portion of the main Ethiopian Rift. *Tectonophysics*.

Griffths, D. a. (1981). *Applied Geophysics for Geologists and Engineers -2nd edition.* UK: Elsevier Science and Technology.

Haile, G. (1998). *Hydrogeology and Hydrochemistry of the lake Ziway areaand the sorrounding.* Unpublished MSc. thesis, Addis Ababa.

Hayatudeen, M. R. (2021). First horizontal and first vertical derivatives from high resolution aeromagnetic data over the Gongola basin upper Benue trough

Northeastern Nigeria. *GLOBAL JOURNAL OF PURE AND APPLIED SCIENCES*, 181 - 192.

Heigold, P. (1979). Aquifer transmissivity from surfcial electrical methods. . 338 -345.

Jacobsen, B. (1987). Case for upward continuation as standard separation filter for potential field maps. *Geophsics, 52*, 1138 - 1148.

Jaferson, D. S., & Fransisco, J. F. (2011). Enhancement of the total horizontal gradient of magnetic anomalies using tilt derivatives. Brazil.

Kazmin, V. a. (1978). *Geology and development of the Nazareth area, Northern Ethiopia rift.* Addis Ababa, Ethiopia: E. I. G. S., .

Kearey, P. B. (2002). *An introduction to geophysical exploration". 3rd edition.* Blackwell science Ltd, UK.

Keating, P., & Pilkington, M. (2004). Euler deconvolution of the analytic signal and its application to magnetic interpretations. *Journal of geological survey of Canada*, 165- 182.

Kebede, A. (2007). *Groundwater flow system and hydrochemistry of Ziway - Koka corrider in the main Ethiopian rift.* Addis Ababa, Ethiopia: Unpublished MSc. thesis.

Kebede, S. L. (2002). LakeGroundwater relationships, oxygen isotope balance and climate and climate sensitivity of the Bishoftu crater lakes, Ethiopia. 261-275.

Keller, G. a. (1996). *Electrical methods in geophysical prospecting.* Oxford: Pergamon Press Inc.

Leu, L. (1982). Use of reduction-to-the-equator process for magnetic data interpretation. *Geophysics*, 445.

Mamo, T. (2010). Delineation of sub-basalt sedimentary basins in hydrocarbon exploration in North Ethiopia. *Marine and petroleum geology,, 27*, 895 - 908.

Maneti, P., Bonini, M., Corti, G., Abebe, T., & Innocenti, F. (2005). Geological map of northern main Ethiopian Rift (Ethiopia): (with the scale of 1: 100,000). *Acta Vulcanologica*.

Manville, V. w. (1998). The saturation behaviour of pumice and some sedimentological implication. *sedimentary geology, 119*, 5 -16.

Melat, E. (2021). Hydro-climatic Variability and Trend Analysis of Modjo River watershed, Awash river basin of Ethiopia. *Journal of environment and earth science*.

Mequanent, B. (2015). *Application of the integrated geophysical method to map geological structure groundwater potential opf Lega Tefo lega Dadi area*. MSc. thesis, Un published, Addis Ababa, Ethiopia.

Miller, H. G., & Singh, V. (1994). Potential Field Tilt a New Concept for Location of Potential Field Sources. *Journal of Applied Geophysics, 32*, 213-217.

Milson J. (2003). *Field Geophysics-The Geological Field Guide Series, Third Edition* (3rd ed.). England: John Wiley & sons Ltd.

Mohamaden, M. e. (2016). Application of electrical resistivity method for groundwater exploration at the Moghra area, Western Desert, Egypt. *The egyptian journal of aquatic research*, 261-268.

MoWIE. (2015). *Assesment of alternative low floride potential water supply sources in selected five woredas in Ethiopian rift valley (Dugda woreda).* Addis Ababa, Ethiopia: Unpublished prefeasibility report.

Nabinghan, M. (1972). The analytic signal of twodimensional magnetic bodies with polygonal cross-section: its properties and use for automated anomaly interpretation:. *gephysics*, 507 -517.

Niwas, S. a. (1981). Estimation of aquifer transmissivity from Dar-Zarrouk parameters in porous media. *journal of Hydrology*, 393 -399.

Okonkwo, A. C., & Ugwu, G. (2015). Determination of Dar-zarrouk parameters for prediction of Aquifer protective capacity: A case of Agbani Sandstone Aquifer, Enugu State, Southeastern Nigeria. *journal of geology and mining*, 12 - 19.

Oladabo, M., & Akintorinwa, O. (2007). Hydrogeophysical study of Ogbese Southwestern, Nigeria. . *journal of pure and applied science*, 55 -61.

Oluwadebi, A. G. (2015). The Significance of Crystallinity in Hydrothermal Alteration Mapping: A Case study of Alemtena area of Main Ethiopian Rift, Ethiopia. *International research journal of Earth science, 3(4)*, 12-17.

Oni, A. G., Eniola, P. J., Oluremfemi, M. O., & Osutuyi, G. (2020). The magnetic method as a tool in groundwater investigation in a basement complex terrain: Modomo Southwest Nigeria as a case study. *Applied water science*.

Phillips, J. D. (2002). Locating magnetic contacts: a comparison of the horizontal gradient, analytical signal and local wavenumber methods. *70th Annual international meeting*, (pp. 402 -405).

Ragunath, H. (1982). *Groundwater hydrogeology 2nd edition.* New Delhi, India: Wiley Eastern Ltd.

Rajagopalan, S. (2003). Analytic Signal vs. Reduction to Pole: Solutions for Low Magnetic Latitudes. *Exploration geophysics*, 1 - 4. doi:10.1071/ASEG2003ab136

Reach. (2020). *report on finding from the Awash river basin.* University of Oxford, Oxford, UK: Mid-programme synthensis.

Reynolds, J. (1997). *An introduction to applied and environmental geophysics – 2nd edition.* Wiley Blackwell Ltd.

Roest, W. R., Veroef, J., & Pilkington, M. (1992). Magnetic interpretation using the 3·0 analytic signal. *Geophysics*, 116 - 125.

Samouelian, A. e. (2005). Electrical resistivity survey in soil science: a review. Soil and Tillage Research. 173-193.

Seifu, K. Y. (2010). *Groundwaters of the Central Ethiopian Rift: diagnostic trends intrace elements and major elements.*

Singh, C., & Singh, S. (1970). Some geoelectrical investigations for potential groundwater zones in part of Azamgar area of UP. *pure and applied geophysics*, 270-285.

Singh, U. K., Das, R. K., & Hodlur, G. K. (2004). Significance of Dar-Zarrouk parameters in in the exploration of quality affected coastal aquifer systems. *Environmental earth science*.

Sisay, L. (2007). *Application of Remote Sensing and GIS for Groundwater Potential Zone Mapping in Northern Ada'a Plain (Modjo catchment).* UnPublished MSc. thesis, Addis Ababa University, Ethiopia.

Springer. (2009). *Groundwater Geophysics a Tool for Hydrogeology* (2nd ed., Vol. II). Verlag Berlin Heidelberg: Library of congress controll number 2008936482.

Tigistu H., a. A. (2014). Electrical resistivity tomography and magnetic surveys: applications for building site characterization at Gubre, Wolkite university site, western Ethiopia. 3-15.

Truneh, A. (2006). Hydrogeology of Modjo River Catchment, Ethiopian Rift Valley. Unpublished MSc. Thesis, Addis Ababa, Ethiopia.

Tsegaye, T. (2008). Application of numerical model for groundwater flow system assesment in the upper awash basin (case study mojo river catchment). msc. thesis, unpuplished, addis ababa, ethiopia.

Utom, A., Odoh, B., & Okoro, A. (2012). Estimation of Aquifer Transmissivity Using Dar Zarrouk Parameters Derived from Surface Resistivity Measurements. *Journal of Water Resource and Protection*, 993 -1000.

Utom, A., Odoh, B., & Okoro, A. (2012). Estimation of Aquifer Transmissivity Using Dar Zarrouk Parameters Derived from Surface Resistivity Measurements: A Case History from Parts ofEnugu Town (Nigeria). *water resource and protection*, 993 - 1000.

Woldegabriel, G., Helken, G., White, T., Asfaw, B., Hart, W., & Renne, P. (2000). Volcanism, tectonism, sedimentation, and the paleoanthropological record in the Ethiopian rift system. *Geological society of America*.

WWDSE. (2008). Evaluation Of Water Resources Of The Ade'a And Becho Plains Groundwater Basin For Irrigation Development Project, Volume-III Evaluation of Groundwater Resources Potential, Federal Democratic Republic of Ethiopia, Ministry Of Water Resources. Addis Ababa, Ethiopia.

Yonas, G. H.; and Tesfa, G. A. (2021). Geospatial and multi-criteria decision approach of groundwater potential zone identification in Cuma sub-basin, Southern Ethiopia. *Heliyon, 7*. doi:10.1016/j.heliyon.2021.e07963

Yusuf, S. N., Imagbe, L. O., Yohanna, O. M., Ibrahim, Y., & Kuku, A. Y. (2022). Imaging magmatic intrusions using derivatives of high-resolution aeromagnetic data over the Nigerian sector of the chad Basin. *scientific African*.

Zohdy, A. E. (1974). *Application of surface geophysics to groundwater investigation.* Department of the enterior geological survey.

Appendix

Resistivity curves

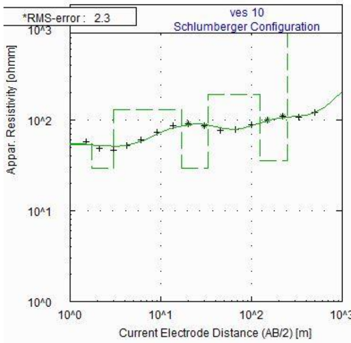

No	Res	Thick	Depth
1	54.4	1.7	1.7
2	29.7	1.3	3.0
3	131.8	14.0	17.0
4	29.3	16.3	33.3
5	191.5	90.3	123.6
6	35.3	126.0	249.6
7	5732.5	-.-	-.-

* RMS on smoothed data

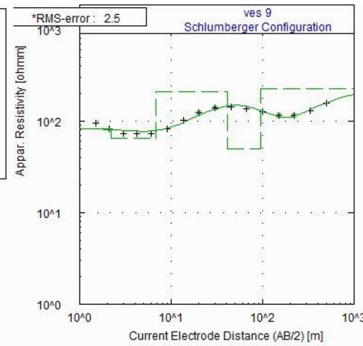

No	Res	Thick	Depth
1	82.5	2.2	2.2
2	64.4	4.6	6.8
3	209.1	34.0	40.7
4	50.3	55.0	95.7
5	228.4	-.-	-.-

* RMS on smoothed data

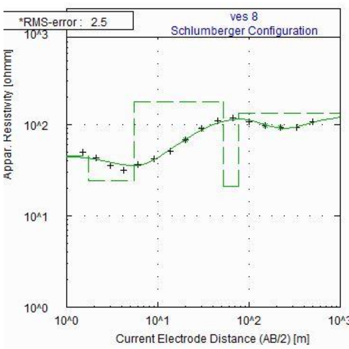

No	Res	Thick	Depth
1	45.2	1.7	1.7
2	24.2	3.8	5.5
3	176.1	46.4	51.9
4	21.2	25.7	77.6
5	132.1	-.-	-.-

* RMS on smoothed data

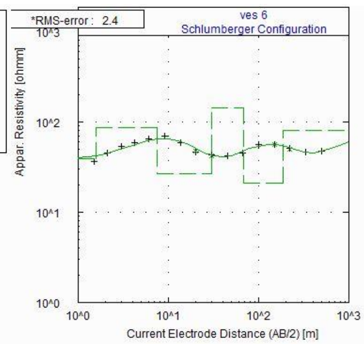

No	Res	Thick	Depth
1	39.6	1.6	1.6
2	87.4	5.9	7.5
3	26.8	22.5	30.0
4	141.9	38.5	68.6
5	21.2	116.2	184.8
6	80.6	-.-	-.-

* RMS on smoothed data

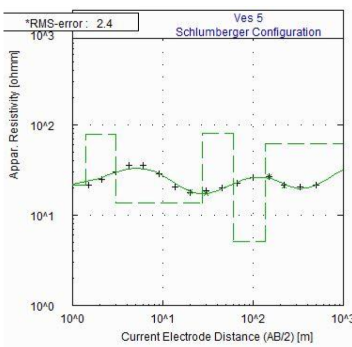

No	Res	Thick	Depth
1	21.4	1.4	1.4
2	78.7	1.6	3.0
3	13.7	24.4	27.4
4	80.8	32.3	59.8
5	5.1	77.7	137.5
6	61.2	-.-	-.-

* RMS on smoothed data

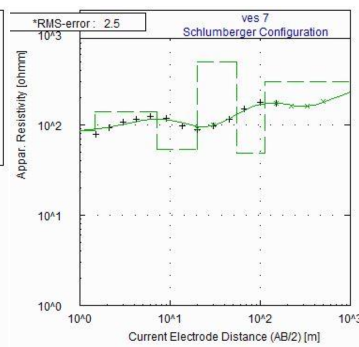

No	Res	Thick	Depth
1	85.9	1.5	1.5
2	140.9	5.6	7.1
3	53.3	12.8	19.9
4	495.4	34.8	54.7
5	48.3	59.2	113.9
6	299.9	-.-	-.-

* RMS on smoothed data

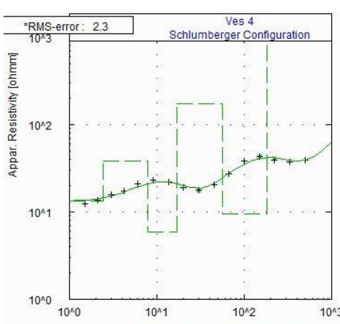

No	Res	Thick	Depth
1	13.3	2.4	2.4
2	37.9	5.5	7.9
3	5.9	9.3	17.1
4	173.6	38.6	55.7
5	9.4	126.1	181.9
6	1805.7	-.-	-.-

* RMS on smoothed data

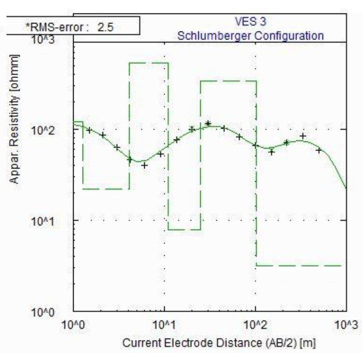

No	Res	Thick	Depth
1	120.0	1.3	1.3
2	21.9	2.8	4.1
3	538.3	6.9	11.0
4	8.0	13.8	24.8
5	337.2	77.6	102.4
6	3.2	-.-	-.-

* RMS on smoothed data

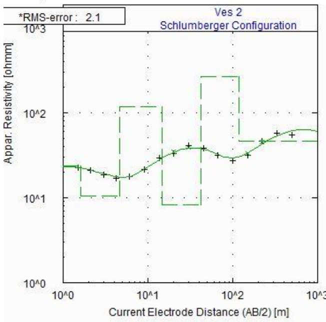

No	Res	Thick	Depth
1	23.7	1.6	1.6
2	10.5	3.0	4.6
3	117.0	10.0	14.6
4	8.2	27.8	42.4
5	266.4	76.0	118.4
6	47.0	-.-	-.-

* RMS on smoothed data

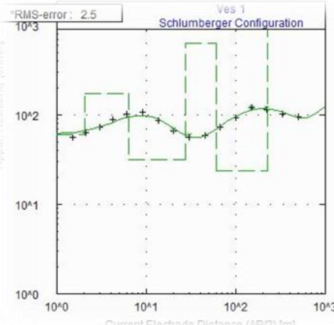

No	Res	Thick	Depth
1	61.1	2.0	2.0
2	175.2	4.2	6.3
3	31.3	21.4	27.7
4	640.6	33.1	60.8
5	23.9	166.3	227.0
6	2670.9	-.-	-.-

* RMS on smoothed data

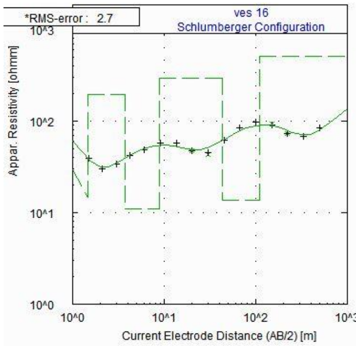

No	Res	Thick	Depth
1	109.7	0.5	0.5
2	14.6	1.0	1.5
3	193.7	2.3	3.8
4	10.9	5.0	8.8
5	296.8	34.0	42.9
6	13.5	67.3	110.2
7	513.5	-.-	-.-

* RMS on smoothed data

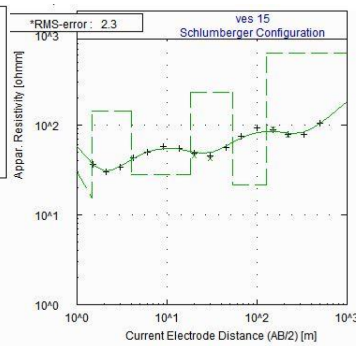

No	Res	Thick	Depth
1	108.1	0.5	0.5
2	15.5	1.0	1.5
3	143.6	2.6	4.1
4	27.8	14.2	18.2
5	233.3	35.8	54.0
6	21.4	73.6	127.6
7	634.8	-.-	-.-

* RMS on smoothed data

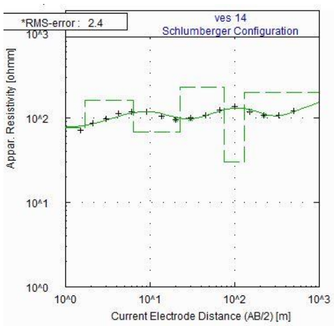

No	Res	Thick	Depth
1	77.2	1.7	1.7
2	161.5	4.7	6.4
3	67.5	16.3	22.7
4	228.9	51.8	74.5
5	30.2	56.9	131.4
6	201.6	-.-	-.-

* RMS on smoothed data

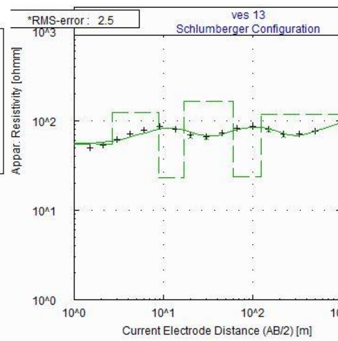

No	Res	Thick	Depth
1	55.3	2.7	2.7
2	125.5	6.3	8.9
3	23.2	7.9	16.8
4	164.4	44.1	60.9
5	23.5	62.0	122.9
6	117.1	-.-	-.-

* RMS on smoothed data

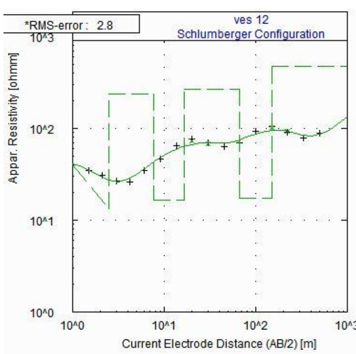

No	Res	Thick	Depth
1	45.8	0.9	0.9
2	13.3	1.6	2.5
3	237.0	5.1	7.6
4	16.6	8.8	16.4
5	265.8	50.3	66.7
6	17.3	83.7	150.3
7	474.5	-.-	-.-

* RMS on smoothed data

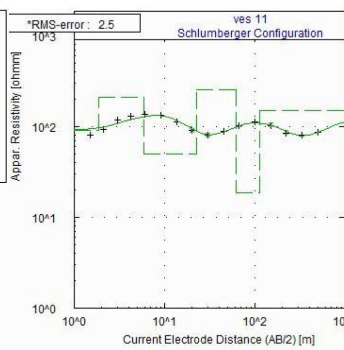

No	Res	Thick	Depth
1	91.0	1.9	1.9
2	208.7	4.0	5.9
3	50.0	16.7	22.6
4	256.3	38.5	61.2
5	18.8	51.3	112.5
6	149.5	-.-	-.-

* RMS on smoothed data

Borehole data

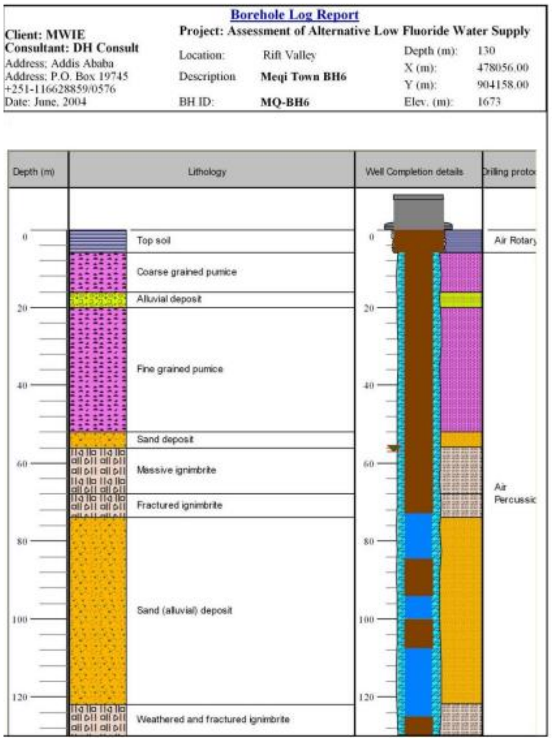

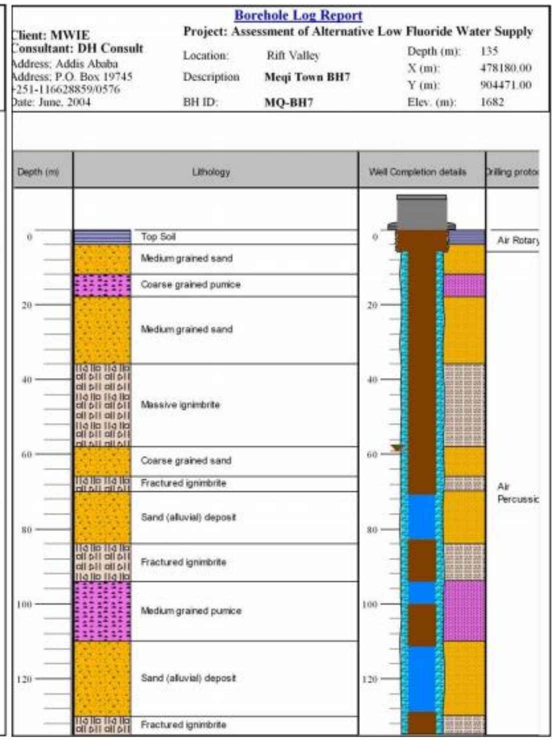

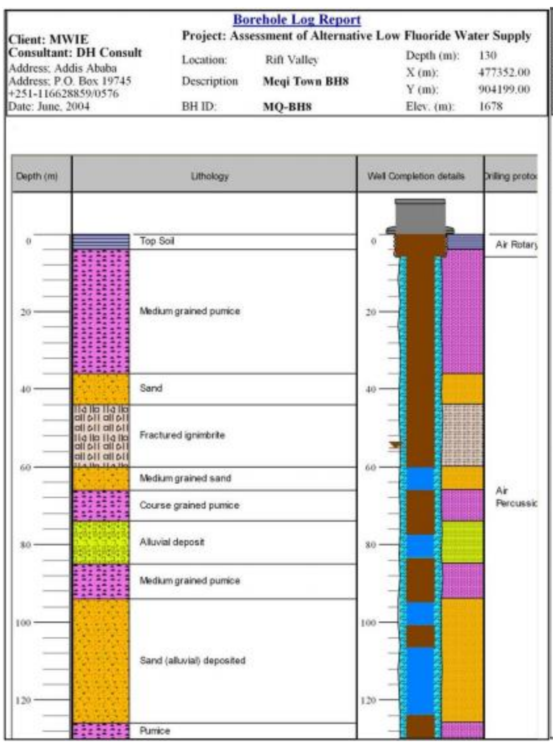

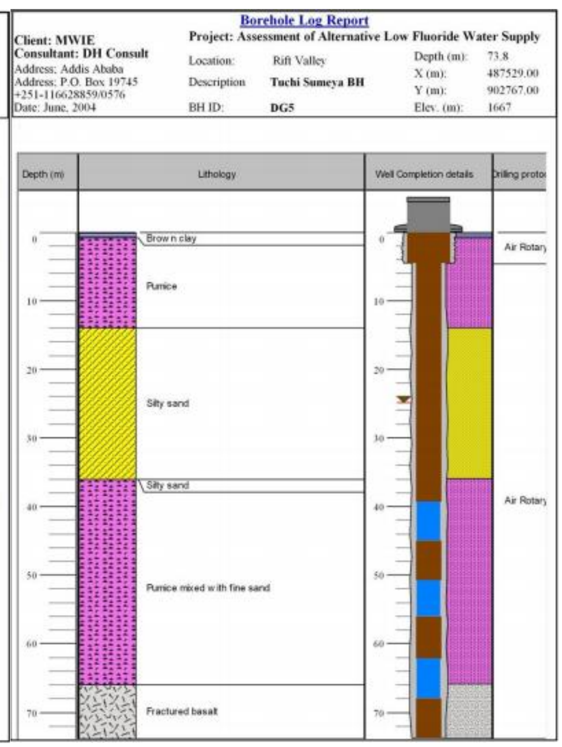

Table 2 litho logical Description of Sera wakele PA

Depth(m)	litho logical Description
0-2	Top soil
2-6	Clay
6-21	Pumice
21-26	Clay
26-100	pumice
100-200	Sand
200-225	Highly weathered ignimbrit

10

Bora District, Bite Dhaba Well Completion Report

August [illegible]

Table 3 Lithological description

Depth Range		Lithological Description
From	To	
0	2	Top soil (Black Cotton Soil)
2	4	Sticky clay
4	16	Fine grained sand
16	128	Pumice
128	132	Scoria
132	138	Massive basalt
138	148	Scoria
148	176	Moderately fractured and weathered basalt with alterations
176	204	Weathered scoracious basalt
204	226	Moderately fractured and weathered Ignimbrite
226	250	Highly fractured and altered Ignimbrite

12

e 2 litho logical Description of Berta Sami PA

th(m)	litho logical Description
	Top soil
)	Pumice
75	Fractured and weathered ignimbrite
240	Circulation loss (no sample)

8